Doctoral Dissertations Graduate School

12-2008

Magnetic Field Effects on Photocurrent and Photovoltaic Processes in Organic Solar Cells

Zhihua Xu
University of Tennessee - Knoxville

Follow this and additional works at: https://trace.tennessee.edu/utk_graddiss

Part of the Materials Science and Engineering Commons

Recommended Citation

To the Graduate Council:

I am submitting herewith a dissertation written by Zhihua Xu entitled "Magnetic Field Effects on Photocurrent and Photovoltaic Processes in Organic Solar Cells." I have examined the final electronic copy of this dissertation for form and content and recommend that it be accepted in partial fulfillment of the requirements for the degree of Doctor of Philosophy, with a major in Materials Science and Engineering.

Bin Hu, Major Professor

We have read this dissertation and recommend its acceptance:

Jimmy Mays, Roberto S. Benson, Bamin Komami

Accepted for the Council:

Carolyn R. Hodges

Vice Provost and Dean of the Graduate School

(Original signatures are on file with official student records.)

To the Graduate Council:

I am submitting herewith a dissertation written by Zhihua Xu entitled "Magnetic Field Effects on Photocurrent and Photovoltaic Processes in Organic Solar Cells." I have examined the final electronic copy of the dissertation for form and content and recommend that it be accepted in partial fulfillment of the requirements for the degree of Doctor of Philosophy, with a major in Materials Science and Engineering.

<div align="right">

Bin Hu
_____

Major Professor

</div>

We have read this dissertation

And recommend its acceptance:

Jimmy Mays
_____

Roberto S. Benson
_____

Bamin Komami
_____

<div align="right">

Accepted for the Council:

Carolyn R. Hodges
_____

Vice Provost and Dean of the Graduate School

</div>

(Original signatures are on file with official student records.)

Magnetic Field Effects on Photocurrent and Photovoltaic Processes in Organic Solar Cells

A Dissertation Presented for

the Doctor of Philosophy Degree

The University of Tennessee, Knoxville

Zhihua Xu

December 2008

ACKNOWLEDGEMENTS

First and foremost, I am deeply indebted to my advisor, Dr. Bin Hu. His great efforts in guiding and supporting my research have been crucial for me to finish this dissertation. I thank him for providing abundant opportunities and resources. Also, I would like to thank my committee members, Dr. Roberto Benson, Dr. Jimmy Mays, and Dr. Bamin Khomami, for their instructive advice and great support.

I owe many thanks to my collaborators at the Oak Ridge National Laboratory (ORNL) for their help in using facilities. They are Dr. David B. Geohegan, Dr. Ilia Ivanov, Dr. Kai Xiao, Dr. Matthew Garrett, Dr. Chengjun Sun and Dr. Jane Howe.

I spent a great time together with my group members, Dr Yue Wu, Liang Yan, Ming Shao, Jaime Sullivan, Huidong Zang, Dr. Youzhi Wu, and Dr. Tho Nguyen. I would like to thank them for useful discussions and enormous support.

Finally, I must express my appreciations to my parents and other family members in China, and my wife, Hui Huang, who provided me the strongest support during the years in the graduate school.

ABSTRACT

Two mechanisms were investigated to understand the magnetic field effects on photocurrent (MFP), a phenomenon whereby an external magnetic field (MF) can increase or decrease photocurrent in organic solar cells (OSCs). The first one relates to MF-modulated intersystem crossing (ISC) between singlet and triplet polaron pairs and charge transfer (CT) complexes, accounting for the positive MFP in low and high magnetic field, respectively. The second mechanism originates from the interaction between triplet excited states and charge carriers, namely triplet-charge reaction (TCR). External magnetic field was found to reduce the rate constant of TCR, leading to negative MFP.

MFP measurements were used to study the dissociation processes of singlet and triplet excitons in single-layer solar cells. It was found that the triplet excitons mainly dissociate directly into free charge carriers at the metal-electrode interface due to their long diffusion length, while the singlet excitons experience significant bulk dissociation into polaron pairs due to their short diffusion length. The interfacial dissociation of triplet excitons at the metal electrode can lead to enhanced photovoltaic (PV) response from phosphorescent materials as compared to the bulk dissociation of singlet excitons in fluorescent materials.

MFP measurements were also applied to study the charge carrier generation and

recombination processes in bulk-heterojunction solar cells. It was found that dissociation of polaron pairs, triplet-charge reaction, dissociation of hot excitons, and photoinduced charge transfer are responsible for charge carrier generation in OSCs. High-field MFP reflects the recombination of dissociated electrons and holes towards the formation of singlet and triplet CT complexes in bulk-heterojunction OSCs. The annealing effect on the formation of CT complexes was also investigated.

The PV efficiency of bulk-heterojunction solar cells was improved by uniformly dispersing phosphorescent heavy-metal complexes. The MFP results suggest that the spin-orbit coupling and the density of triplet excited states in conjugated polymer MEH-PPV were enhanced by external heavy-atom effect. The increased triplet density facilitated exciton dissociation and reduced charge recombination, and consequently improved the PV response in bulk-heterojunction cells.

TABLE OF CONTENTS

LIST OF FIGURES

CHAPTER 1

INTRODUCTION

Since the discovery of photovoltaic (PV) effect by Becquerel in 1839,[1] continuous efforts have been made in academia and industry to improve the efficiency of light-to-electricity conversion.[2-4] The biggest breakthrough was made in 1954 when the first silicon-based solar cell with 6% power conversion efficiency (PCE) was developed at the Bell Laboratories.[5] And now the highest PCE of solar cells has reached 40%.[6] However, due to the relatively high price of the current PV products, the solar energy production accounts for less than 0.01% of the total world energy production.

1.1 Photovoltaic Materials

The dominant PV material today is silicon, which accounts for more than 90% of the PV market share. However, as an indirect band semiconductor, silicon has relatively low light absorption coefficient. To absorb sufficient sun light a thickness on the order hundreds of micrometers is needed for silicon films, and therefore silicon-based solar cells consume much more materials than thin-film solar cells.[7] Furthermore, the fabrication cost of silicon solar cell is high due to its complicated manufacturing processes. To reduce the price of solar energy and keep it competitive with the other renewable energies, the development of new PV materials is of great importance. Along

with the other inorganic thin-film materials such as $CuInSe_2$ (CIS), CdTe and III-V semiconductors, organic semiconducting materials have drawn more and more attention in last two decades.[7, 8]

Organic PV (OPV) materials include conjugated polymers and small molecules that show p-type or n-type semiconducting properties. Due to their alternative single and double bond configuration, organic semiconductors have a σ-bond backbone with the remaining out-of plane p_z-orbital forming π-bonds with neighboring p_z orbitals. The electrons in p_z orbitals, namely π-electrons, can then delocalize over the entire molecule. Because the wavefunction overlap of p_z orbitals forms both bonding (π) orbitals with lower energy and antibonding (π*) orbitals with higher energy, the electronic structures essentially consist of Highest Occupied Molecular Orbitals (HOMO) and Lowest Unoccupied Orbitals (LUMO). The HOMO and LUMO are also named as low-energy valence and high-energy conduction bands. Furthermore, the valence and conduction bands form direct band structures in conjugated molecules, allowing direct electronic transitions for π electrons across the band gap defined as the minimal energy difference between the valence and conduction bands. Figure 1.1 shows the molecular structure of the simplest conjugated polymer polyacetylene and the formation of its band structure. A Conjugated molecule can absorb a photon with energy larger than the band gap. The organic semiconducting materials usually have high absorption coefficients, which enable them to make very thin solar cells (hundreds of nanometers) and consume fewer
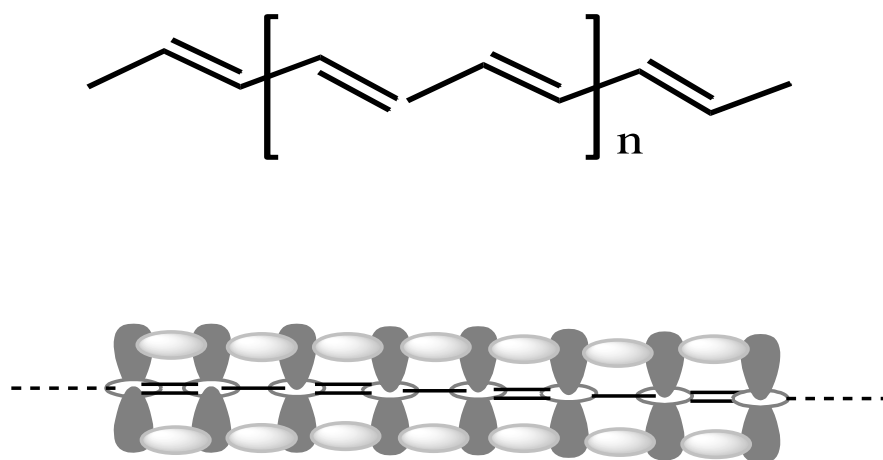
Figure 1.1 Molecular structure of conjugated polyacetylene, and its band structure formed by the overlap of p_z orbital.

materials than crystalline silicon solar cells. High versatility of organic compounds can be achieved by chemical tailoring, providing nearly infinite possibilities of tuning their optical and electrical properties. Most importantly, their good mechanical properties open the possibility to fabricate light, flexible solar cells in large scale using inexpensive "roll-to-roll" fabrication technology. Therefore, OPVs are widely regarded as a promising cost-effective alternative to silicon solar cells.[9]

1.2 Organic Solar Cells

1.2.1 Device Structures

There are three basic device structures of organic solar cells (OSCs), namely single-layer, bilayer-heterojunction and bulk-heterojunction OSCs. The first generation of organic solar cells is single-layer cells, which were fabricated with a single organic layer sandwiched between two metal electrodes with different work functions (Figure 1.2a). The power conversion efficiency of single-layer PV cells was generally very low (lower than 0.1%).[10] The next generation of OSCs is bilayer-heterojunction cells, which include two organic layers with electron donating or electron accepting properties sandwiched between the electrodes (Figure 1.2b). This type of OSCs was first reported by Tang in 1986 using two organic materials (a phthalocyanine derivative and a perylene derivative) sandwiched between a transparent conducting oxide and a semitransparent metal electrode.[11] The power conversion efficiency of this device was about 1%. The highest efficiency of bilayer-heterojunction cells has reached 4%.[12] The third generation and the most promising OSCs are bulk-heterojunction solar cells, in which electron donor and acceptor materials are blended together forming continuous conductive network for electrons and holes collection (Figure 1.2c). Bulk-heterojunction OSCs were first introduced by Heeger's group in early 90s, when efficient photoinduced charge transfer was observed in the blend of a conjugated polymer and fullerene.[13] Around 5% power conversion efficiency has been achieved using this structure.[14, 15]

Al		Al		Al
Organic material		Acceptor		Donor+Acceptor
		Donor		
ITO		ITO		ITO
Glass		Glass		Glass
(a)		(b)		(c)
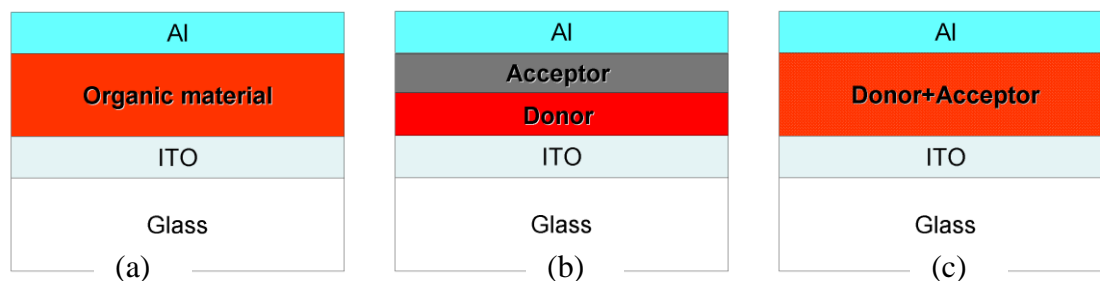
Figure 1.2 Typical device structures of organic solar cells: (a) Single-layer cell; (b) Bilayer-heterojunction cell; (c) Bulk-heterojunction cell.

1.2.2 Photovoltaic Processes

The process of light-to-electricity conversion in an organic photovoltaic cell includes the following consecutive steps: (I) Absorption of sun light leads to formation of excited states, bounded electron-hole pairs (excitons); (II) Excitons diffuse to some regions, where exciton dissociation and charge separation occur; (III) The separated electrons and holes transport to the cathode and anode, respectively. Therefore the photon-to-electron conversion efficiency (or external quantum efficiency, EQE) of PV devices (η_{EQE}) is determined by the product of the efficiency of light absorption (η_A), exciton dissociation (η_D), and charge collection (η_{CC}). In addition to the above-mentioned processes that contribute to charge carrier photogeneration, there exist undesirable charge recombination processes. For example, radiative and nonradiative decay during the

5

exciton diffusion, geminate recombination following exciton dissociation and bimolecular recombination during charge collection. The recombination processes compete with the free charge generation processes, and reduce the PV efficiency of organic solar cells. The important photovoltaic processes involving in charge generation and recombination in OPVs are depicted in Figure 1.3.

1.2.3 Characterization of OPVs

The characterization of OPVs is conducted under standard illumination of AM1.5G simulated white light. The typical current-voltage (I-V) curves of OPVs with or without illumination are shown in Figure 1.4. Three parameters are considered to characterize the power conversion efficiency of solar cells: short-circuit current (I_{SC}), the photocurrent when the device is short circuited; Open circuit voltage (V_{OC}), the voltage that balances the current to zero; Fill Factor (FF), which is determined as $FF=I_M V_M/I_{SC}V_{OC}$, where I_M and V_M is the current and voltage of the maximum power point, the product between current and voltage and hence the power output is the largest. The power conversion efficiency (PCE) of solar cells is defined as:

$$PCE(\%) = \frac{P_{out}}{P_{in}} = \frac{I_{SC} \bullet V_{OC} \bullet FF}{P_{in}} \times 100\% \qquad \text{(Equation 1.1)}$$

1.3 Singlet and Triplet Excited States

When a photon is absorbed by organic semiconductors, either conjugated polymers
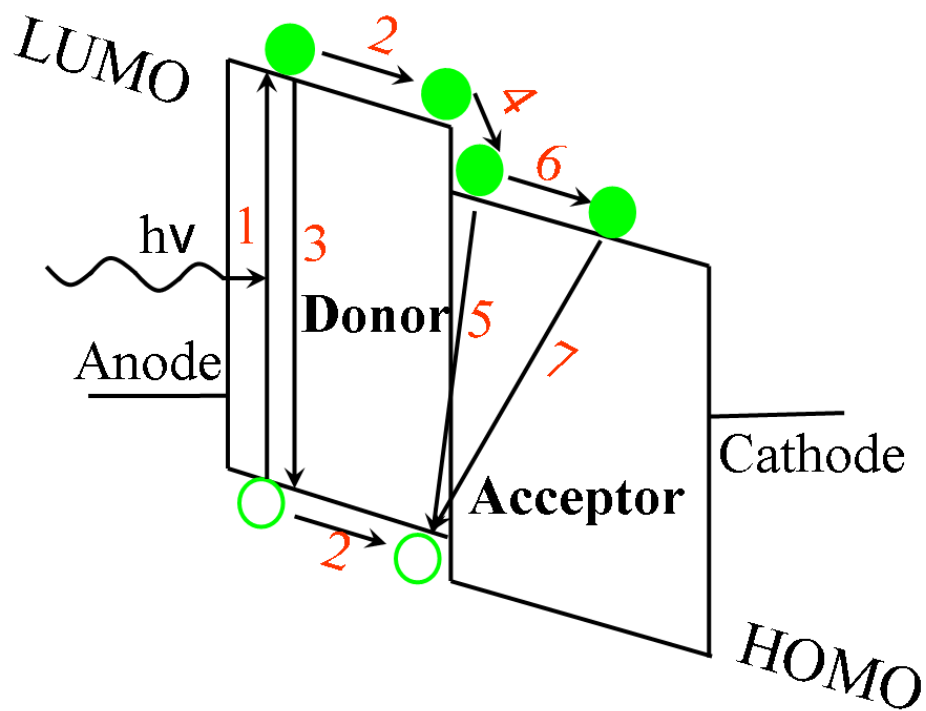
Figure 1.3 Free charge carrier photogeneration and recombination processes in organic solar cells. 1. light absorption and exciton formation; 2. exciton diffusion; 3. exciton recombination (radiative and nonradiative); 4. exciton dissociation; 5. geminate charge recombination; 6. charge collection; 7. bimolecular charge recombination.
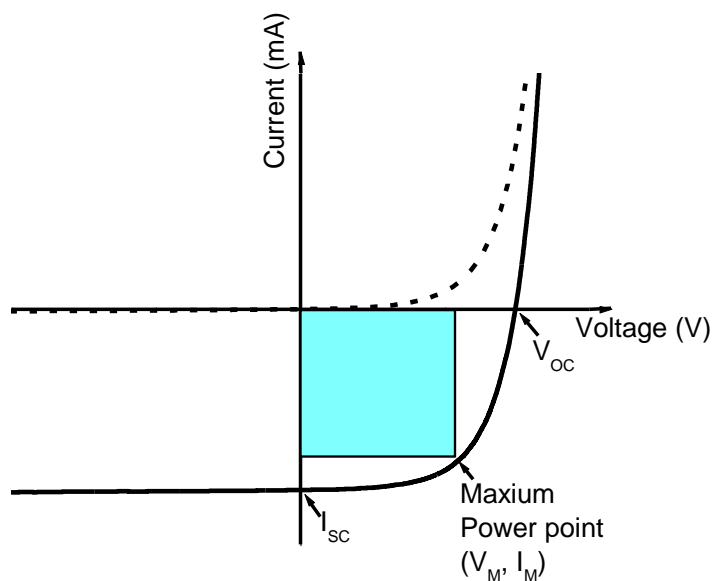
Figure 1.4 Typical current-voltage (I-V) characteristics of organic solar cells in dark

(dash line) and under light illumination (solid line).

or small molecules, an electron in the highest occupied molecular orbital (HOMO) will

be excited to the lowest unoccupied molecular orbital (LUMO), leaving behind a hole

(positive charge) in the HOMO, which is bounded with the electron by the coulomb

attraction. This bounded electron-hole pair is named as an exciton. In inorganic

semiconductors, the screening effect significantly reduces the Coulomb interaction in

electron-hole pair because of large dielectric constant. Therefore, photoexcitation leads to

generation of free electrons and holes, or electron-hole pairs with small binding energy

(on the order of 0.1eV), namely Mott-Wannier exciton.[16] However, the dielectric

constant is usually small in organic materials, and the Coulomb interaction between electron and hole is strong. Therefore, photoexcitation of organic semiconductors generates Frenkel excitons, which have typical binding energy on the order of 1.0 eV.[17,18]

1.3.1 Singlet and Triplet Excitons

As the most important excited state in organic semiconductors, an exciton contains two unpaired charges in different orbitals, which can form different spin combinations. If the electron and hole have parallel spin, the total spin will be S=1, and the spin multiplicity will be m=3 (m=2S+1). In this case, the exciton is in triplet state. If the electron and hole have opposed spin (S=0), their spin multiplicity is m=1. Therefore, the exciton is in singlet state. The vector representation of the triplet and singlet states is shown in Figure 1.5.[19] Because of the repulsive nature of the spin-spin interaction between the electrons with the same spin (exchange interaction), a triplet state usually has lower energy level and larger binding energy than the corresponding singlet state,[20] resulting in a energy gap Δ_{S-T} between singlet and triplet states. The exchange interaction depends on the spatial overlap of π and π^* orbitals, therefore the exchange energy and consequently Δ_{S-T} decrease drastically with increasing separation distance between electron and hole. Since the electrons in the ground state of organic semiconductors are paired, i.e. in singlet state, the transition from singlet excited state to singlet ground state is allowed, resulting in radiative decay with photon emission (fluorescence) or nonradiative
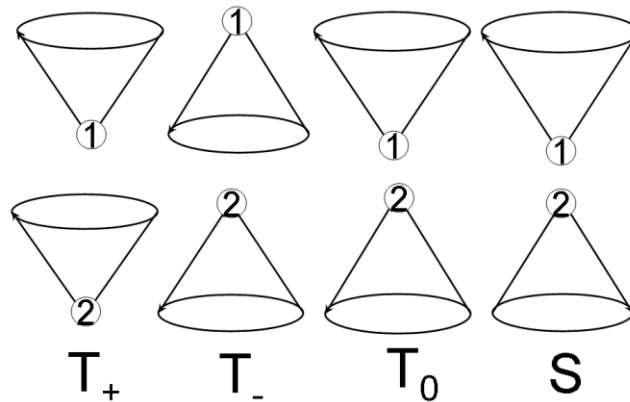
Figure 1.5 Vector representation of the spin states of electron-hole pair: singlet state (S) and triplet states (T_+, T_-, T_0)

decay with phonon emission. While the transition from triplet excited state to ground state is forbidden according to the spin conservation rule. Therefore, triplet excitons are usually nonemissive, having longer lifetime and diffusion length than singlet excitons. The energy-level diagram of singlet and triplet excitons and their decay channels are shown in Figure 1.6.

1.3.2 Intersyetem Crossing

The transition between singlet and triplet state, defined as intersystem crossing (ISC), is usually strongly forbidden because it involves spin flipping of an orbital electron. However, this forbidden transition can be partly allowed by spin-orbit coupling (SOC)
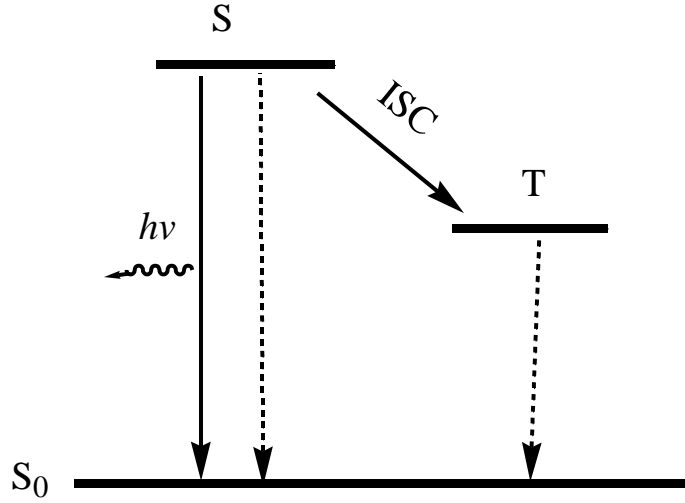
Figure 1.6 Energy-level diagram and decay channels of singlet and triplet excitons. S_0: ground state, S: singlet state, T: triplet state, ISC: intersystem crossing, solid arrow: radiative decay with photon emission (hv), dash arrow: nonradiative decay.

and hyperfine interaction (HFI). Spin-orbit coupling arises from the interaction of the magnetic field associated with the spin angular momentum and the magnetic field associated with the orbital motion of the same electron in the electrostatic field of a nucleus, shown as Figure 1.7. The spin-orbit Hamiltonian H_{SOC} are expressed as

$$H_{SOC} = \xi_{n,l}LS = 2\beta_e^2 \left\langle Z/r^3 \right\rangle_{n,l} LS \qquad \text{(Equation 1.2)}$$

where $\xi_{n,l}$ is the SOC constant, n is the principle quantum number, l is the value of orbital angular momentum, L is the orbital momentum operator, and S is the spin momentum operator, β_e is the Bohr magneton, Z is the nuclear charge, r is the distance between an
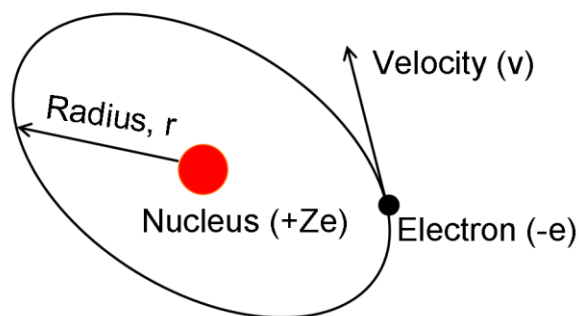
Figure 1.7 Schematic representation of spin-orbit coupling.

electron and a nucleus. In hydrogen-like atoms

$$\left\langle 1/r^3 \right\rangle_{n,l} \approx Z^3/n^3 l(l+1)(l+1/2)$$ (Equation 1.3)

Therefore the SOC constant is proportional to Z^4.[21, 22] This reflects a general principle that heavy atoms can lead to strong spin-orbit coupling. SOC mixex the singlet and triplet wave functions and make their interconversion possible.[23]

Another channel that mixes the singlet and triplet spin multiplicity is the interaction between spin momentum of electrons and the nucleus around them, namely hyperfine interaction, as shown in Figure 1.8. The hyperfine Hamiltonian is written as

$$H_{HFI} = aIS$$ (Equation 1.4)

Where a is the HFI constant, and I is the nuclear spin operator, and S is the electron spin operator. Because the HFI constant a is very small, HFI can only effectively induce spin mixing and intersystem crossing when the energy gap Δ_{S-T} is small.[24] Due to the large
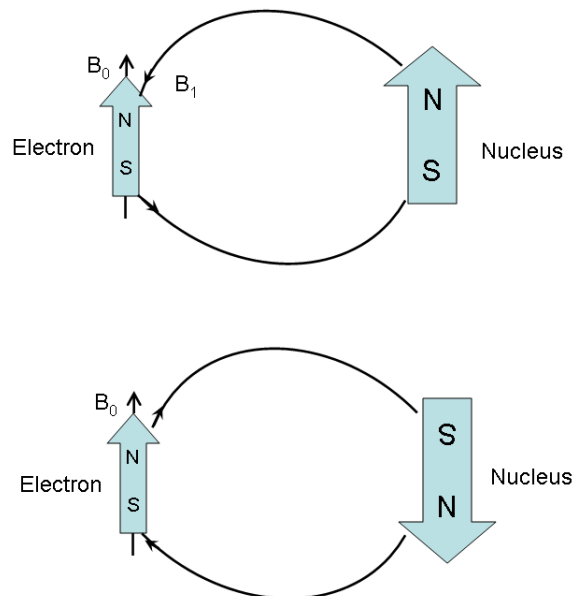
Figure 1.8 Schematic description of hyperfine interaction.

exchange energy between singlet and triplet excitons, Δ_{S-T} is usually too large for HFI to effectively induce ISC in excitonic state.

1.3.3 Singlet and Triplet Charge Transfer Complex

Following the formation of singlet excitons, the bounded electron-hole pair may recombine radiatively with emission of photons or nonradiatively with emission of phonons. The singlet excitons can also convert to triplet excitons through intersystem crossing. Another decay channel for singlet exciton is electron transfer to a neighboring molecule, forming intermolecular charge transfer (CT) complex.[25] The neighboring

molecules can be the same molecules, or molecules with defects or impurities that make the electron transfer energy favorable. Similar to the excitonic state, the charge transfer complex can also be in singlet and triplet state, and SOC induces the intersystem crossing between singlet and triplet CT complexes. On the other side, the separation distance between the electron and hole in CT complexes is larger than that in intramolecular excitons. As a result, the exchange interaction is weaker, and the singlet-triplet energy gap Δ_{S-T} is smaller in CT complexes. Therefore, HFI plays a role in controlling the intersystem crossing between singlet and triplet CT complexes as well as SOC.

1.3.4 Singlet and Triplet Polaron Pair

In CT complexes, the coulomb attraction between electron and hole is largely reduced as compared with excitons. Thermally activated hopping of electrons and holes will lead to formation of distantly-separated and weakly-bounded electron-hole pairs, namely polaron pairs.[26] Further dissociation of polaron pairs generates free electrons and holes and contributes to photocurrent. Because the separation distance between electron and hole in polaron pairs is large (a few nanometers), the exchange interaction is negligible, and the energy splitting between singlet and triplet states is close to zero.[26] As a result, hyperfine interaction becomes an important process to mix the singlet and triplet spin multiplicity in polaron pair state.

Excitons, CT complexes and polaron pairs are the three types of excited states that

generate free charge carrier in OPVs. The singlet and triplet spin multiplicities of these excited states have different energy levels (Figure 1.9), recombination channels and dissociation processes, which will lead to different efficiency of photocurrent generation. For example, the singlet excitons have smaller binding energy and are easier to be dissociated than triplet excitons. This is a favorable character for PV application. However, due to the allowed transition to ground state singlet excitons have fast recombination channel which is not favorable in PV application, because it competes with exciton dissociation. On the other side, triplet excitons have large binding energy, but the forbidden recombination nature allows them have long lifetime to travel to donor/acceptor sites where dissociation of strongly bounded triplet excitons is possible. Therefore, how to control and utilize the singlet and triplet spin state should be an important factor for material selection and structure design of OPVs.

1.4 Triplet States in OPVs

The distinct characteristics between singlet and triplet excited states, such as binding energy, lifetime, diffusion length, dissociation and recombination processes, presumably contribute to their different efficiency of photocurrent generation. However, the researches on OPVs have been predominantly focused on the singlet excited state because the primary photoexcited state in organic semiconductors is in singlet spin multiplicity. Recently, there is slowly increasing interest in utilizing triplet states to
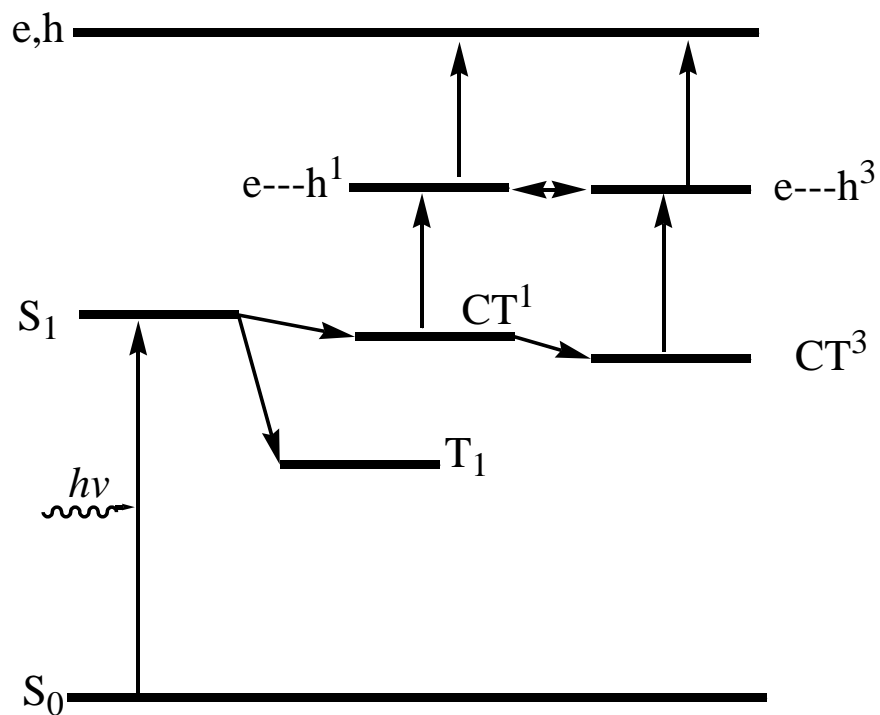
Figure 1.9 General scheme of singlet and triplet excited states of organic semiconductors under photoexcitation, S_0: ground state, S_1: singlet exciton, T_1: triplet exciton, CT^1 and CT^3: singlet and triplet charge transfer complex, $e{-}h^1$ and $e{-}h^3$: singlet and triplet polaron pair, e and h: free electron and hole.

enhance photovoltaic efficiency.

The first study on the photovoltaic processes of singlet and triplet excitons in OPVs was done by Köhler *et al.*[27] By measuring photoluminescence of the blends of an organometallic polymer Pt-poly-yne, which showed both singlet emission (fluorescence) and triplet emission (phosphorescence), and fullerene (C_{60}), a strong electron acceptor, they found that the phosphorescence was completely quenched by C_{60}, while the fluorescence was just partly quenched. Combining with the results from photocurrent measurement, they concluded that the strongly bounded triplet excitons were dissociated by electron acceptor C_{60}, and their long lifetime facilitated their diffusion to the donor/acceptor interfaces where charge transfer happened. More recently, Guo *et al.*[28] synthesized a UV-blue absorbing Platimum-acetylide polymer (PtTh) which is a triplet material due to strong spin-orbit coupling caused by platinum. The solar cells made by the blends of PtTh and a soluble fullerene derivative 1-(3-methyloxycarbonyl)propyl-phenyl [6,6] C_{61} (PCBM) showed PCE around 0.3%. Photoinduced absorption measurement proved the charge transfer from triplet excited states of PtTh to PCBM.

Shao *et al.* [29]reported a successful fabrication of efficient bilayer-heterojunction solar cells using triplet small molecules. In their work, platinum contained 2,3,7,8,12,13,17,18-octaethyl-21*H*,23*H*-porphineplatinum(II) (PtOEP) was selected for the electron-donating material and C_{60} was used as the electron acceptor. PtOEP is a

phosphorescent material due to its strong SOC. Adjusting the film thickness and annealing conditions led to an OPV with 2.1% power conversion efficiency. Even higher efficiency was expected if the mobility and absorption properties of the triplet materials were improved.

In summary, some researches have been done to harness the energy of triplet excitons in organic solar cells. Elaborate design of device structure and selection of materials that can fully take advantage of both singlet and triplet excited states definitely presents a pathway to higher efficiency of OPVs. To achieve this goal, more systematic study about singlet and triplet photovoltaic processes in OPVs is needed.

1.5 Magnetic Field Effect

There is long history in exploring magnetic field effects (MFE) on the kinetics of chemical reactions.[19, 21] Recently, researchers found some interesting MFE phenomena with organic semiconductors, e.g., magnetic field dependent electroluminescence,[30, 31] magnetoresistance (MR),[32, 33] and magnetic field effect on photocurrent (MFP).[26, 34, 35] The fundamental mechanism of the MFEs results from the interaction of external magnetic field and internal magnetic field associated with the paramagnetic excited states in organic semiconducting materials, such as triplet excitons (s=1), free electrons and holes (s=0.5). Exploring detailed mechanisms needs to analyze all the information from MFE measurement including the magnitude of the magnetic field effect, the sign of the

MFE, and MFE as a function of varying magnetic fields, etc.

1.5.1 Magnetic Field Effect on Photocurrent

It has been found that external magnetic field can change the magnitude and even the sign of photocurrent in organic semiconductors, although they are intrinsically nonmagnetic materials. Magnetic field effect on photocurrent (MFP) was defined as

$$MFP(\%) = \frac{PC_H - PC_0}{PC_0} \times 100\%$$ (Equation 1.5)

where PC_H and PC_0 are the photocurrent of organic devices in magnetic field H and in zero external magnetic field, respectively. Photocurrent is the electric current generated by the excited states of organic semiconductors under photoexcitation. Corresponding to photocurrent, dark current is measured without photoexcitation. Figure 1.10 shows an example of MFP measured from an organic device based on poly[2-methoxy-5-(2'-ethylhexyloxy)-1,4-phenylenevinylene] (MEH-PPV). The MFP consists of two components: a rapid increase in low magnetic field and then a very slow decrease in the range of higher field. The increasing and decreasing components are named as positive and negative MFP, respectively.

1.5.2 General Mechanisms of MFP

Although the mechanisms of MFP in different organic semiconductors haven't been fully understood yet, the general magnetic field effects can be used to study MFP. One of
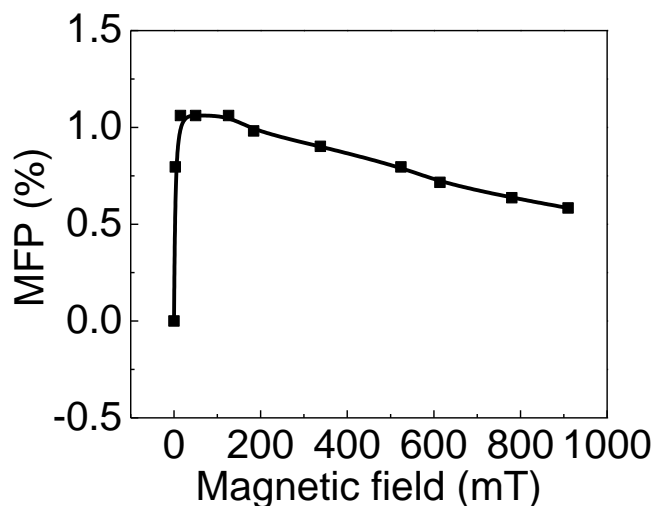
Figure 1.10 Magnetic field effect on photocurrent of ITO/MEH-PPV/Al.

the important effects caused by external magnetic field is Zeeman Effect: a statistic

magnetic field splits the energy levels of three triplet excited states, and consequently

changes the energy gap between singlet and three triplet states. As a result, the ratio of

singlet/triplet is modulated by the external magnetic field because intersystem crossing

based on HFI mechanism largely depends on their energy difference Δ_{S-T}. As shown in

Figure 1.11, in zero magnetic field, the singlet and triplet polaron pairs are nearly in the

same energy level, therefore the singlet and three triplet spin states are fully mixed by

HFI. An external magnetic field splits the T_+ and T_- away from T_0. As a result, the

intersystem crossing between singlet state and T_- and T_+ is suppressed, although the ISC

between singlet and T_0 remains unchanged. Furthermore, the different dissociation (K_S,
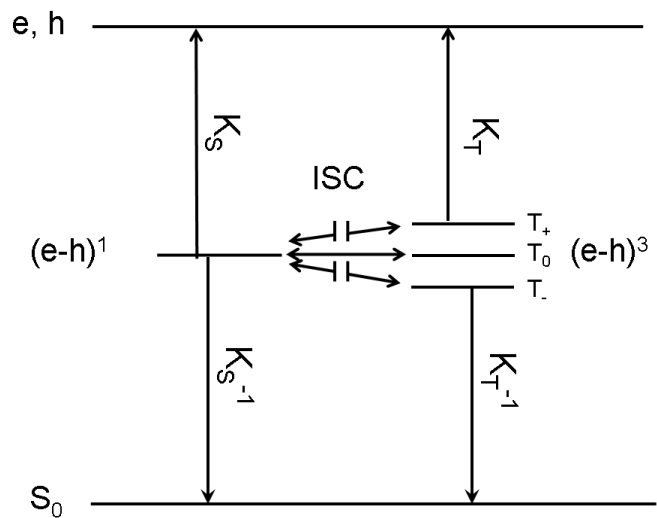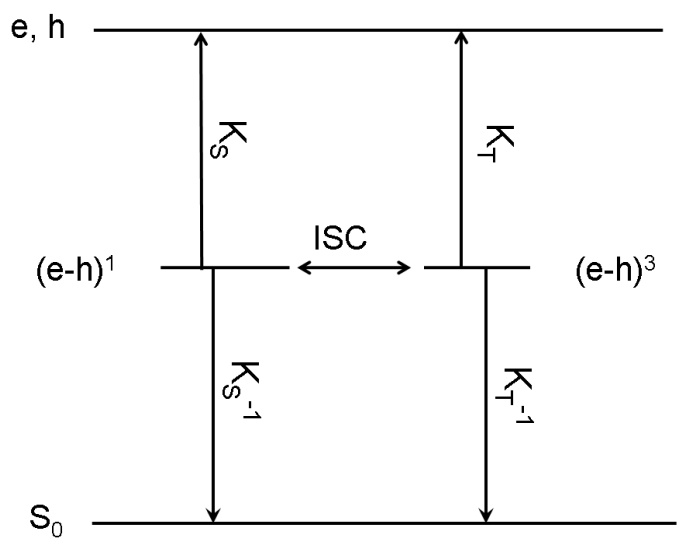
Figure 1.11 Energy diagrams of singlet and triplet polaron pairs in zero magnetic field (a) and in magnetic field H (b). K_S and K_T are the dissociation rate constant of singlet and triplet polaron pairs, K_S^{-1} and K_T^{-1} are the recombination rate constant of singlet and triplet polaron pairs, respectively.

K_T) and recombination (K_S^{-1}, K_T^{-1}) processes between the singlet and triplet states result in their different efficiency of photocurrent generation. So the change of singlet/triplet ratio leads to the change of photocurrent. This explains why the photocurrent of organic semiconductors can be modulated by the external magnetic field.[36]

Another possible mechanism of MFP is the external magnetic field effect on the interactions between the paramagnetic species in the organic materials. The most important paramagnetic interactions in organic solid films are triplet-triplet annihilation (TTA) and triplet-charge reaction (TCR). TTA is the interaction between two triplet excitons (s=1), leading to the generation of a higher energy singlet excited state (S*) and a ground state (S), as shown by equation 1.6.

$$T + T \leftrightarrow (TT) \rightarrow S* + S_0 \qquad \text{(Equation 1.6)}$$
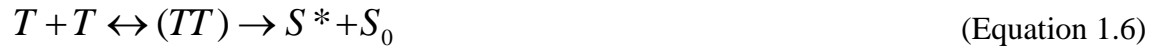
It was known that TTA is sensitive to external magnetic field.[37] As a consequence, the singlet/triplet ratio and photocurrent becomes magnetic field dependent. TCR is the interaction between triplet states and doublet (D) species (free or trapped charges, s=0.5), resulting in the quenching of triplet excited states, and the activation of charge carriers (D*) which directly contributes to photocurrent generation (Equation 1.7).

$$T + D \leftrightarrow (TD) \rightarrow S_0 + D* \qquad \text{(1.7)}$$

Magnetic field is known to reduce the TCR rate constant, and hence change the triplet concentration and free charge carrier density, both of which contribute to the magnetic

field dependent photocurrent.[38, 39]

As reflected from its intrinsic mechanisms, MFP measurement is closely related with the photovoltaic processes of singlet and triplet excited states in organic semiconducting materials. Therefore, it can be potentially utilized as a powerful tool to explore the dissociation, interactions, and recombination processes of the excited states in organic solar cells, based on which we might find new ways to improve the power conversion efficiency of OPVs.

1.5.3 Literature Review about MFP

Utilizing the general principles of magnetic field effects on organic semiconductors, quite a few works have been done to investigate the MFP phenomena shown in different organic materials, including conjugated polymers and small molecules.

Frankevich *et al.*[26, 36, 38] did extensive studies on magnetic field effect on photocurrent in organic devices. They proposed a hyperfine interaction (HFI) mechanism to explain the low field MFP of poly(p-phenylene vinylene) (PPV) and its derivatives.[26, 36] According to HFI mechanism, in polaron pair state where the exchange energy is negligible, the singlet and triplet states are mixed by HFI. External magnetic field can split the degenerated triplet states by Zeeman Effect. As a result, the ISC from singlet polaron pair to triplet polaron pair is reduced. Due to their different recombination rate, the free charge carrier generation, i.e. photocurrent generation, can be modulated by

external magnetic field. The separation distance of the polaron pairs was estimated about 6nm and their lifetime is within the range between 10^{-8}-10^{-9}s. They also presented a triplet-charges reaction (TCR) mechanism to explain the negative MFP in relatively larger magnetic field.[38] They claimed that the interaction between triplet excitons and trapped charges releases the charges from the deep traps and enhance photocurrent. Magnetic field reduces the interaction rate constant, leading to negative MFP. Konarev *et al.* presented a similar mechanism to explain the negative MFP in a series of fullerene complexes.[40]

Kalinowski *et al.*[34] used similar HFI mechanism to explain the low field MFP in organic small molecule tris-(8-hydroxyquinolinato) aluminum (III) (Alq$_3$), but they attributed the positive MFP in low field to the higher dissociation rate of singlet polaron pairs than that of triplet polaron pairs, which differs from the explanation of Frankevich. To explain the negative MFP in high magnetic field, they proposed a level-crossing (LC) mechanism, which applied to the polaron pair state where the exchange energy is not negligible. External Zeeman Effect splits the degenerated triplet polaron pairs and under certain field the energy of singlet state will be in the same level with one of the triplet state, and the intersystem crossing from singlet to triplet will drastically enhanced. But according to this assumption the ISC should be reduced again in the field higher than level-crossing field. Kalinowski explained that the random distribution of separation distance of the polaron pairs in amorphous organic solid state led to a Guassian

distribution of LC field, which accounts for the negative MFP in large magnetic field range.

Ito *et al.* studied the MFP of charge transfer complex based on 1,2,4,5-tetracyanobenzene (TCNB)-doped poly(*N*-vinylcarbazole) (PVK) film.[35] In contrast to the pure PVK film, they observed negative MFP in low field and a positive MFP dip in certain higher field. Although they used similar HFI and LC mechanism to explain the two different MFP components, they attributed the photocurrent generation from triplet CT excitons instead of singlet CT excitons.[41] A hole-hopping model describing the polaron pair formation was also presented in their work.

In summary, most of the works have been focused on investigating the mechanisms of MFP in different organic materials, but there are important issues still need to be further clarified. For example, although the low field MFP has been attributed to the polaron pair state, there is no direct evidence to exclude the involvement of other excited states, such as excitons and CT complexes; there exist different explanations about the negative MFP,   and the true mechanism needs to be elucidated.

1.6 Outline of This Dissertation

From the introduction above, we note that the singlet and triplet excited states experience different photovoltaic processes which affect the power conversion efficiency of organic solar cells. And MFP is potentially a powerful tool to explore the singlet and

triplet photovoltaic processes in organic solar cells. However, the intrinsic mechanism of MFP hasn't been fully understood and thus limits the application of MFP measurement. Based on the research progress in this field, this dissertation was focused on the following issues: (I) Further understanding the physical mechanisms of MFP in organic devices; (II) Applying MFP measurements to study the singlet and triplet photovoltaic processes in organic solar cells; (III) Enhancing PV efficiency of bulk-heterojunction solar cells by controlling singlet and triplet PV processes based on the new findings from MFP measurements.

This dissertation includes seven chapters. Chapter 1 introduces the basic knowledge about organic solar cells, singlet and triplet excited states, magnetic field effect on photocurrent in organic materials, and literature review on MFP, etc. Chapter 2 presents our new understanding of the mechanism of MFP based on MF-modulated ISC in excited states. The magnetic field effect on the three excited states: excitons, CT complexes and polaron pairs, will be investigated individually. The relationship between MFP and the electron-hole separation distance will be addressed. Chapter 3 focuses on illustrating the mechanism of negative MFP component in intermediate and high magnetic field. There are two existing mechanisms: level-crossing (LC) and triplet-charge reaction (TCR), to explain the negative MFP. Our experimental results strongly support the TCR mechanism. In Chapter 4, the application of MFP measurements in studying the dissociation processes of singlet and triplet excitons, which

are the most important excited state in organic semiconductors, is presented. In Chapter 5, MFP measurements are used to investigate the singlet and triplet photovoltaic processes in the most promising bulk-heterojunction solar cells using poly(3-hexylthiophene) (P3HT) and surface-functionalized fullerene 1-(3-methyloxycarbonyl)propyl-1-phenyl [6,6] C_{61} (PCBM) as active materials. The photovoltaic processes and efficiency of the different excited states including excitons, CT complexes and polaron pairs, is studied in bulk-heterojunction cells with different PCBM concentration. The recombination of the charge carriers, which is a limiting factor for higher efficiency in bulk-heterojunction solar cells, is also studied by MFP measurements. Chapter 6 provides an example of improving the efficiency of OPVs by adjusting the singlet/triplet ratio and their photovoltaic processes in bulk-heterojunction solar cells. And the dissertation is summarized in Chapter 7.

CHAPTER 2

MAGNETIC FIELD EFFECT ON THE INTERSYSTEM CROSSING OF PHOTOEXCITED STATES IN ORGANIC SEMICONDUCTORS

2.1 Introduction

Most of the current explanations about magnetic field effect on photocurrent (MFP) of different organic materials are based on a common assumption: magnetic field changes the singlet/triplet ratio of polaron pairs.[34, 36] This assumption relies on the two facts: (I) the dissociation of polaron pairs directly leads to generation of photocurrent. (II) the exchange energy is negligible in polaron pair state because of the long charge separation distance, enabling external magnetic field to modulate intersystem crossing rate. It is theoretically correct, but lacks sufficient experimental evidence. Furthermore, the magnetic field effect on charge transfer (CT) complexes and excitons, which have shorter electron-hole separation distance than polaron pairs, has been rarely addressed in the literatures. In this chapter, magnetic field effect on the intersystem crossing in polaron pairs, excitons, and CT complexes will be investigated individually, providing sufficient experimental evidence to clarify the intrinsic mechanism of MFP in organic semiconducting materials.

2.2 Experimental

Two materials were selected to study the mechanism of MFP: a conjugated polymer poly[2-methoxy-5-(2'-ethylhexyloxy)-1,4-phenylenevinylene] (MEH-PPV) and a surface-functionalized fullerene 1-(3-methyloxycarbonyl)propyl-1-phenyl [6,6] C_{61} (PCBM). Their chemical structures are shown Figure 2.1. MEH-PPV is a well known conjugated polymer that has been used in organic lighting-emitting diodes (OLEDs) and OPVs.[42, 43] The absorption and photoluminescence (PL) spectra are shown in Figure 2.2. PCBM is a strong electron acceptor that has been widely used in organic bulk-heterojunction solar cells.[44]

The procedure of device fabrication includes substrate cleaning, organic film coating, and electrode deposition. Substrates used for device fabrication were half-coated indium-tin-oxide (ITO) glasses. Copper wire contact with the glass and ITO were made using a thermalset silver paste (Figure 2.3a). Then the ITO substrates were cleaned by detergent, deionized water, acetone and chloroform, respectively. MEH-PPV and MEH-PPV:PCBM blends were dissolved into chloroform then spin-coated onto ITO glass using a spin-coater in nitrogen gas filled glove box (Figure 2.3b); Finally, aluminum (Al) electrodes were thermally evaporated onto the organic films in a shadow mask under the vacuum of 2×10^{-6} Torr (Figure 2.3c).

For MFP measurements, organic devices were placed between the two poles of an electromagnet with the light illumination of mono wavelength light through a liquid light

OR

MeO
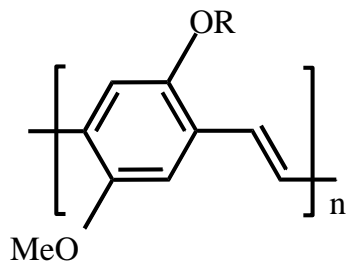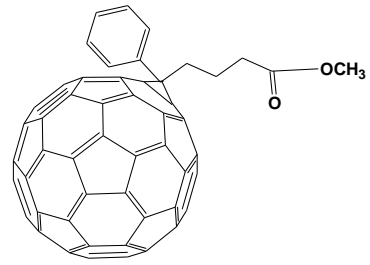
MEH-PPV

PCBM

Figure 2.1 chemical structures of MEH-PPV and PCBM
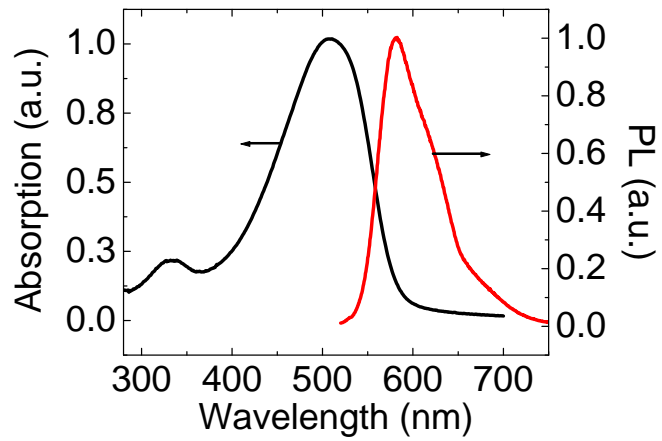
Figure 2.2 PL and Absorption spectra of MEH-PPV.

(a)   (b)   (c)
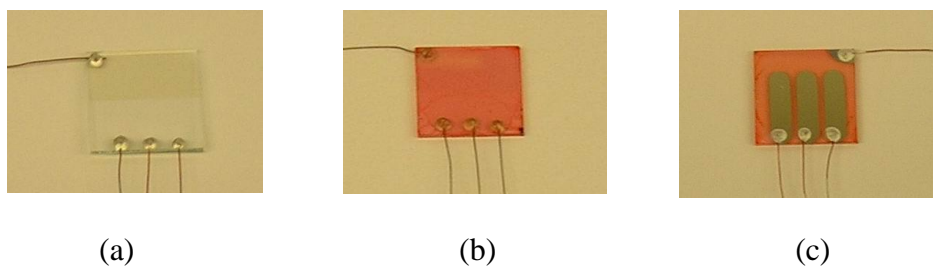
Figure 2.3 ITO glass with copper wire contact (a); A spin-coated MEH-PPV thin film on ITO glass (b); A completed device with the structure of ITO/MEH-PPV/Al (c).

waveguide. The strength of magnetic field were controlled by Sorensen DLM80-7.5 power meter and determined by a Hall-probe gaussmeter placed close to the sample holder. MFP measurements were conducted by monitoring the photocurrent change of the organic devices under different magnetic field using Keithley 2400 sourcemeter. During the measurement, the devices were unbiased or reversely biased to exclude the influence of dark current. The excitation wavelengths were controlled by SPEX Florolog 3 spectrometer. Absorption and emission spectra of organic films were characterized by a Perkin-Elmer Lamda-35 Uv-vis spectrometer and SPEX Florolog 3 spectrometer, respectively.

2.3 Results and Discussion

It is known that photocurrent can be generated by the dissociation and interactions

of excited states including excitons, polaron pairs and CT complexes in organic semiconductors.[45, 46, 47] Therefore, magnetic field effect on photocurrent (MFP) may also originate from these three excited states which coexist in organic semiconductors. To unveil the intrinsic mechanisms of MFP in organic materials, the external magnetic field effect on the intersystem crossing of each of the excited states was investigated.

2.3.1 Magnetic Field Effect on ISC of Excitons

The first photoexcited state in organic semiconductors is singlet exciton, followed by different decay channels, such as intersystem crossing to triplet exciton, dissociation into polaron pairs, and radiative and nonradiative recombination into ground state. Photoluminescence (PL) is a measurable product of radiative recombination of singlet exciton. Therefore, magnetic field effect on PL (MFPL) provides a relatively simple and effective way to investigate MFE on excitons. MFP and MFPL of MEH-PPV are shown in Figure 2.4. MFP comprises an increasing component in low field and a slowly decreasing component in high field. However, no magnetic field effect on PL was observed. MFPL result suggests that the population of singlet excitons is independent on external magnetic field. Therefore, we can conclude that the intersystem crossing between singlet and triplet excitons is unchanged. This result is consistent with the large singlet-triplet energy gap Δ_{S-T} in excitonic state comparing with the small external Zeeman Effect, as shown in Figure 2.5. Hyperfine interaction cannot induce intersystem
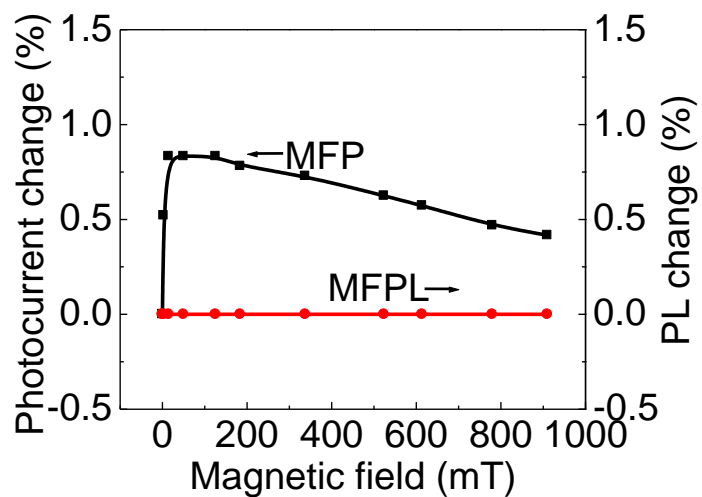
Figure 2.4 Magnetic field effect on photocurrent (MFP) and magnetic field effect on photoluminescence (MFPL) of ITO/MEH-PPV/Al under excitation of light at 500nm.
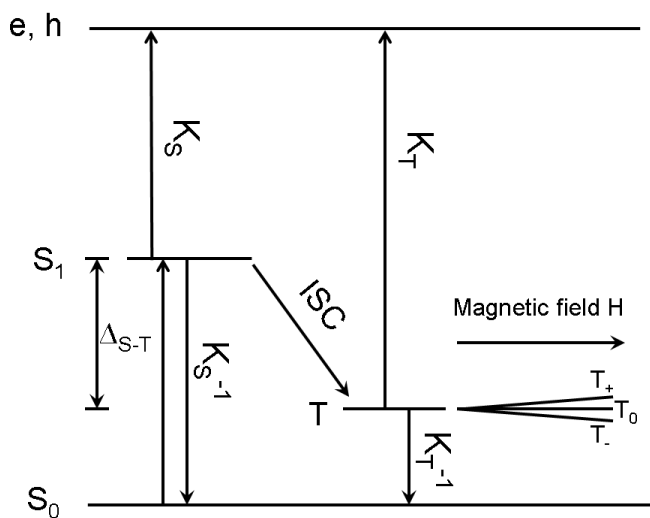
Figure 2.5 Energy level diagrams and photovoltaic processes of singlet and triplet excitons under external magnetic field.

crossing between singlet and triplet excitons. The ISC between singlet and triplet excitons is basically determined by spin-orbit coupling, which is independent process on external magnetic field. Therefore, photocurrent generated by dissociation of excitons is also unaffected by externals magnetic field.

2.3.2 Magnetic Field Effect on ISC of Polaron Pairs

Polaron pairs are non-emissive, and can not be probed by PL measurement. Comparing with excitons, polaron pairs are loosely bounded electron-hole pairs because of their large charge separation distance. Therefore, the dissociation of polaron pairs is much easier than excitons. Small electric field is expected to separate the charges in polaron pair state, and reduce the density of polaron pairs. If MFP does originate from dissociation of polaron pairs, its magnitude should decrease under external electric field. MFP of MEH-PPV under different reverse bias is shown in Figure 2.6. We observe that small electric field can largely change the magnitude of positive MFP. The value of the highest positive MFP decreases from 1.1% under zero bias to 0.35% under 2V. The relative change of MFP is around 70%. While in the same electric field, the PL of MEH-PPV does not show visible change (Figure 2.7), indicating the density of singlet excitons keeps unchanged. Significant quenching of PL in higher electric fields is consistent with the large binding energy of singlet excitons. The different quenching effect of electric field on MFP and PL strongly suggests that the origin of low field MFP
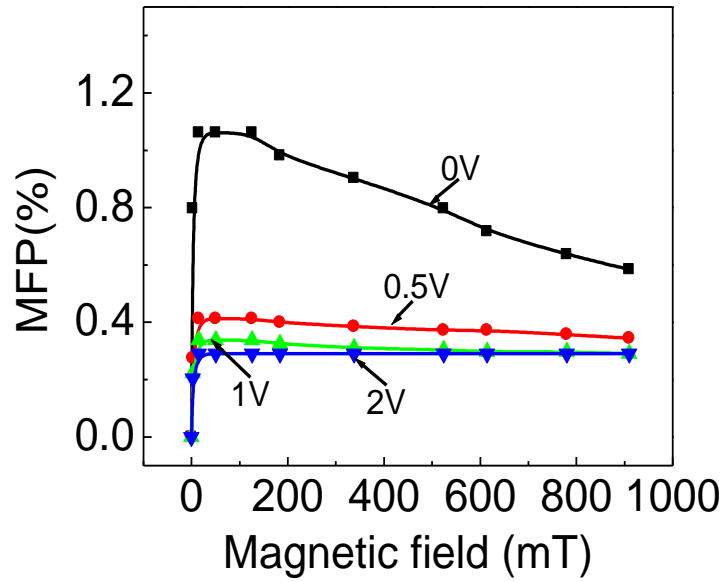
Figure 2.6 MFP of ITO/MEH-PPV/Al under 500nm excitation and different reverse bias.
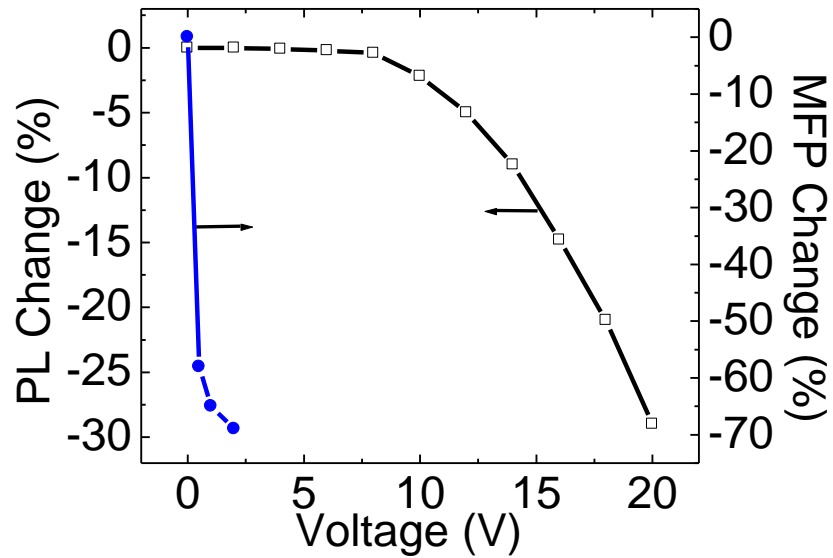
Figure 2.7 Relative change of PL and MFP magnitude under external electric field.

is the dissociation of polaron pairs instead of excitons.

To further confirm that MFP has its origin from polaron pair state, excitation wavelength dependent MFP were measured using the same MEH-PPV sample. It is known that high energy excitation (using short wavelength light), which has photon energy larger than the band gap of organic semiconductors, can direct dissociate excitons with the assistance of excessive photon energy.[48] As a result, high energy excitation can significantly enhance the magnitude of photocurrent by direct dissociation of excitons, which is a MF-independent process as discussed above. Furthermore, the direct dissociation of excitons competes with the thermal-activated dissociation of excitons from which polaron pairs are generated. So the density of polaron pairs is lower under high energy excitation. Combining the above two effects, we can expect that high energy excitation will significantly reduce the magnitude of MFP if it does originate from polaron pairs. The excitation wavelength dependent MFP results are shown in Figure 2.8. We found that the excitations with wavelength longer than 500nm (absorption peak of MEH-PPV) lead to similar MFP response (for clarity only 500nm is shown), while excitations with wavelength shorter than 500nm significantly quench the magnitude of positive MFP. The relative change of the magnitude of positive MFP from 500nm to 350nm is about 80%. This result is consistent with that of electrical field dependent MFP , and further confirms the polaron pair mechanism of MFP in organic semiconductors.

Based on the experimental results shown above, the detailed mechanism of MFP
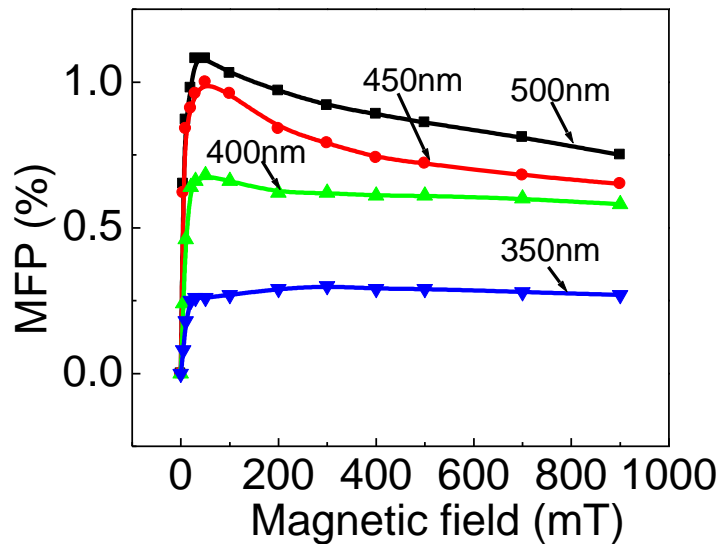
Figure 2.8 MFP curves of ITO/MEH-PPV/Al under different excitation wavelengths.

originated from polaron pairs is proposed as follows. As shown in Figure 2.9, photoexcitation of MEH-PPV leads to formation of singlet excitons (S_1) from which singlet polaron pairs $(e\text{---}h)^1$ are generated. Although small amount of triplet excitons (T) are generated through intersystem crossing (ISC) induced by spin-orbit coupling (SOC),[49] the larger binding energy comparing with the singlet excitons makes their dissociation into triplet polaron pairs $(e\text{---}h)^3$ much more difficult. However, triplet polaron pairs can be generated by ISC from $(e\text{---}h)^1$ which is induced by hyperfine interaction (HFI).[34, 36] Therefore, singlet and triplet polaron pairs coexist in MEH-PPV with dissociation rate K_S, K_T and recombination rate K_S^{-1}, K_T^{-1}, respectively. Because of the negligible exchange energy in polaron pair state, singlet and three triplet states (T_0, T_+, T_-) are fully mixed by
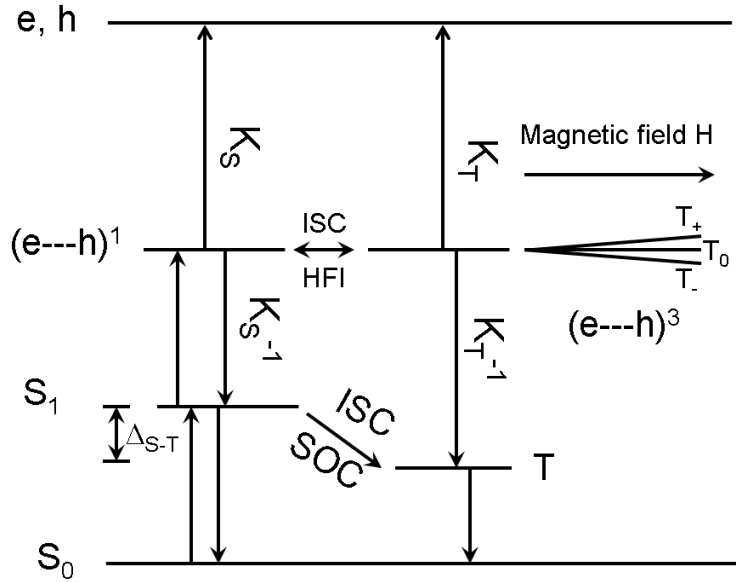
Figure 2.9 Energy level diagrams and photovoltaic processes of singlet and triplet polaron pairs under external magnetic field.

HFI. The singlet/triplet ratio is 1/3. The generation of free electron and hole (e, h), i.e. photocurrent, without external magnetic field can be expressed as:

$$PC_0 = n \bullet \frac{K_S + 3K_T}{K_S + 3K_T + K_S^{-1} + 3K_T^{-1}}$$ (Equation 2.1)

Where n is a constant denoting the total number of singlet polaron pairs evolving from singlet excitons. External magnetic field (H) splits the energy level of three triplet states, resulting in reduced ISC from singlet polaron pair to T_+ and T_-. And consequently the ratio of singlet/triplet in polaron pair state increases. The singlet/triplet ratio becomes 1/1 at magnetic field H where the ISC is completely blocked from singlet polaron pair to T_-

and T_+ states. The photocurrent at field H (PC_H) can be written as

$$PC_H = n \bullet \frac{K_S + K_T}{K_S + K_T + K_S^{-1} + K_T^{-1}}$$
(Equation 2.2)

If the dissociation and recombination rate between singlet and triplet states are different, the change of singlet/triplet ratio will lead to the change of photocurrent. It has been reported that the dissociation rate of singlet polaron pair (K_S) is larger than triplet (K_T) because the relatively stronger ionic nature of singlet states from anti-phase wavefunction configuration allows the singlets to effectively interact with the internal electric field for dissociation.[34, 50] If we assume $K_S \gg K_T$, and singlet and triplet polaron pairs have the same recombination rate ($K_S^{-1} = K_T^{-1} = K^{-1}$) which is generally correct based on the fact that 25% internal quantum efficiency of electroluminescence (EL) can be achieved from fluorescent materials,[51] MFP at magnetic field H is

$$MFP(\%) = \frac{PC_H - PC_0}{PC_0} \times 100\% = \frac{2K^{-1}}{K_S + 2K^{-1}} \times 100\%$$
(Equation 2.3)

According to this mechanism, the MFP should show a increasing component in low magnetic field, then saturate in high field. And the MFP calculated from equation 2.3 is the magnitude of saturated positive MFP achieved based on polaron pair mechanism. However, we note that MFP of MEH-PPV shows a slowly decreasing component in high field which can not be readily explained based on polaron pair mechanism. The mechanism of this negative MFP will be discussed in Chapter 2.

2.3.3 Magnetic Field Effect on ISC of Charge Transfer Complexes

Charge transfer complexes are the intermolecular electron-hole pairs with charge separation distance r longer than intramolecular excitons and shorter than polar pairs. Therefore, they have smaller binding and exchange energy than excitons, but larger than polaron pairs. As an intermediate excited state that widely coexists with excitons and polar pairs, magnetic field effect on CT complexes has been scarcely investigated.[35] In order to identify the MFP from CT complexes state, MEH-PPV was blended with high concentrations of PCBM, which were expected to dissociate all the excitons and polaron pairs, and form CT complexes at the interfaces of MEH-PPV/PCBM. The energy band diagram of MEH-PPV and PCBM is shown in Figure 2.10a. The large energy difference in LUMOs between MEH-PPV and PCBM provides sufficient driving force for exciton dissociation.[52, 53, 54] One the other side, CT complexes are expected to form at the MEH-PPV/PCBM interfaces by the geminate electron-hole pairs which fail to escape the coulomb attraction after exciton dissociation or by mutual capture of counter free charge carriers during their transport to electrodes,[55] as shown in Figure 2.10b.

It was found that high concentrations of PCBM almost completely quench photoluminescence (Figure 2.11) and low field MFP (Figure 2.12) and of MEH-PPV, indicating that PCBM does dissociate both excitons and polaron pairs. And for the samples with high concentrations of PCBM (MEH-PPV:PCBM=1:0.6, 1:4), a positive MFP appears in the magnetic field higher than 150 mT. Since the CT complexes are the
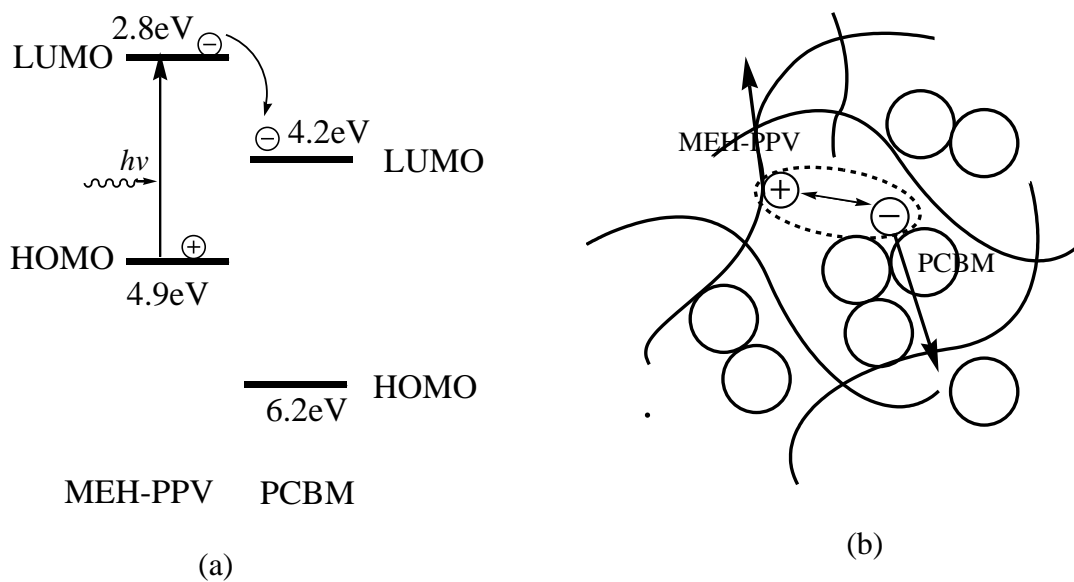
Figure 2.10 Energy band alignment and charge separation at MEH-PPV/PCBM interface

(a), charge transfer complexes formation at MEH-PPV/PCBM interface (b).
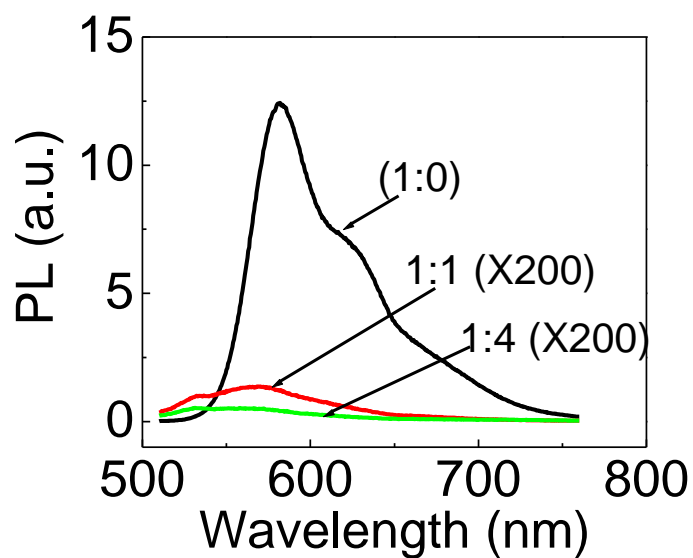
Figure 2.11 Photoluminescence spectra of MEH-PPV, MEH-PPV: PCBM (1:1) and

MEH-PPV:PCBM (1:4).
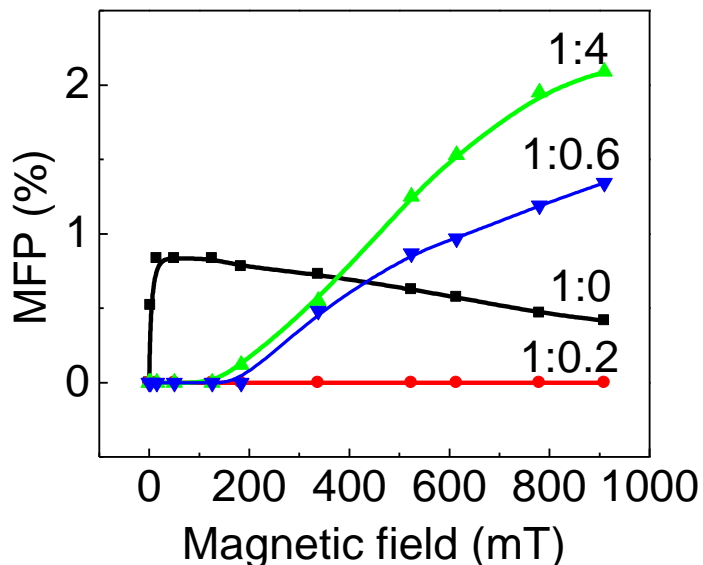
Figure 2.12 MFP curves of ITO/MEH-PPV:PCBM(1:x)/Al excited by 500nm.

only excited state in those samples, it is reasonable to attribute the high-field MFP to the MFE on CT complexes. The high-field MFP does not change with excitation wavelengths, as shown in Figure 2.13. This result further excludes the possibility of its origin from dissociation of polaron pairs, which shows strong dependence on excitation wavelength. The independence of high-field MFP on excitation wavelength can be reasonably explained by the nature of CT complexes. As mentioned above, CT complexes are the product of charge transfer or charge recombination processes at the donor/acceptor interfaces, both of which are not influenced by the excitation photon energy.

According to the intermolecular nature of CT complexes, the mechanism of high-
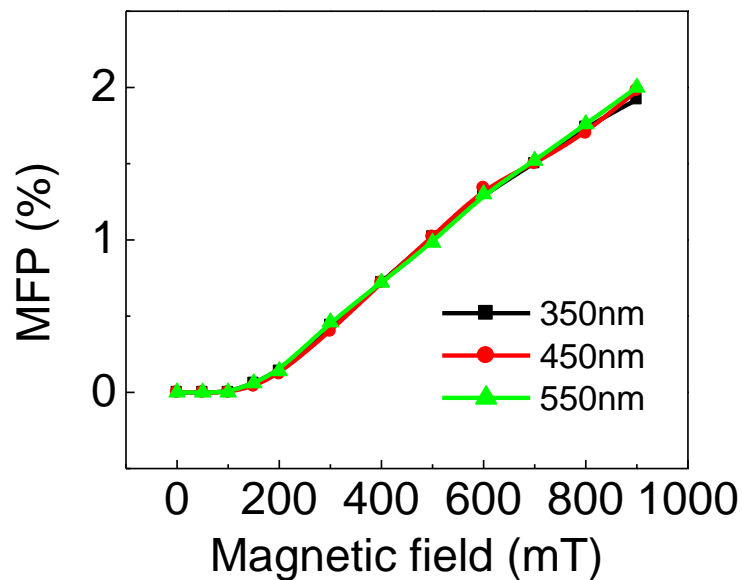
Figure 2.13 MFP curves of ITO/MEH-PPV:PCBM(1:4)/Al under different photoexcitation.

field MFP is proposed using the diagrams shown in Figure 2.14. In MEH-PPV:PCBM devices, photocurrent comes from two processes: direct dissociation of excitons by charge separation which is not sensitive to external magnetic field, and the dissociation of CT complexes which shows magnetic field dependence. The photocurrent comes from the former processes is defined as PC_1, the photocurrent from CT complexes is PC_2. As described above, CT complexes are formed following the photoinduced charge transfer from MEH-PPV to PCBM. Due to the large energy difference (1.4 eV) of the LUMOs between MEH-PPV and PCBM, the energy levels of singlet and triplet CT complexes are

expected to be lower than those of the singlet and triplet excitons, as shown in Figure 2.14. The singlet/triplet ratio of CT complexes depends on the intersystem crossing rate K_{ISC} which are determined by SOC and HFI. SOC is weak in MEH-PPV, and HFI can not induce intersystem crossing because the singlet-triplet energy gap Δ_{S-T} in CT complexes are relatively larger than polaron pairs. Therefore the CT complexes are basically in singlet state in zero external magnetic field. Photocurrent from CT complexes (PC_2) writes as

$$PC_2 = n \bullet \frac{K_S}{K_S + K_S^{-1}}$$ (Equation 2.4)

where n is the total number of singlet charge transfer complexes. As we can see from Figure 2.14, the Δ_{S-T} in CT complexes state is much smaller than the one in exciton state. Therefore, as the external magnetic field split the energy of T_+ away from T_0, Δ_{S-T} between CT^1 and T^+ becomes smaller and at certain point HFI mechanism becomes effective on ISC, and consequently triplet CT complexes are generated. The photocurrent originated from CT complexes becomes:

$$PC_2(H) = n \bullet \left[\frac{(1 - \gamma_T)K_S}{K_S + K_S^{-1}} + \frac{\gamma_T K_T}{K_T + K_T^{-1}} \right]$$ (Equation 2.5)

where γ_T is the triplet yield resulting from intersystem crossing. We note that the direct recombination of triplet CT complexes into singlet ground state is not allowed according to the spin conservation rule. Therefore, it is reasonable to assume $K_T \gg K_T^{-1}$, and Equation 2.4 becomes

e, h

S_1

ISC

K_S K_T

Δ_{S-T} T

CT^1 Magnetic field H

ISC T_+

K_S^{-1} K_T^{-1} T_0 CT^3

T_-

S_0
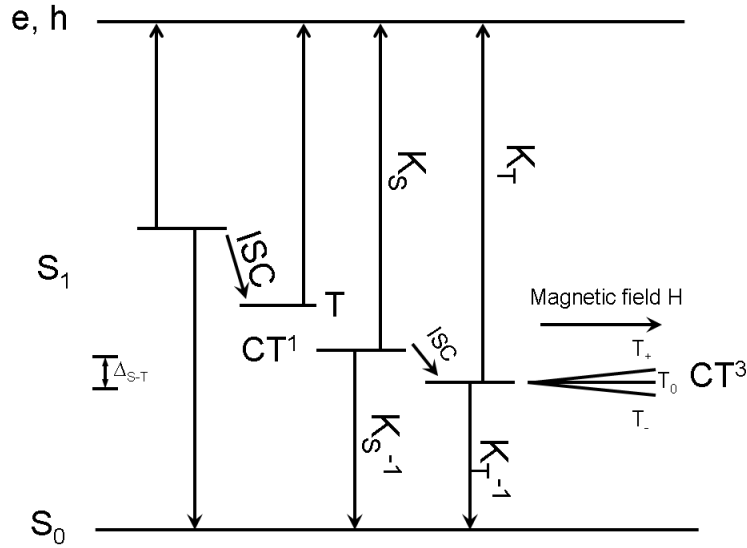
Figure 2.14 Magnetic field effect on energy levels and photovoltaic processes of CT complexes.

$$PC_2(H) = n \bullet \frac{K_S + \gamma_T(K_T K_S + K_T K_S^{-1} - K_S)}{K_S + K_S^{-1}} \qquad \text{(Equation 2.6)}$$

Considering the existence of two component of photocurrent (PC$_1$ and PC$_2$), MFP in MEH-PPV:PCBM should be calculated by

$$MFP(\%) = \frac{PC_2(H) - PC_2}{PC_1 + PC_2} \times 100\% = \frac{\gamma_T\left(K_T K_S + K_T K_S^{-1} - K_S\right)}{PC_1\left(K_S + K_S^{-1}\right)/n + K_S} \times 100\% \qquad (2.7)$$

The Equation 2.7 was used to explain the PCBM concentration dependent MFP result shown in Figure 2.12. There is significant difference in the magnitude of MFP and turn-on magnetic field (H$_0$), the field where start to show MFP, among the samples of

MEH-PPV:PCBM (1:0.2), MEH-PPV:PCBM (1:0.6) and MEH-PPV:PCBM (1:4). MEH-PPV:PCBM (1:0.2) does not show MFP in the whole field range, while MEH-PPV:PCBM (1:0.6) shows lower magnitude and higher turn-on field than MEH-PPV:PCBM (1:4). According to Equation 2.7, the turn-on field should be the point where γ_T start to change. The change of γ_T comes from MF-dependent ISC induced by HFI. From Figure 2.14, we can find out that the energy gap between singlet and triplet CT complexes Δ_{S-T} is the most critical parameter to determine the H_0. At H_0, T_+ is lifted so close to the singlet state of CT complexes that HFI start to induce spin mixing and increase γ_T. Therefore, smaller Δ_{S-T} will lead to lower turn-on field. It is known that Δ_{S-T} is determined by the exchange energy which decreases with the increasing charge separation distance (r) in CT complexes. Following this reasoning, we get to the conclusion that turn-on field is determined by the value of r, i.e., larger r smaller H_0, and vice versa. In MEH-PPV:PCBM (1:0.2), PCBM is uniformly distributed in MEH-PPV matrix, and the holes and electrons are fixed at the MEH-PPV/PCBM interfaces. The charge separation distance r is small and leads to large turn-on field H_0 which is out of the range of our measurement. While in MEH-PPV:PCBM (1:4), PCBM and MEH-PPV form aggregations which facilitate the transport of electrons and holes, respectively.[56] Therefore, electrons and holes are not fixed at the MEH-PPV/PCBM interfaces, and can move around the interfaces. This interface morphology leads to larger average distance r, and lower turn-on field. This also explains why MEH-PPV:PCBM (1:0.6) have H_0

located between the former two samples.

Now we turn to the magnitude of high-field MFP. According to the Equation 2.7, the magnitude of MFP is determined by triplet yield γ_T and the population of singlet CT complexes n and PC_1, the photocurrent generated by direct dissociation of excitons. As discussed above, γ_T is determined by the turn-on field H_0 and charge separation distance r. Larger r leads to lower H_0, and consequently leads to higher γ_T at certain magnetic field strength H. The population or density of CT complexes determines the relative ratio between PC_2 and PC_1, which are magnetic field dependent and independent, respectively. Higher population of CT complexes leads to larger PC_2 and larger MFP. We note that r, n and PC_1 may not be independent parameters, which provide complicated situation for the analyzing of the magnitude of MFP in a specific material system.

We can also use the CT complex mechanism to explain electric field dependent MFP in MEH-PPV:PCBM, shown in Figure 2.15. The samples with different compositions between MEH-PPV and PCBM show different responses of MFP on external electric field. External electric field significantly enhances the magnitude and reduces the turn-on field of MFP in MEH-PPV:PCBM (1:0.2), while does not visually change the MFP from the sample of MEH-PPV:PCBM (1:0.6). For the sample of MEH-PPV:PCBM (1:4), electrical field drastically reduce the magnitude of MFP, but does not change the turn-on field. In general, external electric field has two effects on CT complexes: enlarging the charge separation distance r and reducing the population n by dissociating CT complexes
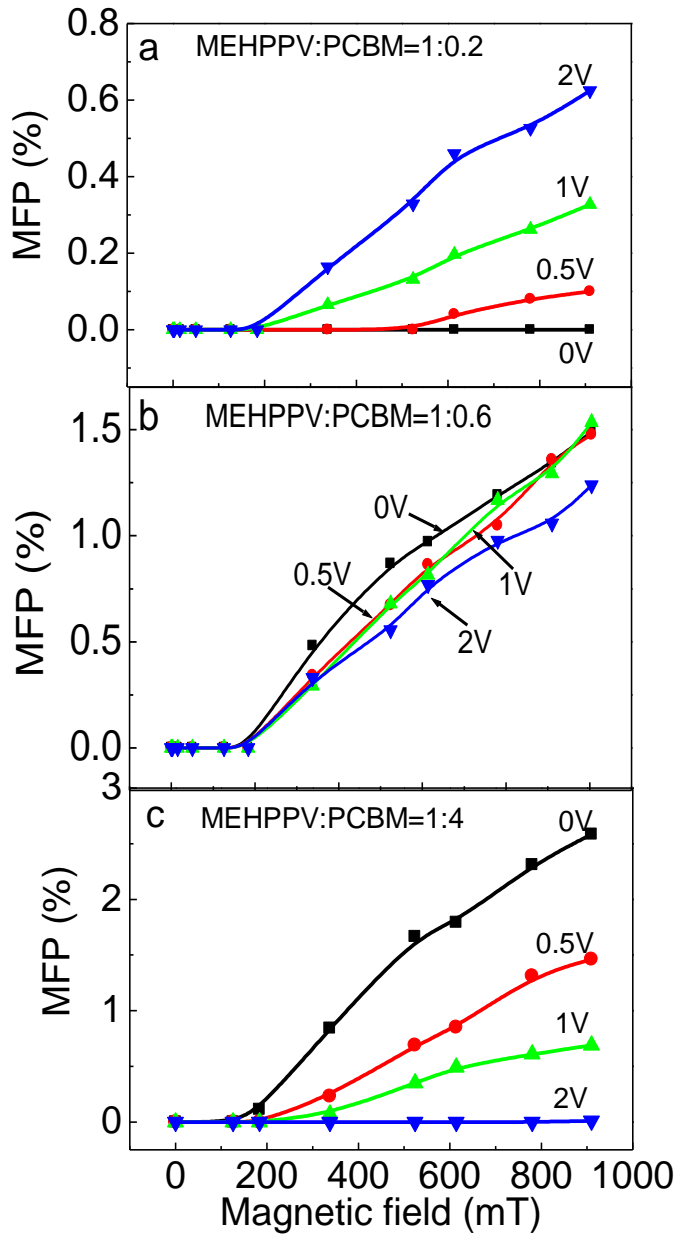
Figure 2.15 Electrical field effect on MFP of ITO/MEH-PPV:PCBM (1:0.2)/Al (a), ITO/MEH-PPV:PCBM (1:0.6)/Al (b), and ITO/MEH-PPV:PCBM (1:4)/Al (c) under photoexcitation at 500nm.

into free electrons and holes. In MEH-PPV:PCBM (1:0.2), the charge separation distance of CT complexes is small and the binding energy is relatively large as we discussed above. Therefore the major effect from small external electric field is enlarging the value of r, leading to lower turn-on field and larger magnitude of MFP. For the sample of MEH-PPV:PCBM (1:4), the large charge separation distance r results in small binding energy between electron-hole pairs. Further enlarging of r by external electric field leads to completely dissociation of CT complexes, and decreases the population n. Consequently, the magnitude of the MFP is reduced. The sample of MEH-PPV:PCBM (1:0.6) has the value of r located between the values of the two previous samples, the two effects from electric field cancel with each other. Therefore the MFP does not show clear dependence on small electrical field. But under higher electric field, the dissociation effect is expected to become predominant and the magnitude of MFP will be quenched. This has been proved by our experiment (the result is not shown here).

2.4 Conclusions

The magnetic field effects on ISC of excitons, polaron pairs and CT complexes have been studied based on MEH-PPV and MEH-PPV:PCBM. MFPL measurement confirmed that external magnetic field does not affect the intersystem crossing in excitonic state due to large Δ_{S-T}. Electric field and excitation wavelength dependent MFP results confirmed that the low field MFP originates from the MF-dependent intersystem crossing in polaron

pair state. Introducing PCBM into MEH-PPV can dissociate all the excitons and polaron

pairs in polymer matrix, providing an opportunity to study the magnetic field effect on

CT complexes. The high-field MFP from MEH-PPV:PCBM was attributed to the

MF-dependent intersystem crossing in CT complexes. The turn-on field of MFP from CT

complexes is determined by the charge separation distance *r*. And the magnitude of

high-field MFP is determined by *r*, the population of CT complexes *n* and the

nonmagnetic photocurrent PC_1.

The essence of the MFP discussed in this chapter is the magnetic field effect on the

intersystem crossing between singlet and triplet excited state. We named it as Type I MFP.

As we mentioned, this mechanism can not explain the negative MFP observed in

MEH-PPV. In the next chapter, we will present the Type II MFP, which originates from

magnetic field effect on triplet-charge reaction, to explain the mechanism of negative

MFP.

CHAPTER 3

MAGNETIC FIELD EFFECT ON TRIPLET-CHARGE REACTION IN ORGANIC SOLID FILMS

3.1 Introduction

In principle, there are two types of magnetic field effects on organic semiconductors: MFE on the intersystem crossing between singlet and triplet excited states (Type I),[34, 36] and MFE on the interactions between paramagnetic excited states (Type II).[39, 57] In the field on MFP, most of the research was focused on Type I MFP, which has been discussed in Chapter 2. However, the negative MFP component in MEH-PPV can not be explained by the Type I mechanism, providing the necessity to investigate Type II MFP. The most important paramagnetic interactions in organic solid films are triplet-triplet annihilation (TTA) and triplet-charge reaction (TCR). TTA is the interaction between two triplet excitons (s=1), leading to the generation of a higher energy singlet excited state (S*) and a ground state (S); TCR is the interaction between triplet states and doublet (D) species (free or trapped charges, s=0.5), resulting in the quenching of triplet excited states and the activation of charge carriers (D*) which directly contributes to photocurrent generation. In this chapter, MFE on TCR will be investigated to explain the negative MFP which widely exists in most of the organic semiconducting materials.

3.2 Experimental

The materials used in this work include MEH-PPV, PCBM, poly(3-hexylthiophene) (P3HT), poly(9,9-dioctylfluorenyl-2,7-diyl) (PFO), *fac* tris (2-phenylpyridine) iridium (Ir(ppy)$_3$), Iridium (III) tris(2-(4-totyl)pyridinato-N,C^2) (Ir(mppy)$_3$), Bis(2-(9,9-dibutylfluorenyl)-1-isoquinoline(acetylacetonate) (DFIr) tris-(8-hydroxylquinoline) aluminum (Alq$_3$), their chemical structures are shown Figure 3.1.

The procedure of device fabrication is similar to what has been described in the Chapter 2. The polymer films were deposited by spin-coating, and the small molecule films were deposited by vacuum evaporation. MFP, absorption and PL spectra were measured as described in Chapter 2. The photocurrent (PC) spectra of the organic devices were measured by recording the short circuit current of the samples illuminated by mono-wavelength light illumination selected from SPEX Florolog 3 spectrometer. For electroluminescence (EL) spectra measurement, the devices were put in liquid nitrogen gas and the EL was collected by a liquid light guide to the Florolog 3 spectrometer.

3.3 Results and Discussion

The MFP of a series of organic materials including small molecules and conjugated polymers were measured and the results are shown in Figure 3.2. In general, there are three types of MFP curves. PFO shows the first types of MFP which includes a sharp

PFO   P3HT   Alq₃

Ir(ppy)₃   Ir(mppy)₃   DFIr
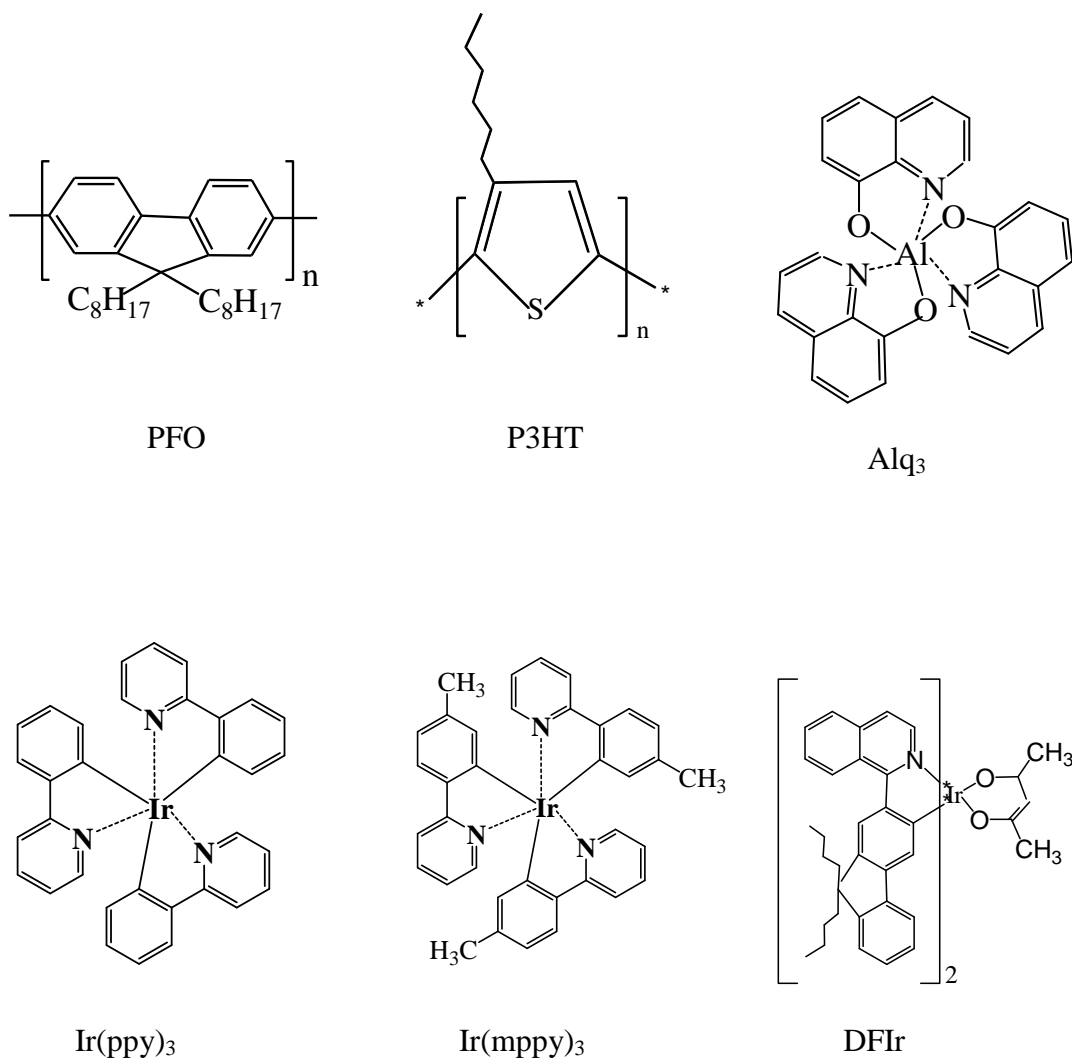
Figure 3.1 Chemical structure of PFO, P3HT, Alq₃, Ir(ppy)₃, Ir(mppy)₃, and DFIr.
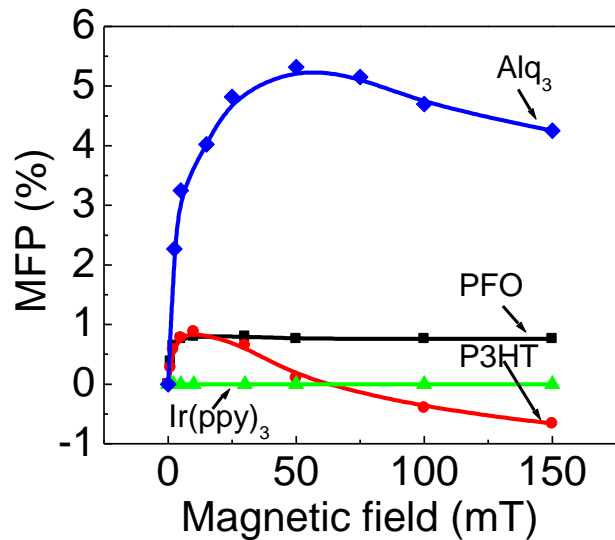
Figure 3.2 Magnetic field effect on photocurrent of PFO, P3HT, Alq_3, $Ir(ppy)_3$ measured in the device structure of ITO/organic material/Al.

increasing component in low field, and a saturated component in higher field. Most of the materials such as MEH-PPV, P3HT, Alq_3, shows the second type of MFP which includes an increasing component in low field followed by a decreasing component in higher field. The magnitude of the decreasing component varies among the materials. For example, MEH-PPV just shows a slightly decreasing response as shown in previous chapter, while P3HT shows much significant negative component. The Iridium dyes including $Ir(ppy)_3$, $Ir(mppy)_3$, and DFIr present the third kind of MFP, which has neither increasing nor decreasing components.

3.3.1 Level Crossing and Triplet-Charge Reaction

One of the distinct differences among these materials is the ratios of singlet/triplet excitons. It is known that the heavy atoms can significant enhance SOC in organic materials. PFO comprises of only light elements carbon and hydrogen, and therefore has very weak SOC and the triplet yield was reported lower than 1%.[49] Alq_3 has Aluminum linked with carbon hydrogen group and has slightly higher SOC than PFO. The triplet yield has been reported about 20% in Alq_3.[24] P3HT contains heavy atom Sulphur, and triplet yield is about 70% in liquid.[49] $Ir(ppy)_3$ has been reported to have 100% intersystem crossing due to the heavy atom Iridium.[58] By comparing the MFP of PFO, Alq_3 and P3HT, we observe that the magnitude of the negative MFP component increases with triplet density. Therefore, it is reasonable to assume that the negative component of MFP is from MFE on triplet-charge reaction. The triplet-charge reaction can be dependent of magnetic field if the triplet exciton ratio or reaction rate constant is magnetically modified. The absence of magnetic field effect on PL suggests that the negative component in the magnetic field effects of photocurrent can be attributed to field-dependent reaction rate constant. In principle, a magnetic field can decrease the reaction rate constant by removing the degeneracy or reducing triplet mobility due to external Zeeman splitting.[59] As a result, the magnetic field effects on photocurrent contain both positive and negative components based on the dissociation of polaron pairs and the triplet-charge reaction. On contrast, we also noted that the positive and negative

magnetic field effects of photocurrent can be also attributed to level-crossing between singlet and triplet polaron-pair states.[34, 35] Specifically, the external Zeeman splitting can cause an intersect point between singlet and triplet (m=-1) levels, leading to a level-crossing in polaron-pair states. As a consequence, the intersystem crossing rate becomes increasing and decreasing, respectively, when the singlet and triplet (m=-1) levels move towards and away from the level-crossing point as applied magnetic field continuously increases. This non-monotonic change in intersystem crossing rate can yield an increase and decrease in the photocurrent due to the different dissociation rates between singlet and triplet polaron pairs.   Nevertheless, an external magnetic field can have both positive and negative effects on photocurrent in organic semiconductors, although the two possible mechanisms: (I) level-crossing and (II) dissociation and triplet-charge reaction, still remain controversial.

3.3.2 Effect of Triplet Ratio on Negative MFP

To clarify the true mechanism of negative MFP, The effect of triplet ratio on MFP was investigated by continuously adjusting triplet exciton density in PFO. Two particular materials: phosphorescent $Ir(ppy)_3$[60] and fluorescent Alq_3[61] molecules, which have similar electronic levels, were selected to uniformly disperse into organic semiconducting polymer PFO matrix, respectively. The uniform molecular dispersion can be obtained in the PFO matrix up to 5 wt% for the $Ir(ppy)_3$ and Alq_3.[62] In general, dispersing molecules

can cause three possible consequences: tuning of singlet-to-triplet exciton ratio by energy transfer, modification of spin-orbit coupling by intermolecular magnetic interaction, and dissociation of bound electron-hole pairs at polymer/molecule interface. Most importantly, the dispersed $Ir(ppy)_3$ can significantly increase the triplet exciton ratio in the PFO matrix under photoexcitation.[63, 64] The increase of triplet excitons is established by three processes: (I) the efficient Förster process transfers the photoexcited singlet excitons from PFO to $Ir(ppy)_3$ due to the spectral overlap between PFO emission and $Ir(ppy)_3$ absorption and the close physical contacts between the PFO chains and $Ir(ppy)_3$ molecules; (II) the near 100% intersystem crossing coverts the singlets into triplets in excitonic states in the $Ir(ppy)_3$ molecules due to strong spin-orbit coupling; (III) the Dexter process transfers the triplet excitons from the $Ir(ppy)_3$ molecules back to the PFO chains due to the triplet energy difference and sufficient intermolecular PFO-$Ir(ppy)_3$ contact (Figure 3.3a). The efficient Dexter energy transfer is supported by the absence of phosphorescence emission from $Ir(ppy)_3$ in PFO:$Ir(ppy)_3$ (Figure 3.3b). On contrast, in the PFO+Alq_3 system the singlet excitons can not be sufficiently converted into triplet excitons in the dispersed Alq_3 molecules due to insignificant intersystem crossing after the Förster transfer from the PFO matrix to the Alq_3 dopants, and lacking backward Dexter energy transfer (Figure 3.4a). As a result, the fluorescence emission from Alq_3 (500nm) is observed in the PL spectra of PFO:Alq_3 (Figure 3.4b). Therefore, dispersing Alq_3 does not increase the triplet exciton ratio in the PFO matrix.
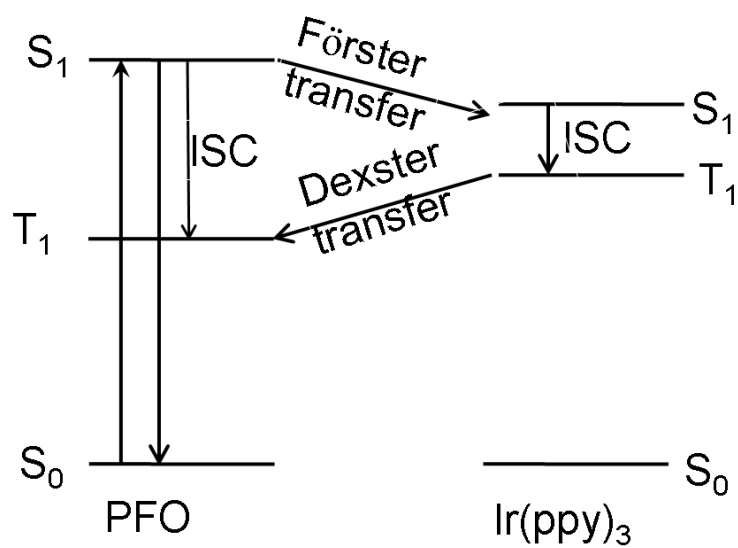
(a)
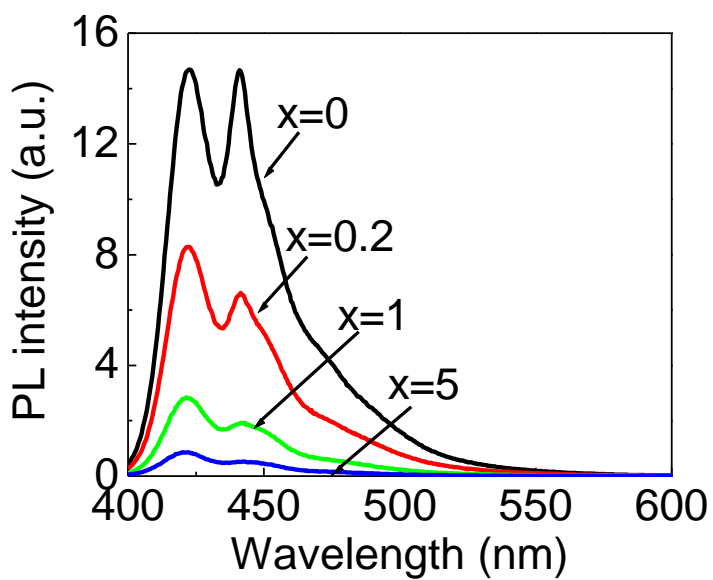
(b)

Figure 3.3 Energy transfer processes in PFO:Ir(ppy)$_3$(a) and PL spectra of PFO:x%Ir(ppy)$_3$ (b).
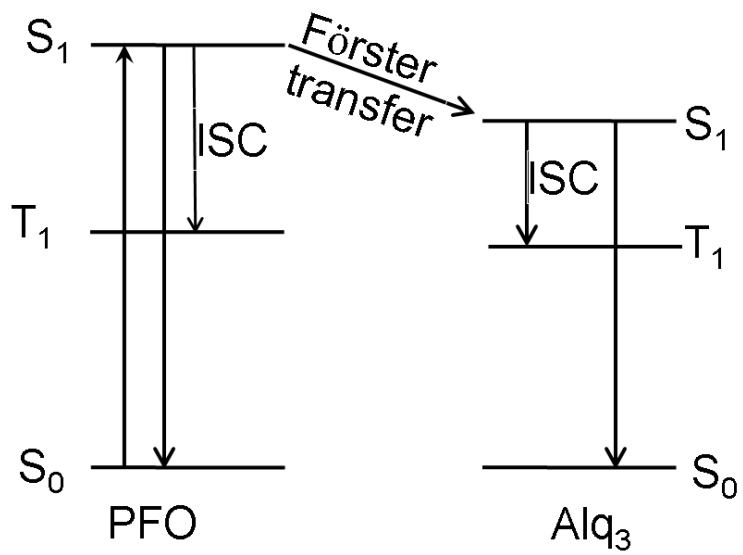
(a)
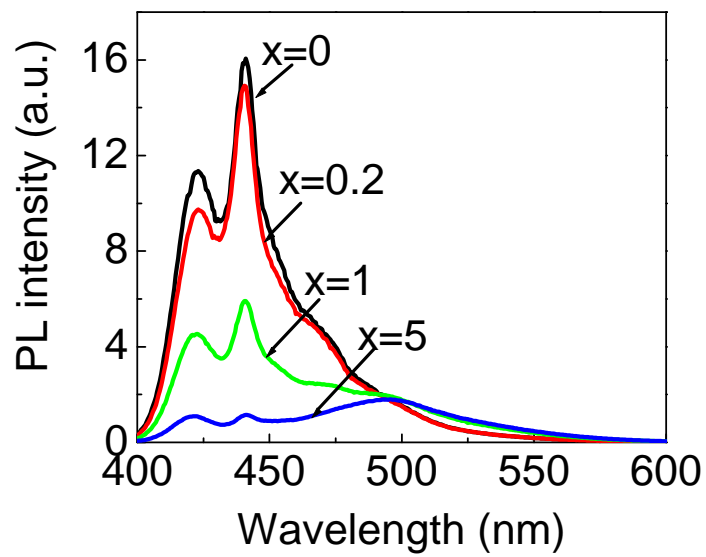
(b)

Figure 3.4 Energy transfer processes in PFO:Alq$_3$(a) and PL spectra of PFO:x%Alq$_3$ (b).

Figure 3.5a shows that dispersing the Ir(ppy)$_3$ molecules causes two appreciable changes: introducing a negative component and decreasing the positive component in the magnetic field effects on photocurrent in the PFO+Ir(ppy)$_3$ system. However, in the PFO+Alq$_3$ system the magnetic field effects on photocurrent remain approximately unchanged with the Alq$_3$ dispersion (Figure 3.5b) The comparison between PFO+Ir(ppy)$_3$ and PFO+Alq$_3$ systems clearly suggests that introducing triplet excitons yields a negative component in magnetic field effects on photocurrent. It can be thus assumed that the negative MFP comes from triplet exciton-charge reaction.

It is known that triplet-charge reaction (TCR) results in quenching of triplet excitons and activation of trapped charges (Equation 1.7). Therefore, TCR contributes to the photocurrent generation in organic materials. The photocurrent spectra of ITO/PFO:x%Ir(ppy)$_3$/Al and ITO/PFO:x%Alq$_3$/Al are shown in Figure 3.6a and 3.6b, respectively. We observe that doping of Ir(ppy)$_3$ significantly enhances the photocurrent in PFO, while doping of Alq$_3$ reduces the PC in PFO. The enhancement of PC by Ir(ppy)$_3$ strongly supports the TCR mechanism in PFO: Ir(ppy)$_3$. The reduction of PC in PFO:Alq$_3$ can be attributed to the exciton trapping effect from Alq$_3$ molecules.

3.3.3 The Effect of Charge Density on Negative MFP

The mechanism of negative MFP has been attributed to triplet-charge reaction because the tuning of the ratio of singlet/triplet excitons can control the magnitude of
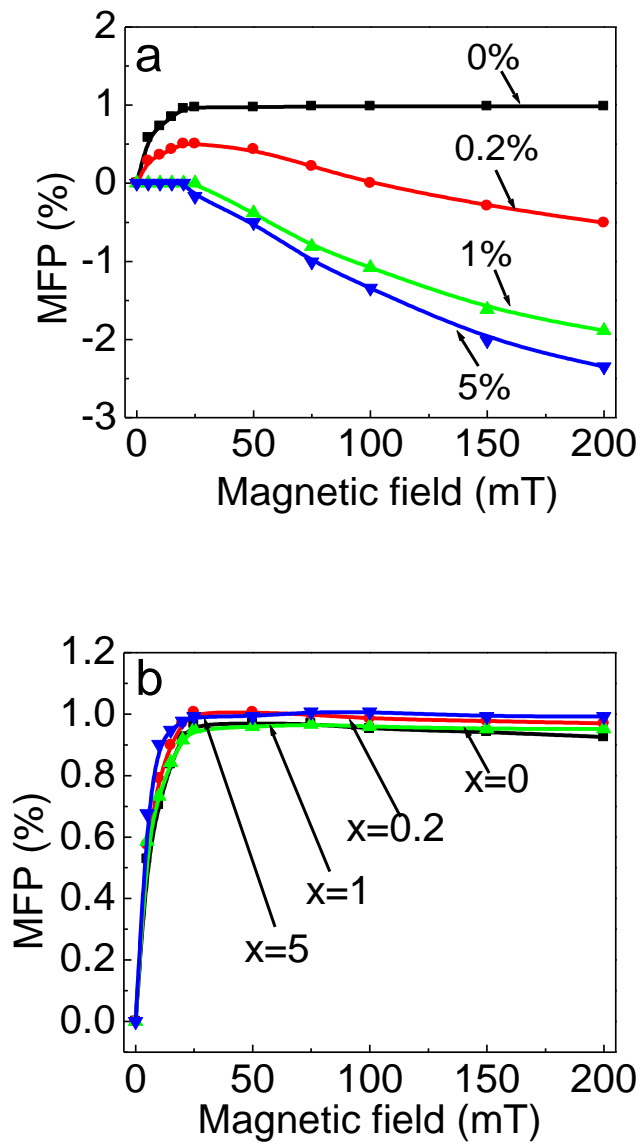
Figure 3.5 MFP of ITO/PFO:x%Ir(ppy)$_3$/Al (a) and ITO/PFO:x%Alq$_3$/Al (b) under 400nm photoexcitation.
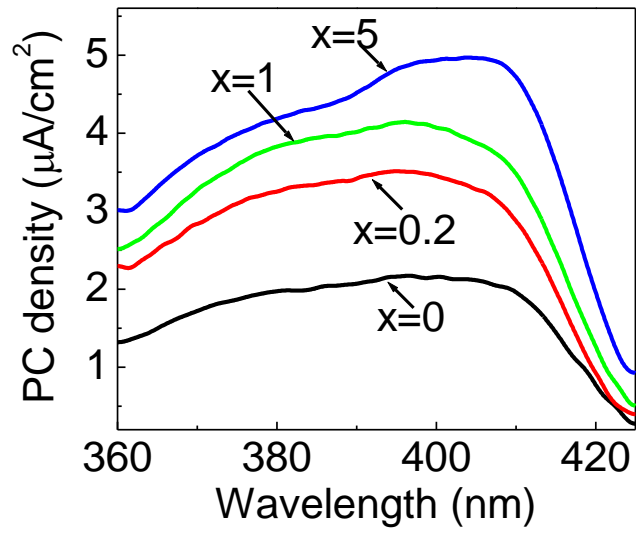
(a)
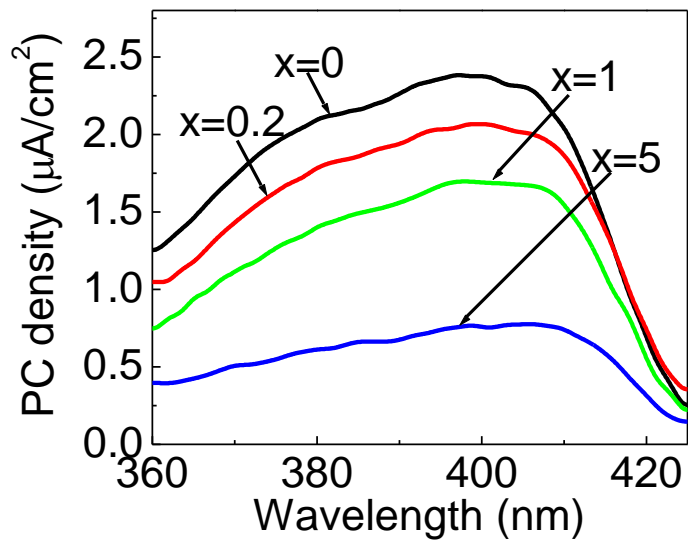
(b)

Figure 3.6 PC spectra of ITO/PFO:x%Ir(ppy)$_3$/Al (a) and ITO/PFO:x%Alq$_3$/Al (b).

negative MFP. However, triplet-charge reaction involves triplet excitons and trapped charges, either of which can lead to the change of TCR. To further confirm the TCR mechanism of negative MFP, the effect of trapped charge needs to be investigated.

To control the density of trapped charge, low concentrations of PCBM was dispersed into the MEH-PPV matrix. As discussed in the Chapter 2, the strong electron accepting character enables PCBM to dissociate all the excited states in MEH-PPV. However, low concentrations of PCBM are supposed to dissociate small amount of excited states, and due to the isolated distribution of PCBM the dissociated electrons and holes are randomly trapped in PCBM and MEH-PPV, respectively (Figure 3.7). As a result, the density of trapped charges can be increased by doping of PCBM, and thus the TCR is enhanced. However, it needs to be noted that the control of doping concentration of PCBM is critical to get enhanced TCR, because increasing concentration of PCBM can dissociate triplet excitons leading to reduced TCR. The MFPs of MEH-PPV doped with low concentrations of PCBM are shown in Figure 3.8. Low doping of PCBM enhances the negative MFP of MEH-PPV. This result strong supports the TCR mechanism of negative MFP.

3.3.4 SOC Effect on MFP

By investigating the dependence of MFP on the density of triplet excitons and trapped charges, the origin of the negative MFP has been determined as the triplet-charge
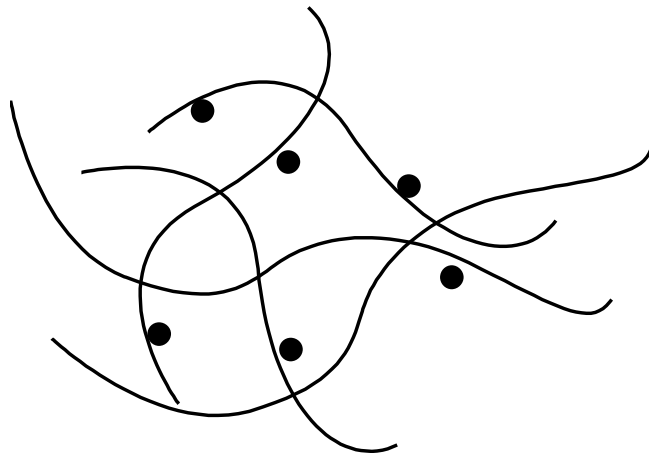
Figure 3.7 Schematic representation of charge trapping in MEH-PPV:PCBM.
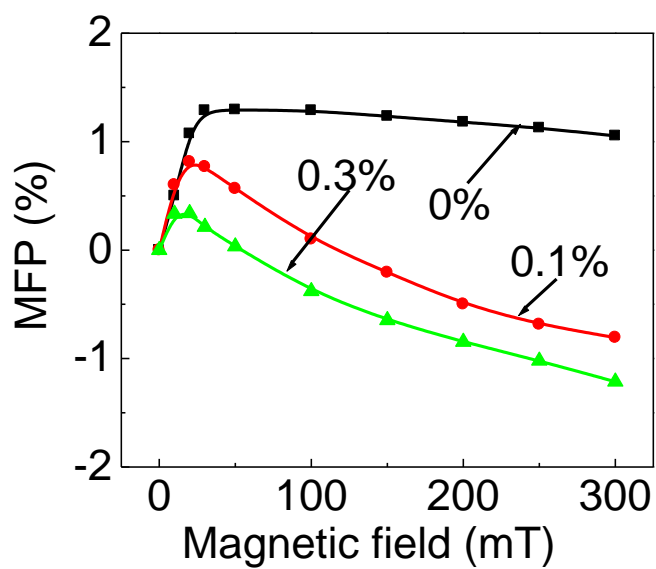
Figure 3.8 MFP of ITO/MEH-PPV:x%PCBM/Al under photoexcitation at 500nm.

reaction. According to Merrifield,[39] the reaction of a triplet exciton (s=1) and a trapped

charge (s=1/2) generates an intermediate doublet-quartet mixtures which has six spin

states. There are two outcomes from the mixture states: spin-independent triplet back

scattering, and spin-dependent triplet quenching. The quenching of the triplet exciton

involves a transition from the intermediate spin state to a purely doublet state:

$$T + D \underset{K^{-1}}{\overset{K}{\rightleftarrows}} (TD) \xrightarrow{K_l} S_0 + D \qquad \text{(Equation 3.1)}$$

where K is collision rate of triplet and doublet species, K^{-1} is the back scattering rate, K_l

is the triplet quenching rate of the l-th spin states of the intermediate complex (TD).

Therefore, the total quenching rate of triplet excitons Q is:

$$Q = \frac{1}{6} K \sum_{l=1}^{6} \frac{K_l}{K^{-1} + K_l} \qquad \text{(Equation 3.2)}$$

The value of Q has a maximum when the doublet component is uniformly distributed

over all six intermediate spin states. And the minimum of Q occurs when the intermediate

state comprises completely separated doublet and quartet. In zero magnetic field (ZMF),

the doublet is uniformly distributed and the quenching rate is maximal. With the

increasing of the external magnetic field, Zeeman splitting increases and the doublet

component gradually concentrates on four states and the value of Q decrease.[65]

Therefore, external magnetic field reduces the net rate constant of triplet-charge reaction

and consequently reduces the generation of free charge carriers, leading to negative MFP.

Now it turns to the question of what parameters affect the MFE on the TCR rate constant. By investigating the MFP in PFO+Iridium dyes, we found that SOC plays important role in determining MFE on the rate constant of TCR. Figure 3.9 shows the MFPs in PFO blended with different concentrations of $Ir(mppy)_3$, a green Iridium dye having energy level similar to $Ir(ppy)_3$ but having better solubility in organic solvents. Similar to $Ir(ppy)_3$, doping of $Ir(mppy)_3$ introduced significant negative MFP in PFO, which can be attributed to the enhanced TCR in PFO due to the increased triplet density achieved through the energy transfer processes shown in Figure 3.3a. The stronger negative MFP in PFO:5%$Ir(mppy)_3$ than PFO:0.2%$Ir(mppy)_3$ is consistent with its higher triplet density. However, we observe that the saturation field of the negative MFP in PFO:5%$Ir(mppy)_3$ is lower than PFO:0.2%$Ir(mppy)_3$ which has its negative MFP extended to more than 900 mT.

It needs to be noted that the strength of negative MFP reflects the strength of TCR, while the saturation field reflects the MFE on TCR rate constant. The different MFE on TCR rate constant between PFO:5%$Ir(mppy)_3$ and PFO:0.2%$Ir(mppy)_3$ can be attributed to their difference in spin-orbit coupling strength, which is supported by the EL spectra measured in liquid nitrogen gas, shown in Figure 3.10. It is known that the injected charge carriers form polaron pairs with singlet/triplet ratio 1:3 in EL devices. So the difference in singlet/triplet ratio of the excited states is not significant among PFO, PFO:0.2%$Ir(mppy)_3$ and PFO:5%$Ir(mppy)_3$ under electric field excitation. But we found
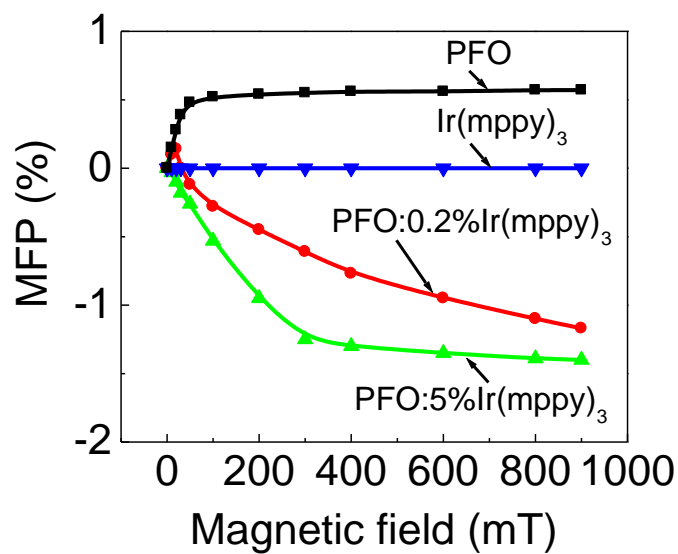
Figure 3.9 Magnetic field effect on photocurrent of PFO, Ir(mppy)$_3$, PFO:0.2%Ir(mppy)$_3$

and PFO:5%Ir(mppy)$_3$ in the device structure of ITO/organic material/Al.
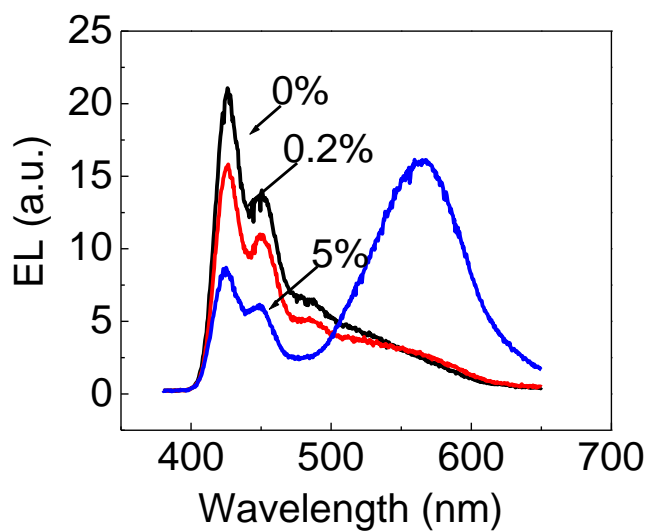
Figure 3.10 EL spectra of PFO, PFO:0.2%Ir(mppy)$_3$ and PFO:5%Ir(mppy)$_3$ in the device

structure of ITO/organic materials/Al.

that the EL spectra show distinct difference among these samples. In addition to the PFO

fluorescent emission peaks (400nm-460nm), the EL spectra of PFO:5%Ir(mppy)$_3$ shows

a new peak in 580nm which can be assigned to the phosphorescence of PFO.[66, 67]   The

existence of phosphorescence in PFO:5%Ir(mppy)$_3$ indicates stronger SOC in the this

sample than PFO:0.2%Ir(mppy)$_3$. Therefore, SOC has two effects on the negative MFP in

PFO. On the one side, SOC can increase the triplet ratio and consequently enhance the

negative MFP. On the other side, SOC reduce MFE on TCR rate constant which will lead

to quenching of negative MFP. The quenching effect of SOC on MFP might be due to the

enhanced spin-lattice relaxation, which destroys the spin-coherency in the excited

states.[21] This might be the same reason for the absence of positive MFP in strong

spin-orbit coupling such as Ir(ppy)$_3$ and Ir(mppy)$_3$.

Figure   3.11   shows   the   MFPs   of   PFO:0.5%PCBM,

PFO:0.2%Ir(mppy)$_3$:0.5%PCBM and PFO:5%Ir(mppy)$_3$:0.5%PCBM. We observe that

PCBM removes the positive MFP in PFO and PFO: Ir(mppy)$_3$ due to its dissociation

effect on polaron pairs. Only negative MFP can be observed in these samples,

simplifying the comparison of negative MFP among different samples. Similar

dependence of the saturation field on the concentration of Ir(mppy)$_3$ has been observed in

PCBM doped samples. This result further demonstrates that SOC plays an important role

in determining the MFE on the rate constant of TCR.
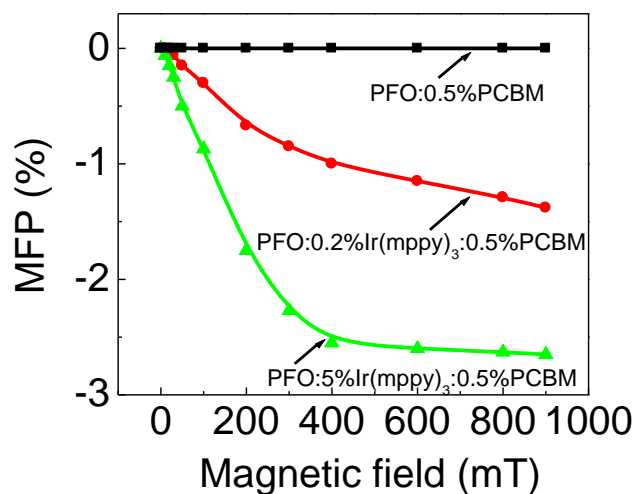
Figure 3.11 Magnetic field effect on photocurrent of PFO:0.5%PCBM, PFO:0.2%Ir(mppy)$_3$:0.5%PCBM and PFO:5%Ir(mppy)$_3$:0.5%PCBM in the device structure of ITO/organic materials/Al.

3.4 Conclusions

The magnitude of the negative MFP in PFO has been enhanced by tuning the triplet ratio in PFO using phosphorescent Iridium dyes as dopants. And the negative MFP in MEH-PPV has been enhanced by increasing the density of trapped charges using low doping of PCBM. Based on these results, the mechanism of the negative MFP, which can be observed in most of the organic semiconductors, has been determined as magnetic field effect on triplet-charge reaction. It has been further investigated that spin-orbit coupling strength is important parameter in determining the magnetic field effect on the rate constant of triplet-charge reaction.

CHAPTER 4

DISSOCIATION PROCESSES OF SINGLET AND TRIPLET EXCITONS IN SINGLE-LAYER ORGANIC PHOTOVOLTAIC CELLS

4.1 Introduction

Since last decade fluorescent organic materials have been heavily used in both bilayer- and bulk-heterojunction PV cells. It is known that an organic PV response is determined by three processes: light absorption, exciton formation and dissociation, and charge collection. The PV efficiencies have been continuously improved by controlling these dynamic processes of singlet excitons.[12, 14, 15, 52, 68, 69] It should be noted that the singlet exciton generated by light absorption can be partially converted into triplet excitons due to hyperfine interaction and spin-orbit coupling, leading to both singlet and triplet excited states in organic molecules.[70] As compared to the singlet excitons, the triplet excitons exhibit high binding energy and long life time. Therefore, the triplet excitons may impact the PV process in organic solar cells.[27, 28, 29, 71] In this chapter, the dissociation processes of singlet and triplet exciton were investigated based on organic PV cells prepared by two organic materials: fluorescent Alq_3 and phosphorescent $Ir(ppy)_3$ dye molecules with mutually similar electronic parameters.

4.2 Experimental

The fluorescent Alq_3 and phosphorescent $Ir(ppy)_3$ used in this research were purchased from Aldrich and American Dye Sources Inc., with the melting temperatures of 415 °C and 447 °C, respectively. The LUMO (lowest unoccupied orbital) and HOMO (highest occupied orbital) are 3.2 eV and 5.7 eV for Alq_3 [61] and 3.0 eV and 5.4 eV for $Ir(ppy)_3$.[60] The organic molecular thin films were deposited with evaporation rate of 0.2 nm/s at their melting temperatures under the vacuum of $2x10^{-6}$ Torr onto the precleaned indium tin oxide (ITO) glass substrates. The organic PV cells were then fabricated by evaporating semitransparent aluminum (Al) metal electrode on the organic thin films, forming the device architecture of ITO/dye/Al. The light illumination of 8 mW/cm^2 was obtained from a xenon lamp with a mono wavelength ranging from 300 nm to 600 nm for the photocurrent measurements.

4.3 Results and Discussion

4.3.1 PV Response from Singlet and Triplet Excitons

Figure 4.1 shows the absorption spectra of $Ir(ppy)_3$ and Alq_3 films on ITO glass. The two films have the same absorption at 400nm. Therefore, 400 nm light was selected for the PV characterization. The current density-voltage (J-V) curves (Figure 4.2) indicate that the photocurrent from the $Ir(ppy)_3$ PV cell is a factor of 15 relative to that from the Alq_3 PV cell at zero bias. Under short-circuit condition, the external quantum efficiencies
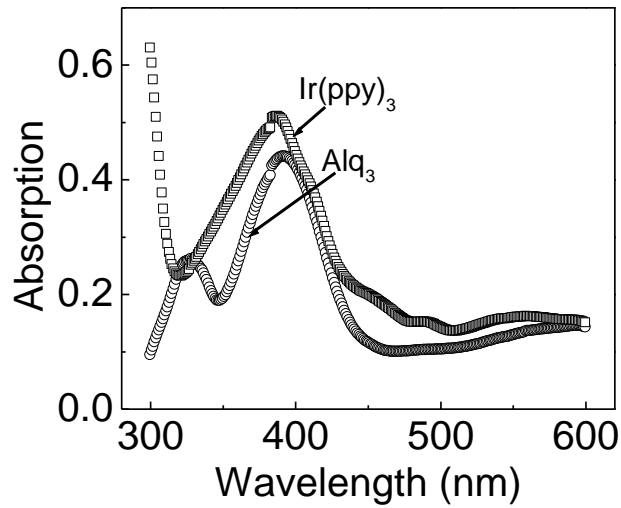
Figure 4.1 UV-Vis absorption spectra for Ir(ppy)$_3$ and Alq$_3$ solid films with thickness of 80 nm.

(η_{EQE}) were determined to be 0.4% and 0.03% for Ir(ppy)$_3$ and Alq$_3$ single-layer devices, respectively. It is known that the external quantum efficiency η_{EQE} of an organic PV cell can be given by

$$\eta_{EQE} = \eta_A \bullet \eta_D \bullet \eta_{CC} \qquad \text{(Equation 4.1)}$$

where η_A, η_D, and η_{CC} are defined as light absorption, exciton dissociation, and charge collection efficiencies. It is noted that η_A can be calculated from optical absorption spectrum while η_{CC} is mainly determined by charge mobilities of an organic semiconducting material.[9] Ir(ppy)$_3$ and Alq$_3$ show very similar η_A at the illumination wavelength of 400 nm. The time-of-flight transient photocurrents have indicated that the
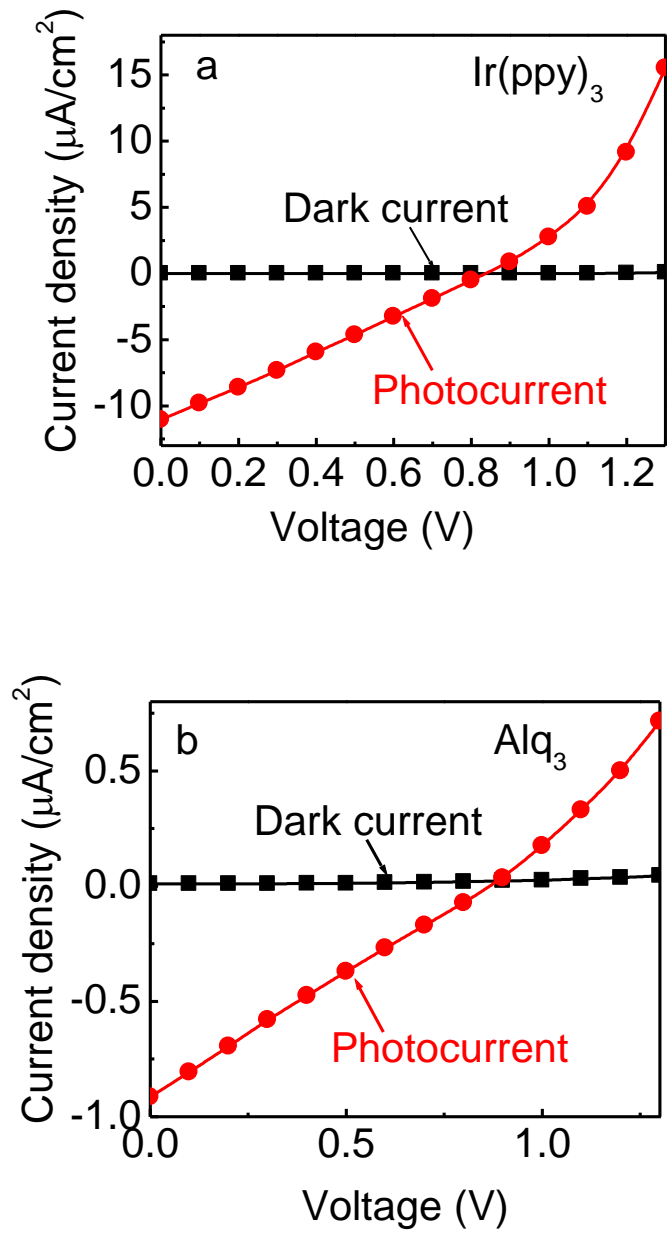
Figure 4.2 Current density-voltage (J-V) characteristics of for ITO/Ir(ppy)$_3$(80nm)/Al (a)

and ITO/Alq$_3$(80nm)/Al (b) PV cells measured under dark (squares) and the light

illumination at 400 nm (dots).

electron and hole mobilities are lower in Ir(ppy)$_3$ than that in Alq$_3$ [72, 73]. It can be therefore assumed that the η_{CC} in the Ir(ppy)$_3$ is not greater than that in the Alq$_3$. As a result, the higher PV efficiency essentially corresponds to a more efficient exciton dissociation η_D in the Ir(ppy)$_3$ PV cell, according to Equation 4.1. We note that the light absorption-generated excited states are mainly triplet excitons in the Ir(ppy)$_3$ due to its near 100% singlet-triplet intersystem crossing[58] while singlet excitons are dominant excited states in the Alq$_3$ due to its low singlet-triplet intersystem crossing of 20% [74]. It can therefore be suggested that the triplet excitons in the phosphorescent Ir(ppy)$_3$ molecules experience a more efficient dissociation than the singlet excitons in the fluorescent Alq$_3$ molecules.

The PL quenching (PLQ) measurement (Figure 4.3) further suggests that the dissociation for triplet excitons in the Ir(ppy)$_3$ PV cell is much more efficient with respective to the singlet excitons in the Alq$_3$ PV cell. In general, excitons experience both bulk and interface dissociation in a PV cell. With longer diffusion length, the interface dissociation can be more significant as compared to the bulk dissociation component for triplet excitons. However, the interface potential barrier (possibly due to relatively larger band gap energy or interfacial dipole) can hinder the triplet excitons to diffuse from bulk to metal electrode. As a consequence, an electric field can largely enhance such interface dissociation. The characteristics of PC versus electrical field (Figure 4.4) measured from the neat Ir(ppy)$_3$ and Alq$_3$ PV cells shows consistent result with PLQ. The triplet excitons

74
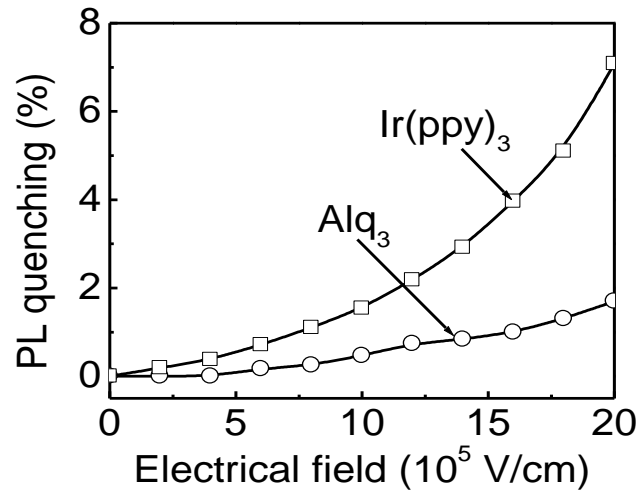
Figure 4.3 Photoluminescence quenching as a function of applied electric field for ITO/Ir(ppy)$_3$(80nm)/Al (squares) and ITO/Alq$_3$(80nm)/Al (dots) PV cells.
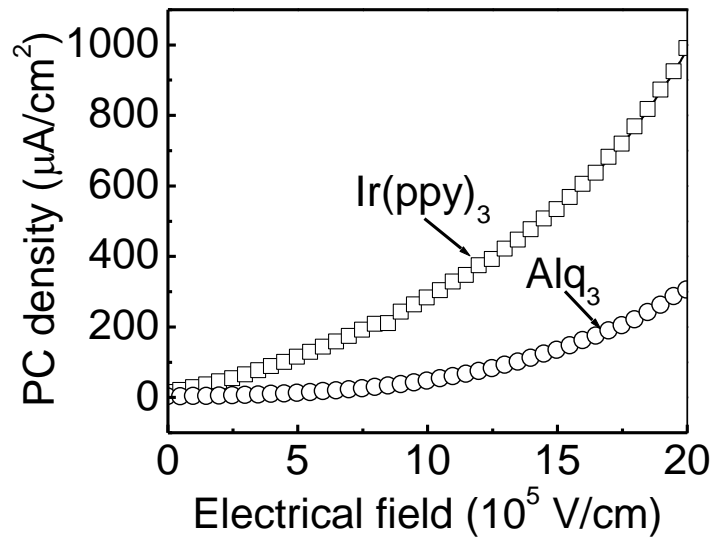
Figure 4.4 Characteristics of photocurrent versus electrical field for ITO/Ir(ppy)$_3$(80nm)/Al (squares) and ITO/Alq$_3$(80nm)/Al (dots) PV cells.

yield a much higher photocurrent in the $Ir(ppy)_3$ as compared to the singlet excitons in

the Alq_3 under reverse bias

4.3.2 Photocurrent Action Spectra

Figure 4.5 shows the normalized short-circuit PC action spectra and UV-Vis

absorption spectra for the $Ir(ppy)_3$ and Alq_3 PV cells. It can be seen that when the

$Ir(ppy)_3$ was illuminated from ITO side, the PC action demonstrates an "antibatic"

response to the light absorption. Specifically, the photocurrent spectrum shows a

minimum at maximal light absorption but a maximum at minimal light absorption. When

the illumination is applied from Al side, the PC action shows a "symbatic" response, i.e.,

the maximal and minimal photocurrents coincide with the greatest and lowest light

absorption, respectively. The "antibatic" response is evidence that the excitons are

diffused to the metal electrode and then dissociate into free charge carriers at the

metal/dye interface to yield a photocurrent.[75] In the Alq_3 PV cell the light illumination

through the ITO and Al electrodes leads to two "symbatic" responses (Figure 4.5b),

implying that the excitons undergo a significant bulk dissociation before a photocurrent is

produced at electrode. Therefore, it can be suggested from the PC and absorption spectra

that the triplet excitons mainly experience a dissociation at the $Ir(ppy)_3$/Al interface in the

phosphorescent $Ir(ppy)_3$ PV cell, while the singlet excitons exhibit a bulk dissociation in

the fluorescent Alq_3 PV cell. This dissociation difference between the triplet and singlet
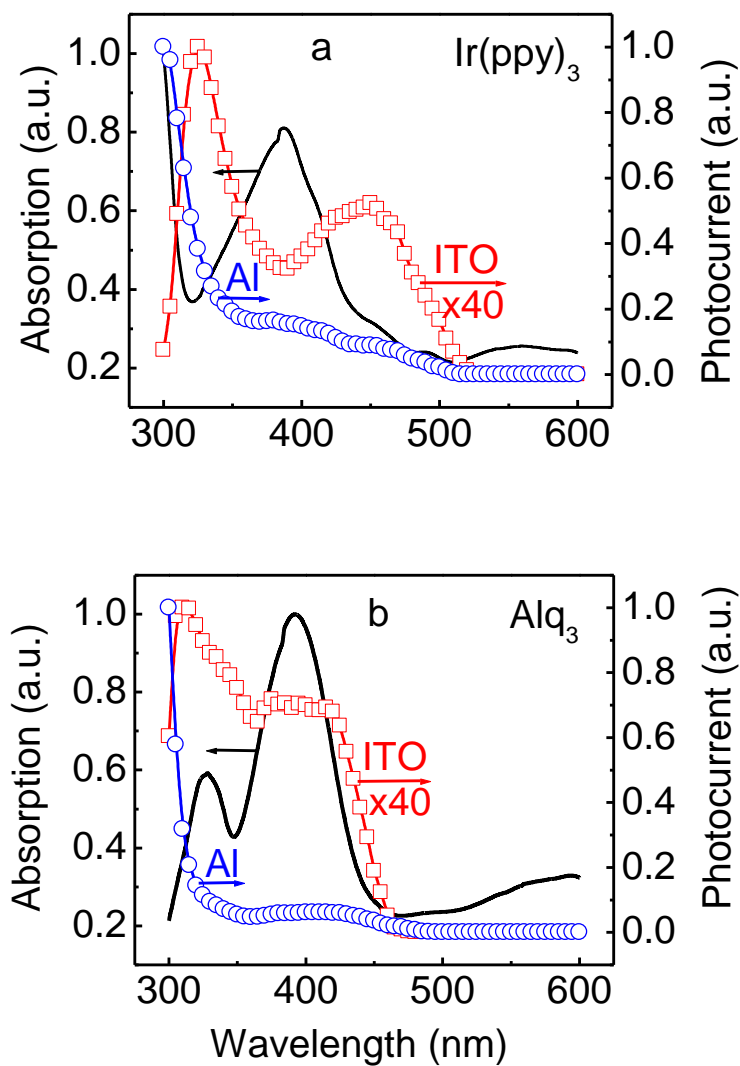
Figure 4.5 Normalized short-circuit PC action spectra and absorption spectra for ITO/Ir(ppy)$_3$(300nm)/Al (a) and ITO/Alq$_3$(300nm)/Al (b) devices. Squares and dots represent the PC action spectra when the light illumination was applied from the ITO and the Al sides, respectively.

excitons can be attributed to their long and short diffusion lengths.

The transport of excitons in the Ir(ppy)$_3$ PV cell can be described by the diffusion equation:

$$D\frac{\partial^2 n}{\partial x^2} - \frac{n}{\tau} + \alpha\phi N\exp(-\alpha x) = 0 \qquad \text{(Equation 4.2)}$$

where D is the exciton diffusivity, n is the number of excitons, τ is the exciton lifetime, α is the absorption coefficient, Φ is the quantum efficiency of exciton generation, and N is the incident photon density. When n = 0 at the ITO and Al electrode interfaces and $\exp(-L/L_D) \ll 1$, in which L and $L_D = (D\tau)^{1/2}$ are the film thickness and the exciton diffusion length, the short-circuit photocurrent J_{Al} due to the interface dissociation under the Al-side illumination can be expressed as [75]

$$\frac{1}{J_{Al}} = (1 + \frac{1}{L_D}\frac{1}{\alpha})(N\phi q)^{-1} \qquad \text{(Equation 4.3)}$$

where q is the charge of an electron. From the characteristics of $1/J_{Al}$ versus $1/\alpha$ (Figure 4.6) plotted by the PV action spectral data, the triplet exciton diffusion length L_D can be calculated to be about 60 nm in the Ir(ppy)$_3$. This long diffusion length must be due to the long triplet lifetime of 2 μs.[76] As compared to the Ir(ppy)$_3$, the singlet exciton diffusion length L_D has been determined to be about 10 nm in the Alq$_3$.[77] This short diffusion length can be attributed to the short singlet lifetime of 15 ns.[78] The long and short diffusion lengths can be further suggested by the thickness-dependent photocurrents from the Ir(ppy)$_3$ and Alq$_3$ PV cells, as shown in Figure 4.7. We should note that the Ir(ppy)$_3$
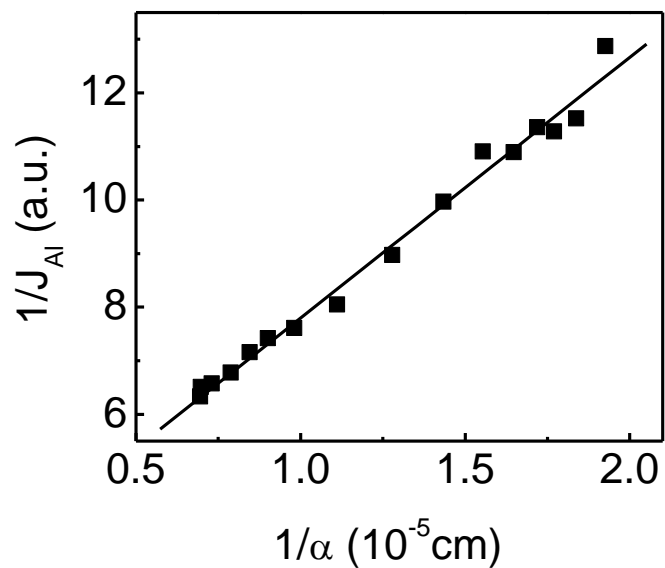
Figure 4.6 $1/J_{Al}$ versus $1/\alpha$ characteristics for ITO/Ir(ppy)$_3$(300nm)/Al.
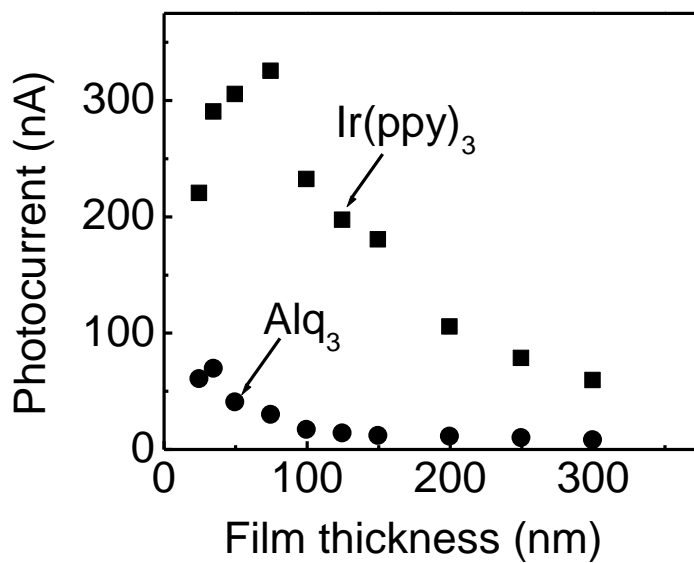
Figure 4.7 Thickness-dependent photocurrent for ITO/Ir(ppy)$_3$/Al and ITO/Alq$_3$/Al cells

and Al can act as an electron donor and acceptor, respectively, to facilitate the exciton dissociation at the $Ir(ppy)_3/Al$ interface in the $ITO/Ir(ppy)_3/Al$ PV cell. The triplet excitons can therefore dissociate at the metal/dye interface due to their long diffusion length. In addition, the exciton dissociation at $Ir(ppy)_3/Al$ interface increases charge collection, reducing the recombination probability of dissociated electrons and holes, which is considerably high in bulk dissociation process.[79] Therefore, the longer diffusion length L_D essentially enhances the PV efficiency η_{EQE} in the $Ir(ppy)_3$ solar cell. On contrast, the singlet excitons can experience significant bulk dissociation due to their short diffusion length and thus lead to a low PV response in the Alq_3.

4.3.3 MFP Measurements

To further understand the exciton dissociation processes in the Alq_3 and $Ir(ppy)_3$ PV cells, we studied magnetic field effects on the photocurrent, namely MFP. It can be seen in Figure 4.8 that the Alq_3 PV cell shows a significant MFP: rapid increase from 0 to 50 mT and then slow decrease from 50 mT up to 350 mT. However, the $Ir(ppy)_3$ PV cell does not exhibit an appreciable MFP in the magnetic field from 0 to 350 mT. In general, photocurrent results from the generation of excitons upon photoexcitation, formation of polaron pairs due to the dissociation of excitons, and development of free charge carriers through the dissociation of polaron pairs in organic PV cells. It is noted that an intersystem crossing can occur between singlet and triplet polaron pairs due to hyperfine
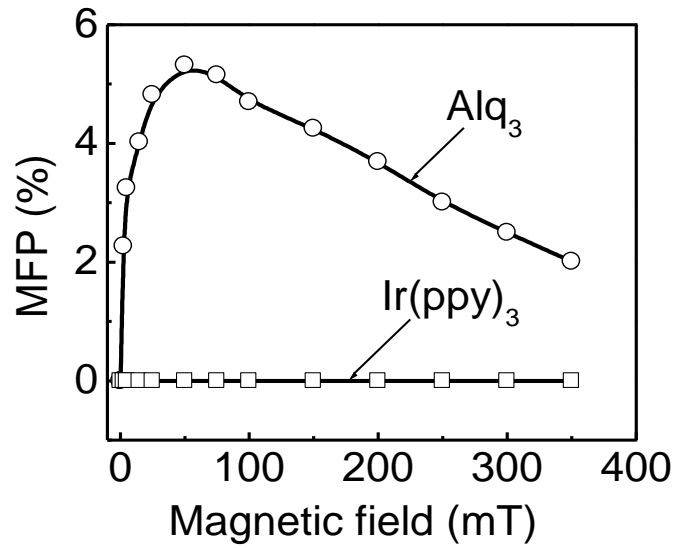
Figure 4.8 MFP of the ITO/Ir(ppy)$_3$(80nm)/Al (squares) and ITO/Alq$_3$(80nm)/Al (dots) PV cells under photoexcitation at 400nm.

interaction and spin-orbit coupling in organic materials. Especially, the intersystem crossing in polaron pair state is sensitive to an external magnetic field due to Zeeman effect,[34],[80] leading to a MFP, based on the fact that the dissociation of singlet polaron pairs is largely greater than that of the triplet polaron pairs in bulk materials.[34, 50] A low external magnetic field can reduce the intersystem crossing rate K_{ISC} and thus boosts the singlet polaron pairs, leading to an increase in the MFP. On the other hand, triplet excitons can react with trapped charges due to its long lifetime and significant diffusion length, contributing to the photocurrent. A relative high magnetic field can reduce this triplet-charge reaction rate and consequently causes a decrease in the MFP.[38, 39]

We now particularly consider why the dissociation in the $Ir(ppy)_3$ PV cell gives riseto an unappreciable MFP. In principle, there are two possibilities: extremely strong spin-orbit coupling or direct dissociation from excitons into free charge carriers that can eliminate the MFP in organic materials. First, Zeeman effect caused by an external magnetic field becomes negligible relative to an extremely strong spin-orbit coupling. Secondly, the excitons do not experience polaron-pair states in the direct dissociation into free charge carriers. In both cases the MFP becomes unappreciable in organic PV cells. It should be noted in Figure 4.9a that the considerable MFP is observed in the $Ir(ppy)_3$ PV cell when the 2,9-dimethyl-4,7-diphenyl-1,10-phenanthroline, named as Bathocuproine (BCP),[81] is used as an exciton-blocking layer. It should be noted that this BCP layer provides two functionalities: generating trapped charge carriers due to the offset between the LUMOs of $Ir(ppy)_3$ and BCP, and blocking the triplet excitons within the $Ir(ppy)_3$ layer (Figure 4.9b). The largely reduced photocurrent by the BCP layer suggests that the triplet excitons are significantly confined in the $Ir(ppy)_3$ (Figure 4.9c). Therefore, the triplet-charge reaction can be enforced by the addition of BCP layer in the double-layer ITO/$Ir(ppy)_3$/BCP/Al PV cell. We observe in Figure 4.9a that a relative high magnetic field (> 50 mT) reduces the triplet-charge reaction rate and thus leads to a decrease in the photocurrent in the double-layer $Ir(ppy)_3$ PV cell. As the BCP thickness increases, the triplet-charge reaction can be further enhanced, leading to a more significant decrease in the MFP. It should be noted that the photoexcitation of 400 nm used in the experiment
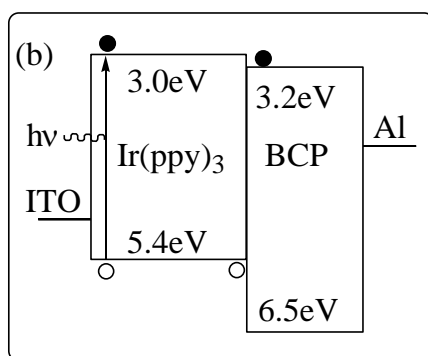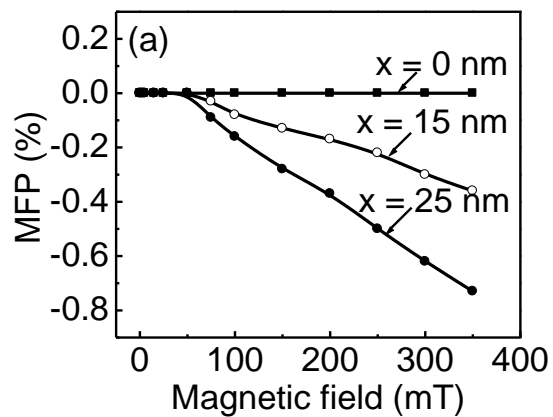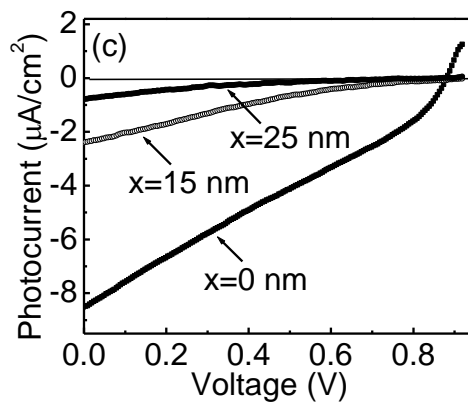
Figure 4.9 (a) The MFP for double-layer PV cell of ITO/Ir(ppy)$_3$(80nm)/BCP(x nm)/Al.

(b) Band diagram together with enforced triplet-charge (T-C) reaction in the double-layer

Ir(ppy)$_3$ PV cell. (c) Photocurrents from ITO/Ir(ppy)$_3$(80nm)/BCP(x nm)/Al PV cells.

does not generate both appreciable photocurrent and MFP in the neat BCP device. As a result, the MFP induced by the BCP blocking layer confirms that the unappreciable MFP is partly due to the direct dissociation from triplet excitons into free charge carriers at the $Ir(ppy)_3$/Al interface in the single-layer ITO/$Ir(ppy)_3$/Al PV cell. This direct exciton dissociation must result from the long diffusion length and the donor-acceptor interaction at the $Ir(ppy)_3$/Al interface.

4.4 Conclusions

In conclusion, the photocurrent and MFP studies indicate that the triplet excitons mainly dissociate directly into free charge carriers at the metal-electrode interface due to their long diffusion length in the phosphorescent $Ir(ppy)_3$ PV cell while the singlet excitons experience a significant bulk dissociation into polaron pairs due to their short diffusion length in the fluorescent Alq_3 PV cell. The interfacial dissociation of triplet excitons at the metal electrode leads to an enhanced PV response from phosphorescent materials as compared to the bulk dissociation of singlet excitons in fluorescent materials. As a result, the control singlet-to-triplet exciton ratio presents a unique pathway to improve PV efficiencies in organic solar cells.

CHAPTER 5

SINGLET AND TRIPLET PHOTOVOLTAIC PROCESSES IN P3HT:PCBM BULK-HETEROJUNCTION OPVS

5.1 Introduction

In general, light absorption by conjugated polymers leads to formation of coulombically bounded electron-hole pairs, namely excitons, with binding energy from several hundred meV to 1eV.[82, 83] To overcome the large binding energy and dissociate the photoexcited electron-hole pairs, electron acceptors (the most commonly used is PCBM) were blended with conjugated polymers to form bulk-heterojunction donor-acceptor interface, where charge separation happens. Then the dissociated electrons and holes are collected by the electrodes for the generation of photocurrent. To improve photovoltaic efficiency of conjugated polymer solar cells, understanding the detailed photovoltaic processes in these semiconducting polymers and their blends is of critical importance. Different techniques such as temperature and field dependent photocurrent,[46, 84 - 86] ultra-fast spectroscopy,[87] photoinduced absorption,[88] flash-photolysis time-resolved microwave conductivity (FP-TRMC),[89] THz time domain spectroscopy (THz-TDS),[90] have been used to study the photon-to-electron processes in conjugated polymers. Although the researchers agree that charge carriers originate from neutral excitons, there is no agreement on the time scale and intermediate processes of

exciton dissociation.

P3HT:PCBM solar cells are so far the most prominent bulk-heterojuction OPVs. About 5% power conversion efficiency (PCE) has been obtained in OPVs using P3HT:PCBM as active materials.[14, 15] In this chapter, the study of the singlet and triplet photovoltaic processes in P3HT:PCBM by MFP measurement will be presented.

5.2 Experimental

Regioregular P3HT with the average molecular weight of Mn = 87,000 was purchased from Aldrich, and PCBM was from American Dye Sources, Inc. Thin films of pure P3HT and P3HT: PCBM blends with the thickness of 100nm were made by spin coating their chloroform solutions on ITO glass substrate under nitrogen atmosphere. Thin films of P3HT:PCBM blends with the thickness of 100nm were made by spin coating their chlorobenzene solutions on glasses or ITO coated glass substrates modified with a thin layer of poly(3,4-ethylenedioxythiophene): poly(styrene sulfonate) (PEDOT:PSS) (Baytron P 4083). Organic solar cells were fabricated by using vacuum deposition of aluminum (Al) onto the spin-coated films. Thermal annealing was carried out under nitrogen gas atmosphere by putting organic films or devices on a digital controlled hotplate. A Keithley 2400 source meter was used to measure current-voltage (I-V) curves for PV devices in dark or under AM1.5G 100 mW/cm^2 illumination from a Thermal Oriel 96000 300 W solar simulator. Absorption spectra were measured with a

Perkin-Elmer Lamda-35 Uv-vis spectrometer. Photoluminescence (PL) spectra were measured using a SPEX Florolog 3 spectrometer.

5.3 Results and Disscussion

In organic solar cells, photocurrent is generated by the dissociation and interactions of the excited states includingexcitons, CT complexes and polaron. And MFP has been demonstrated as a powerful tool to understand the singlet and triplet photovoltaic processes of these excited states. In this chapter, MFP was applied to investigate the PV processes in P3HT:PCBM solar cells with different PCBM concentrations.

5.3.1 Charge Generation in Single-Layer P3HT Solar Cells

Figure 5.1 shows the photocurrent and absorption spectra of P3HT film. The PC spectrum can be roughly divided into two parts, one with wavelengths longer than 500 nm, and the other one shorter than 500 nm. In the first part, photocurrent is relatively low, and the photocurrent generation efficiency is almost wavelength independent if considering the absorption coefficient. In the short wavelength part, photocurrent generation efficiency is much higher and strongly dependent on excitation wavelength. Similar phenomena have been observed in P3HT film by Dicker *et al*.,[89] and in ladder-type poly(para-phenylene) (MeLPPP) by Arkhipov *et al*.[46] Dicker attributed charge carrier generation under low energy photon excitation to exciton interchain
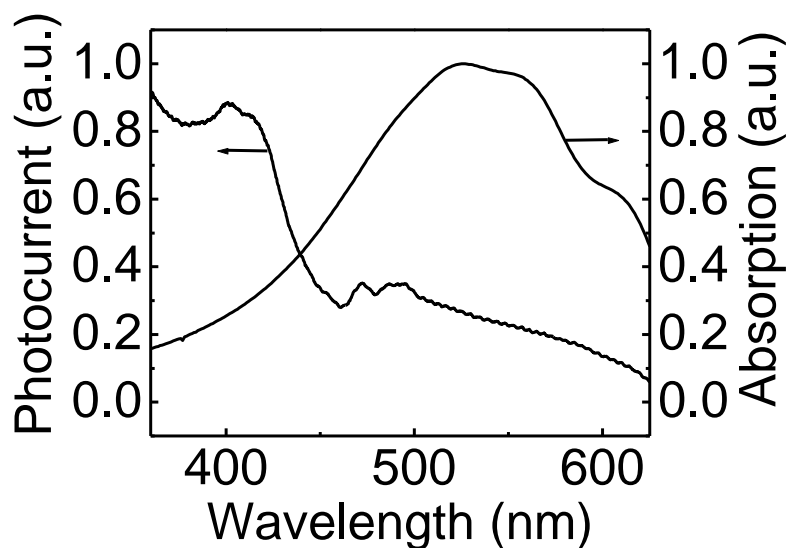
Figure 5.1 Photocurrent and absorption spectra of P3HT film.

dissociation, and higher carrier generation efficiency under higher energy photon excitation to autoionization of S_n states. Arkhipov proposed a tandem mechanism and on-chain dissociation of hot excitons mechanism for charge carrier generation under low and high photon energy excitation, respectively. In this work, we studied the carrier generation processes of P3HT thin films under different photon energy excitation by measuring wavelength dependent MFP, shown as Figure5.2. The MFP results can also be divided into two groups by excitation wavelength at 500 nm. When P3HT sample is excited by light with wavelength longer than 500nm, MFP is wavelength independent (for clarity only MFP of 520 nm is shown in Figure 5.2) and consists of a sharp
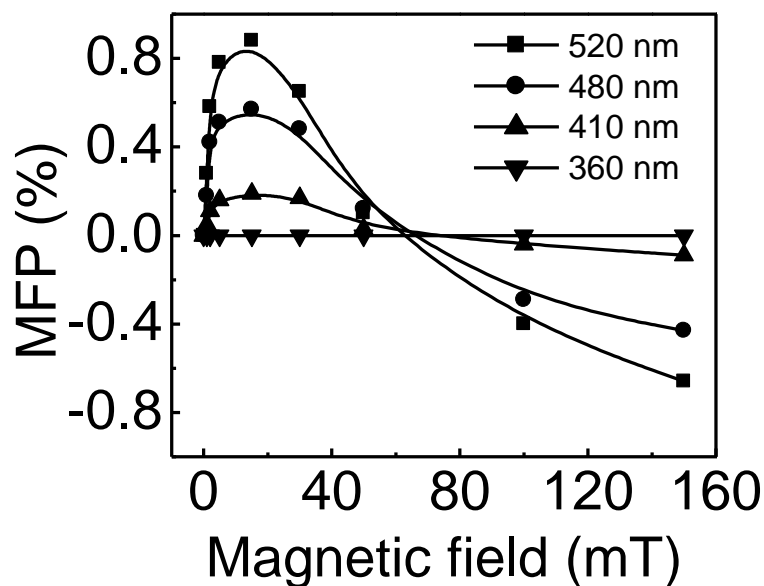
Figure 5.2 MFP of ITO/P3HT/Al under excitation of different wavelength lights.

increasing component in low magnetic field and a decreasing component in higher magnetic field; MFP has strong wavelength dependence when the sample is excited by light with wavelength shorter than 500 nm. The magnitude of MFP reduces with increasing photon energy, and no MFP can be observed when excitation wavelength is shorter than 380 nm.

The positive and negative components of MFP in P3HT can be attributed to the polaron pairs mechanism and triplet-charge reaction mechanism, respectively, as has been discussed in the previous chapters. To have significant positive MFP, the lifetime of polaron pairs should be longer than spin evolution time, which is around 10^{-9} s, and

shorter than spin lattice relaxation time, which is around 10^{-7} s.[26] MFP based on polaron pair mechanism usually saturates at low magnetic field of a few hundreds Gauss. While the negative MFP based on the CTR mechanism does not saturate in low magnetic field.[38]

It can be seen from Figure 5.2 that P3HT exhibits both positive and negative MFP when excited by low photon energy light. Existence of positve MFP indicates that thermal and field assisted dissociation of polaron pairs is one of the mechanisms for free charge carriers photogeneration in P3HT, which is similar to other conjugated polymers such as poly(2,5-diheptyloxy-*p*-phenylene vinylene) (HO-PPV).[36] The dynamics of generation and dissociation of polaron pairs have been addressed by other authors.[36, 46] Significant negative MFP suggests a TCR-assisted free charge carrier generation processes. It is known that either impurities or defects can form deep traps in semiconducting polymers. These traps can serve as charge transfer centers to dissociate excitons or polaron pairs, and lead to trapped electrons and free holes.[84, 85] Due to their long lifetime, triplet excitons can interact with the trapped electrons and "kick" them out of the deep traps to contribute to photocurrent. It has been reported that relative efficient intersystem crossing occurs in P3HT and poly(3-octylthiophene) (P3OT) due to the "heavy atom" sulfur induced spin-orbit coupling in the these polymers,[91] and the triplet exciton quantum yield of 77% has been reported in P3OT solution.[49] Therefore, it could be expected that significant amount of triplet excitons will be populated in P3HT films under photoexcitation. This explains why negative MFP and triplet-charge reaction

assisted charge carriers photogeneration is significant in P3HT films.

It has been demonstrated that the magnitude of positive MFP based on polaron pair mechanism strongly depends on the excitation wavelength. But the negative MFP based on TCR mechanism is diffusion limited, and it should not show wavelength dependence. However, with increased excitation photon energy both positive and negative MFE reduce, indicating that a new charge carrier generation process becomes more predominant. To explain similar high quantum yield of free charge carriers of MeL-PPP under high energy optical excitation, Arkhipov *et al.* proposed a mechanism called "on-chain dissociation of hot excitons",[85, 86] which suggests neutral excitons can acquire part of excess photon energy to facilitate their ultrafast dissociation into completely separated charge carriers. This mechanism is consistent with our results from MFP measurement. The dissociation rate of hot excitons, which was suggested to be subpicoseconds, is out of the time scale of spin evolution. Therefore no positive MFE can be observed. In addition, this dissociation is an intra-chain process with no diffusive steps involved and more efficient than diffusion limited TCR-assisted photocurrent generation process. It thus leads to diminution of negative MFP.

In summary, the charge carrier photogeneration processes in P3HT single-layer solar cells under low energy photoexcitation include dissociation of polaron pairs and triple-charge reaction. And dissociation of hot excitons becomes the dominant charge carrier generation process under high energy photoexcitation.

5.3.2 Charge Generation in P3HT:PCBM Bulk-Heterojunction Solar Cells

We now discuss the donor-acceptor interaction effects on the photovoltaic channels of dissociation and charge reaction in bulk-heterojunction solar cells by using positive and negative magnetic field effects on photocurrent. It is noted that donor-acceptor interaction can occur in ground states[92,93] and excited states[13] to dissociate electron-hole pairs when two different types of organic molecules are mixed at molecular level. Here we consider the donor-acceptor interaction occurring in excited states in bulk-heterojunction solar cells. In principle, the donor-acceptor interaction is determined by two factors: intermolecular distance and electronegativity difference between donor and acceptor molecules. The donor-acceptor interaction provides the necessary internal electric field to compete with the electron-hole attractive interaction for the dissociation of photoexcited states in the generation of photocurrent in organic solar cells.[34, 79] When the acceptor material PCBM[52, 53] is used in bulk-heterojunction solar cells, the effective donor-acceptor interaction can be tuned by changing the PCBM concentration if the uniform dispersion is obtained. Figure 5.3 shows that at low concentrations (< 1 wt%) the PCBM gradually decreases the positive component and enhance the negative component of the MFP of P3HT in low field from 0 to 150 mT. At 1 wt% concentration the PCBM completely destroys the positive component but remains the negative component in the magnetic field effects on photocurrent. This result clearly shows that the weak donor-acceptor interaction at low PCBM concentration (< 1wt%) dissociates polaron
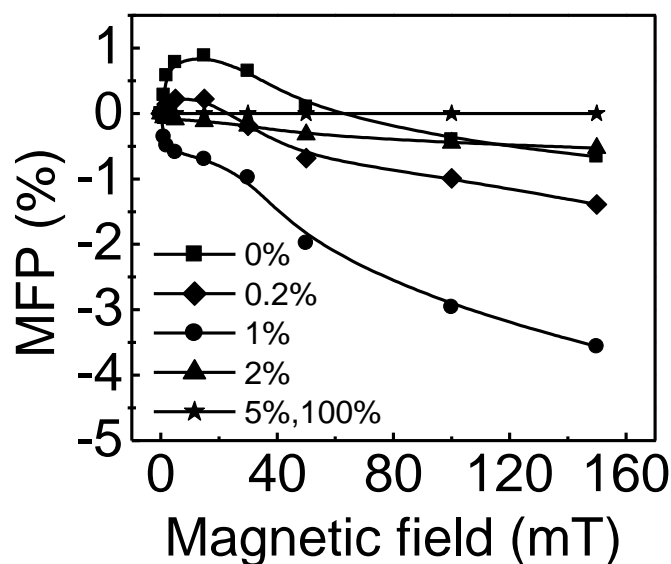
Figure 5.3 MFP of P3HT doped with different concentrations of PCBM under excitation of 520 nm.

pairs but enhances triplet-charge reaction.

It is well known that very efficient photoinduced charge transfer happens between PCBM and P3HT. However, due to the low concentration of PCBM, electrons transferred from P3HT are trapped in isolated PCBM molecules. This means PCBM acts as extrinsic deep traps for charge carrier generation in P3HT, enhancing triplet excitons-traps assisted photocarriers generation and negative MFP. Since dramatically increased quantity of trap sites are formed by doped PCBM, polaron pairs with long separation distance and low columbic bounding, can be easily dissociated by charge transfer to these deep traps instead of thermal or field assisted dissociation. Therefore, positive MFP is quenched.

Increased photocurrent at long wavelength part (Figure 5.4) suggests higher free carrier generation efficiency of triplet excitons-traps assisted dissociation than thermal and field assisted polaron pair dissociation.

Enhanced triplet excitons-traps assisted dissociation has also been found to compete with on-chain dissociation of hot excitons. Negative MFP was observed for P3HT doped with 1 wt% of PCBM even excited by 360 nm light (Figure 5.5). While no negative MFP was observed for pure P3HT film excited at 360 nm, indicating dissociation of hot excitons is the dominant PV processes for charge carrier generation. Comparing the PC spectra of P3HT and P3HT:1%PCBM, we observe that the photocurrent of P3HT:1%PCBM is lower than that of P3HT at short wavelength part (Figure 5.4), suggesting lower efficiency of triplet-charge reaction than dissociation of hot excitons in free charge carrier generation.

We note that further increasing the PCBM concentration (> 1 wt%) within uniform dispersion regime leads to a decrease in the amplitude of negative magnetic field effect on photocurrent. The 5 wt% PCBM dispersion gives a flat magnetic field dependence of photocurrent in low field from 0 to 150 mT. The flat magnetic field dependence of photocurrent indicates that the strong donor-acceptor interaction at high PCBM concentration removes both dissociation of polaron pairs and the exciton-charge reaction. This implies that high-concentration PCBM directly dissociates singlet and triplet excitons to generate photocurrent in bulk-heterojunction solar cells. Consequently,
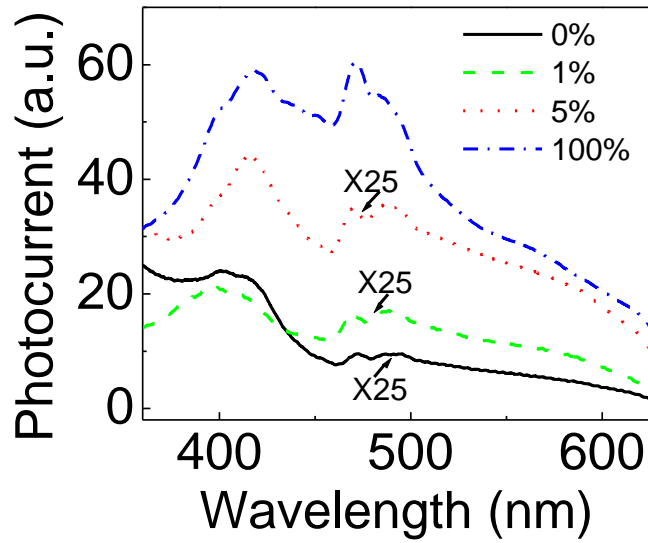
Figure 5.4 Photocurrent spectra of P3HT doped with different concentrations of PCBM.
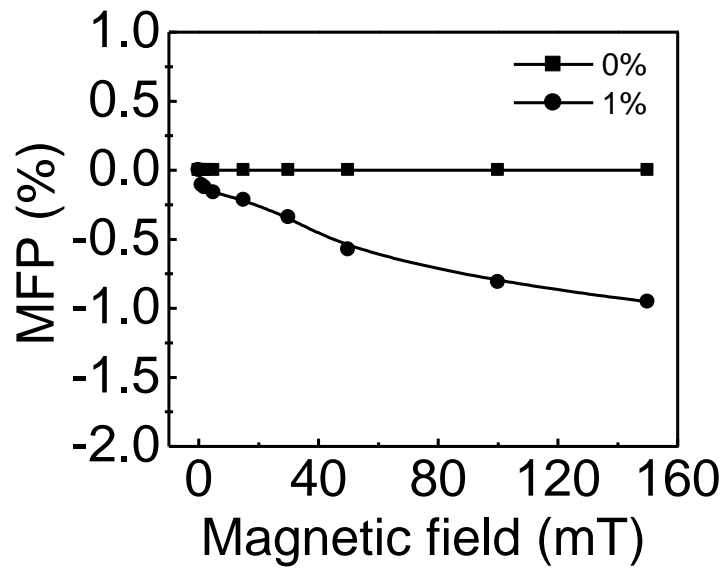
Figure 5.5 MFP of ITO/P3HT/Al and ITO/P3HT:1% PCBM/Al under photoexcitation at

360 nm.

photocurrent is largely enhanced in the whole range of wavelength (Figure 5.4).

As a result, MFP at low field reveals that the photovoltaic channels in P3HT doped with low concentrations of PCBM include (I) the polaron pair dissociation and the triplet-charge reaction under low energy photoexcitation, and (II) direct dissociation of hot excitons and triplet-charge reaction under high energy photoexcitation. When P3HT was doped with high concentrations of PCBM, the predominant photovoltaic channel is photoinduced charge transfer at donor/acceptor interface. In terms of photocurrent generation, photoinduced charge transfer is the most efficient PV channel, followed by direct dissociation of hot excitons. Dissociation of polaron pairs has the lowest efficiency for free charge carrier generation.

5.3.3 Charge Recombination in P3HT:PCBM Bulk-Heterojunction Solar Cells

The photoinduced absorption studies have found that the dissociation of photoexcited states occurs within the time scale of femtoseconds at polymer/fullerene in bulk-heterojunction solar cells.[13, 54, 94-96] There are two inevitable products, namely useful and non-useful outcomes, for the dissociated electrons and holes to yield. First, the dissociated charge carriers can transport through respective networks to generate photocurrent, leading to a useful outcome. Second, the dissociated charge carriers can form bound electron-hole pairs: charge transfer (CT) complexes due to attractive Coulomb interaction, at the donor-acceptor material interfaces, giving a non-useful

outcome. Clearly, the ratio of useful and non-useful outcome affects the photovoltaic efficiency in organic solar cells.

In general, there are two factors: charge mobility and dielectric constant that determine the probability to form charge-transfer complexes from the dissociated electrons and holes. The charge mobilities affect the probability for electrons and holes to escape from their effective Coulomb capture radius. The dielectric constant controls the effective Coulomb capture radius through electric screening effect for the electrons and holes to pair up at the donor-acceptor interfaces when the electrons and holes transport in an average dielectric field. In essence, the charge-transfer complexes can be considered as quasi polaron pairs (Figure 5.6). The wavefunction combination of dissociated electrons and holes can yield both singlet and triplet charge-transfer complex states, respectively, with intersystem crossing. An external magnetic field can modify the singlet/triplet charge-transfer complex ratio by perturbing the intersystem crossing rate. It can be further assumed that the charge-transfer complexes can develop into free charge carriers through dissociation and charge reaction channels.

We observe in Figure 5.7a that the highly dispersed PCBM leads to a positive magnetic field effect on photocurrent in relative high field range between 150 mT and 900 mT while in low field the magnetic field effects on photocurrent remain flat from 0 up to 150 mT in the bulk-heterojunction PCBM+P3HT solar cell. This high-field positive magnetic field effect of photocurrent can be suggested as the signature of charge-transfer

97
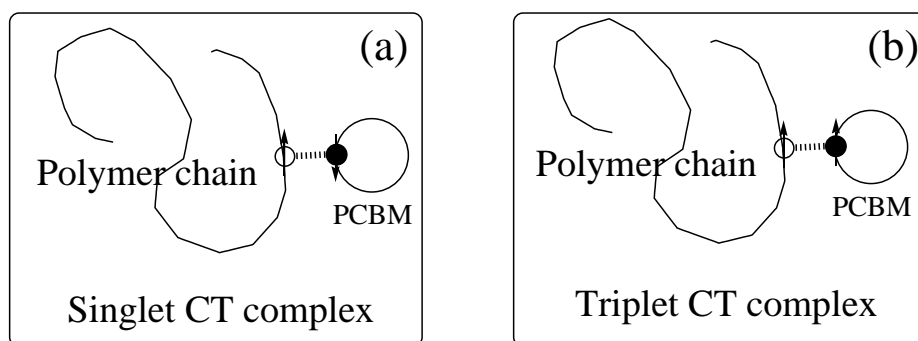
Figure 5.6 Schematic diagrams for singlet (a) and triplet (b) charge-transfer complexes formed from dissociated electron and hole at the P3HT-PCBM interface.

complex states formed from dissociated electrons and holes at the P3HT-PCBM interfaces. It can be seen in Figure 5.7a that the amplitude of this high-field MFP depends on the PCBM weight ratio in the P3HT+PCBM solar cell, while there is no visible difference in turn-on field (H_0) of different samples which indicates that CT complexes have similar value of the charge separation distance r. Therefore, the decrease of positive MFP upon increasing the PCBM weight ratio from 0.2 to 0.8 shows that the density of formed charge-transfer complexes decreases with increasing the PCBM weight ratio in bulk-heterojunction organic solar cells, according to Equation 2.7. Further increasing the PCBM concentration to 1:2 with ratio of P3HT:PCBM leads to an increase of positive magnetic field effect on photocurrent. This backward change in the amplitude of positive magnetic field effect of photocurrent can be related to the reduction of effective
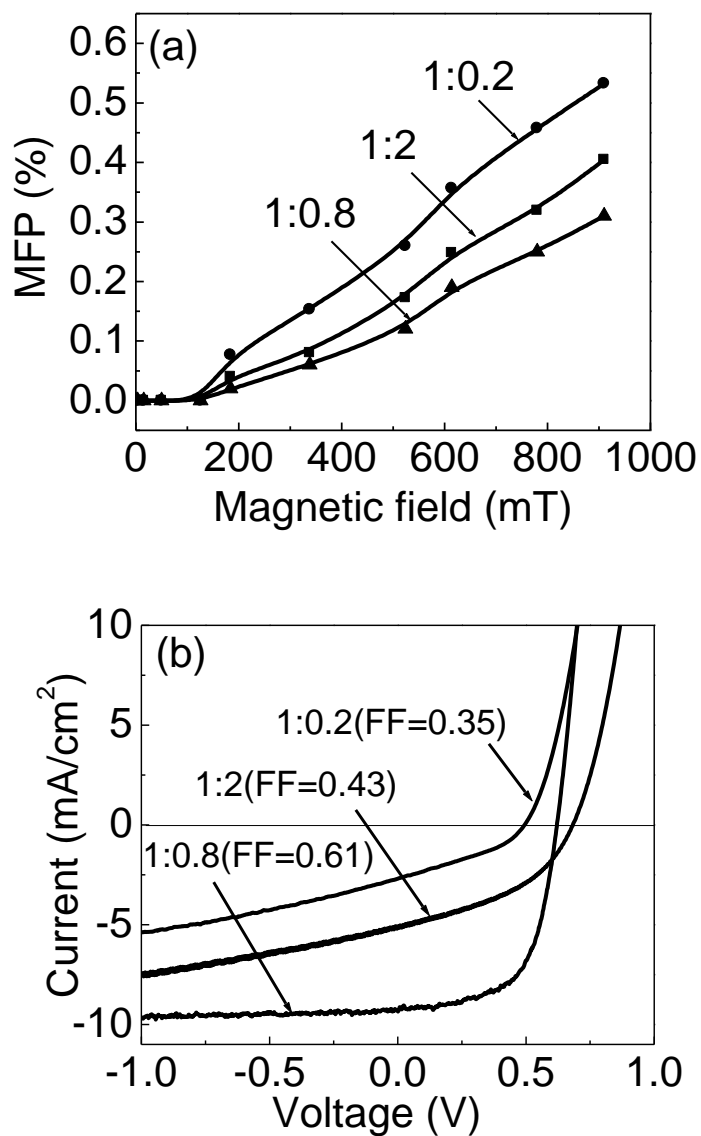
Figure 5.7 High-field MFP (a) and Photocurrent-voltage characteristics (b) for ITO/PEDOT/P3HT+PCBM/Al solar cells with different P3HT:PCBM weight ratios.

donor-acceptor interaction due to more significant PCBM aggregation at higher concentration. Clearly, the 1:0.8 weight ratio of P3HT:PCBM yields a lowest density of charge-transfer complexes. This lowest density of charge-transfer complexes corresponds to an optimized fill factor of 0.61 and highest power conversion efficiency in the ITO/P3HT+PCBM/Al solar cell (Figure 5.7b).

5.3.4 Annealing Effect on CT Complexes in P3HT:PCBM Solar Cells

It is well known that annealing can significantly improve PV efficiency of the P3HT:PCBM solar cells.[97] Around 5% power conversion efficiency (PCE) have been achieved by thermal annealed P3HT:PCBM devices.[15] Similar efficiency has also been reported by Li *et al.,* by controlling solvent annealing effect on P3HT:PCBM cells.[14] Using MFP measurement, we found that the formation of CT complexes in P3HT:PCBM is largely affected by thermal annealing.

The experimental results of thermal annealing in our work were shown as Figure 5.8a. The power conversion efficiency (PCE) under illumination of 100 mW/cm^2 AM1.5G simulated white light was improved from 1.4% for the unannealed devices (I_{SC}=6.5 mA/cm^2, V_{OC}=0.49V, FF=0.42) to 3.5% for the best annealed devices (I_{SC}=9.6 mA/cm^2, V_{OC}=0.61V, FF=0.60). Although the PV enhancement was attributed to the improvement of absorption and charge mobilities induced by morphology change during temperature annealing,[98-100] the fundamental mechanism hasn't been fully understood.
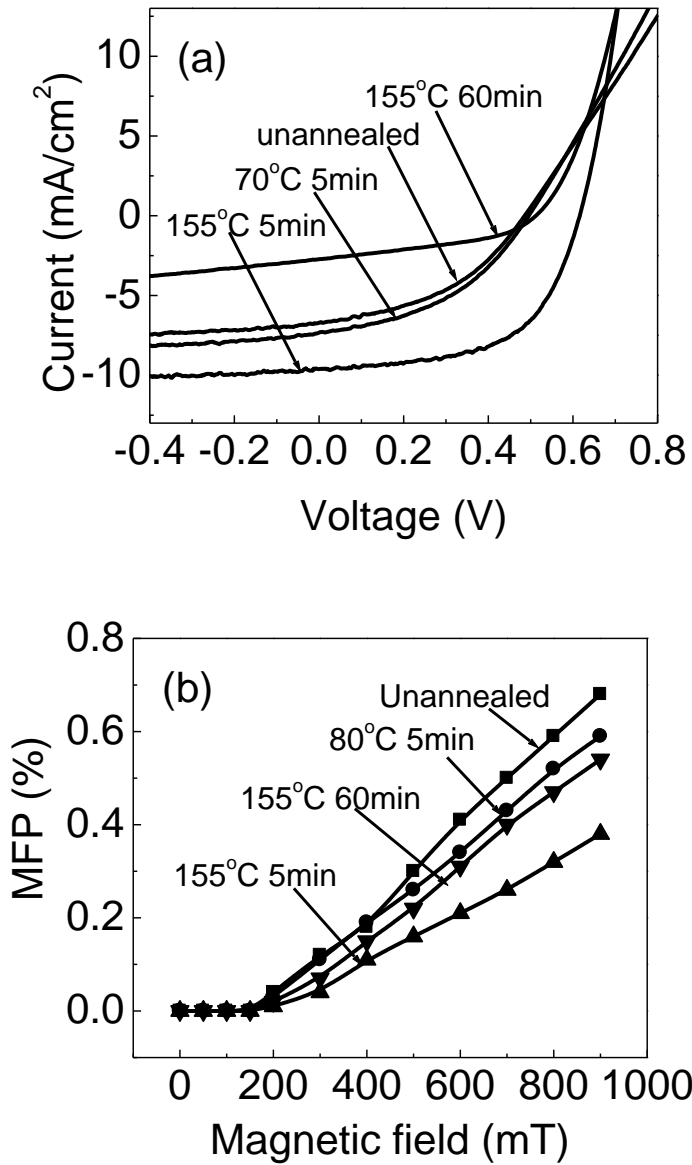
Figure 5.8 Current density-Voltage characteristics (a) and MFP (b) of ITO/Pedot/P3HT:PCBM(1:0.8)/Al devices with different heat treatment under illumination of 100 mW/cm^2 AM1.5 simulated white light.

The MFP measurement in our work suggests that the reduction of CT complexes also contribute to the PV efficiency enhancement upon thermal annealing. Figure 5.8b shows that temperature annealing significantly reduces the amplitude of high-field MFP, while do not change the turn-on field. The unannealed devices have largest high-field MFP, while the annealed device with the highest PV efficiency coincidently shows the smallest MFP.

In bulk-heterojunction solar cells, photocurrent may come from direct dissociation of intramolecular excitons, which shows no dependence on external magnetic field; On the other hand, photocurrent may come from dissociation of CT complexes, which is dependent on external magnetic field. As a result, the change of the density of CT complexes will modify the ratio between magnetic dependent PC and magnetic independent PC, and consequently change the amplitude of MFP. Therefore, the decreased MFP shown in Figure 5.7b suggests that temperature annealing reduces the density of CT complexes in P3HT:PCBM cells. As we mentioned, CT complexes are strongly associated with geminate charge recombination which is a limiting factor to achieve high PV efficiency. So it is not surprising to see that the most efficient device shows the lowest MFP.

Now we consider how temperature annealing can remove certain amount of CT complexes. CT complexes can be formed either by the geminate electron and hole which fail to escape the coulomb attraction after excitons dissociation, or by mutual capture of

counter free charge carriers during their transport to electrodes. Basically, CT complex formation is determined by the attractive force and escaping force involved in the coulombic scattering of electrons and holes, as shown in Figure 2.10b. The attractive force between electron and hole is largely determined by their separation distance which depends on the donor-acceptor interfaces. The escaping force is determined by charge carrier mobilities which influences not only the escaping ratio of coulombically bound charge, but also the transport time for free carriers getting to the electrodes and consequently the probability of the mutual capture of opposing charge carriers. Furthermore, both donor-acceptor interfaces and charge mobilities in organic bulk-heterojunction solar cells can be influenced by the film morphology.[14] Therefore, morphology reorganization upon temperature annealing might account for the change of CT complex formation.

To study the morphology change induced by temperature annealing on P3HT:PCBM films, absorption and photoluminescence measurements were carried out and the results were shown in Figure 5.9a, and 5.9b, respectively. It can be found that temperature annealing gradually increases long wavelength absorption and the vibronic structures for P3HT:PCBM films, which indicates higher crystallinity and stronger interchain interaction between P3HT chains. Similar phenomenon was also found by solvent annealing on P3HT:PCBM films.[101] On the other hand, PL intensity of P3HT:PCBM films was monotonically enhanced by temperature annealing. This suggests aggregation
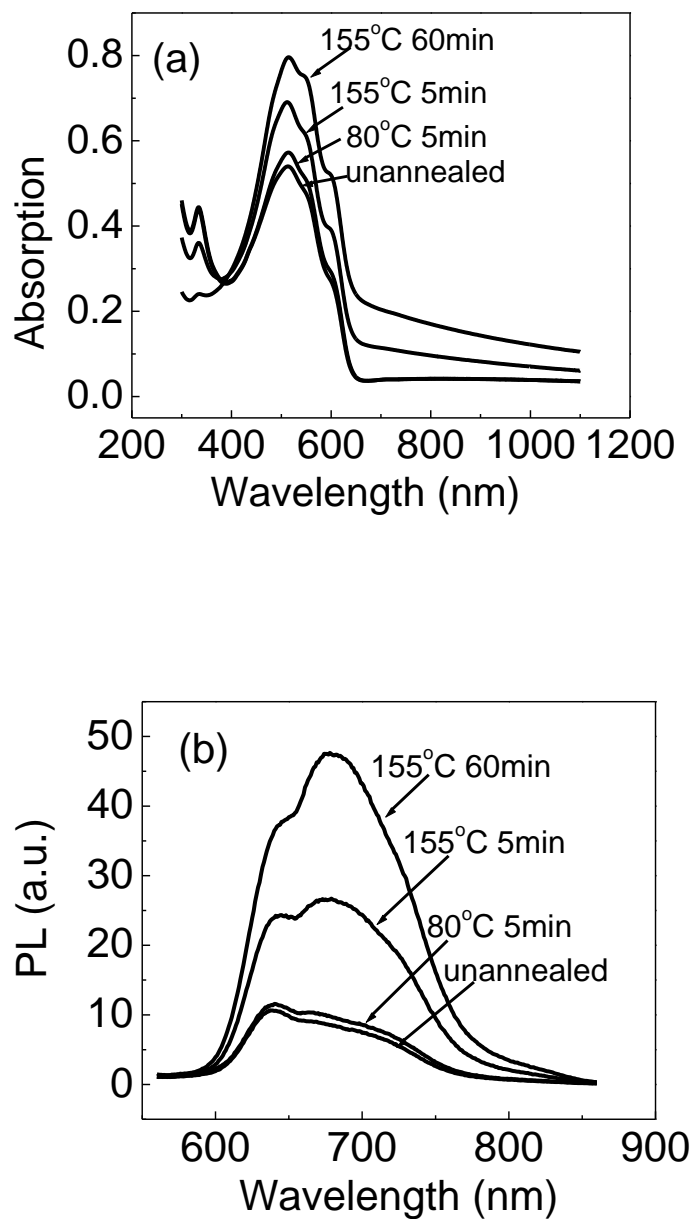
Figure 5.9 Absorption (a) and photoluminescence spectra (b) of P3HT:PCBM(1:0.8)

films with different temperature annealing.

of PCBM and reduced donor-acceptor interface areas. Combining absorption and PL measurement results, we propose that morphology reorganization of both P3HT and PCBM induced by temperature annealing increases the size of phase separation domains and reduces the total area of donor-acceptor interfaces, and consequently increases the average electron –hole separation distance at the interfaces. Therefore, the attractive force between electrons and holes is reduced and the probability of CT complex formation is then suppressed. Furthermore, enlarged phase separation leads to the formation of bicontinuous transporting paths for electron in PCBM and holes in P3HT separately, which will enhance both electron and hole mobilities. The overall charge mobility enhancement is supported by significant enhancement of the dark currents shown in Figure 5.10. The enhancement in charge mobilities increases the probability for electrons and holes to escape from coulumbic attraction and mutual capture, and consequently suppresses the formation of CT complexes.

Our experimental results also show that over annealing the P3HT:PCBM solar cells results in further reduction of interface area, decrease of charge mobility and increase of CT complex density, and consequently deteriorate the PV performance. Therefore, temperature annealing is associated with sophisticated processes involving morphology, interface, mobility, absorption, and excited states, etc. And MFP measurement presents a relatively simple parameter to determine the best annealing conditions by visualizing the dynamics of CT complexes.
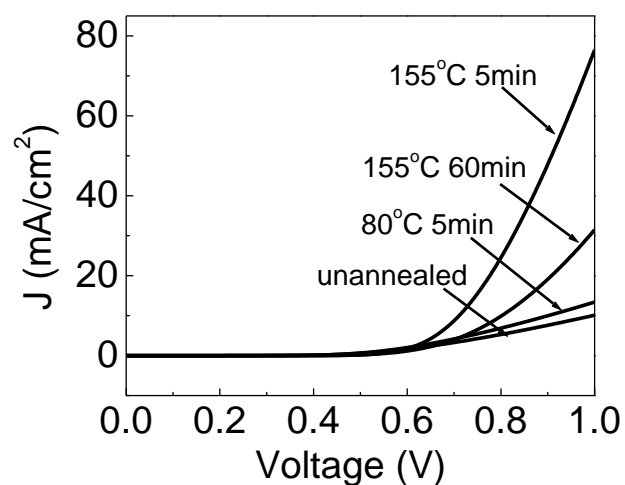
Figure 5.10 Dark current density-Voltage characteristics of ITO/Pedot/P3HT:PCBM(1:0.8)/Al devices with different temperature annealing.

5.4 Conclusions

MFP measurements were used to study the charge carrier photogeneration processes in P3HT and P3HT:PCBM solar cells. It was found that dissociation of polaron pairs, triple-charge reaction, and dissociation of hot excitons are the main carrier generation process in cells of P3HT or P3HT doped with low concentrations of PCBM. When P3HT was doped with high concentrations of PCBM, the predominant photovoltaic channel is the photoinduced charge transfer at donor/acceptor interface. In terms of photocurrent generation, photoinduced charge transfer in the most efficient PV channel, followed by direct dissociation of hot excitons. Dissociation of polaron pairs has the lowest efficiency for free charge carrier generation.

Furthermore, high-field magnetic field effect on photocurrent reflects the recombination of dissociated electrons and holes towards the formation of singlet and triplet charge-transfer complexes in bulk-heterojunction organic solar cells. It is also indicative that the recombination of dissociated electrons and holes is a function of intermolecular donor-acceptor density and morphology. It was found that thermal annealing significantly reduces the density of CT complexes formed at the donor-acceptor interfaces by adjusting the film morphology and charge mobilities. This result suggests that completely removing the formation of CT complexes will further enhance the PV efficiency of organic bulk-heterojunction solar cells.

In conclusion, magnetic field effects on photocurrent provide a unique experimental tool to experimentally visualize the photovoltaic processes of exciton dissociation and charge recombination in organic solar cells.

CHAPTER 6

IMPROVEMENT OF PHOTOVOLTAIC RESPONSE BASED ON ENHANCEMENT OF SPIN-ORBIT COUPLING AND TRIPLET STATES IN ORGANIC SOLAR CELLS

6.1 Introduction

The conversion of sun light into electricity involves three necessary processes: generation of excited states upon light absorption, dissociation of excited states, and charge transport. The selection rule in the electronic dipole transitions indicates that the photon absorption can only generate singlet states in organic semiconducting materials. However, the hyperfine interaction (HFI) or spin-orbit coupling (SOC) can flip electronic spin polarization and thus induces an intersystem crossing between singlet and triplet states. As a consequence, singlet and triplet excited states coexist in organic semiconducting materials under photoexcitation. Due to different binding energies, lifetimes, and diffusion lengths, the singlet and triplet excitons can have different contributions to the generation of photocurrent. The relative lower binding energy makes singlet excitons more effectively dissociate into free charge carriers. However, the longer diffusion length can facilitate the triplet excitons to diffuse to the donor-acceptor interface for dissociation.[27, 29] Therefore, the control of singlet and triplet ratios may form a new mechanism to enhance the PV response in organic solar cells.

It is known that the spin-orbit coupling determines the intersystem crossing and consequently the singlet and triplet ratios in organic materials. The organic conjugated materials with aromatic structures have weak spin-orbit coupling and thus limited triplet states under photoexcitation. There are two ways to increase the SOC: chemically attaching heavy metal atoms to organic molecules,[102] namely internal heavy atom effect, or physically dispersing heavy metal particles into organic materials,[103, 104] so called "external heavy atom effect". The internal heavy-atom effect requires delicate organometallic reactions to systematically change the spin-orbit coupling strength. The external heavy-atom effect can be readily obtained by dispersing heavy metal atoms into organic materials. However, the insolubility of metal particles together with the large discontinuity of dielectric constant at the material interface creates a significant difficulty in obtaining a uniform dispersion and an effective interfacial interaction in organic metallic material composites. We find that mixing two soluble organic materials: strong-SOC $Ir(ppy)_3$ molecules and weak-SOC MEH-PPV can increase the effective spin-orbit coupling in organic solar cells. This enhancement of spin-orbit coupling leads to a decrease of singlets but an increase of triplets through intersystem crossing, consequently improving the PV efficiency in the bulk-heterojunction $Ir(ppy)_3$:MEH-PPV:PCBM solar cell. This PV enhancement can be attributed to the optimization of exciton dissociation, exciton-charge reaction and reduction of charge recombination.

6.2 Experimental

The MEH-PPV with the average molecular weight of Mn = 50,000 was used as a polymer matrix in the organic solar cells. The PCBM and Ir(ppy)$_3$ were mixed with the MEH-PPV in chloroform solution for spin cast to form bulk-heterojunction films with the thickness of 90 nm under nitrogen atmosphere. An organic solar cell was then fabricated by vacuum-depositing aluminum (Al) onto the thin film of bulk-heterojunctions coated on indium tin oxide (ITO) glass substrate. Temperature dependent PL was measured in a Helium-cooled cryostat (Advanced Research System, Inc) with optical windows. Morphology study of bulk-heterojunction solar cells was conducted using a Hitachi 200 KV field emission Transmission Electron Microscope (TEM).

6.3 Results and Discussion

6.3.1 Ir(ppy)$_3$ Effect on PV Response

Figure 6.1a shows the current-voltage (I-V) curves for the devices of PCBM:MEH-PPV (1:1) composite without and with 5wt% Ir(ppy)$_3$ dopant, respectively. These two devices show similar open-circuit voltage (V$_{OC}$) of 0.82 V and fill factor (FF) of 0.29. However, the short-circuit current (I$_{SC}$) was enhanced from 0.6 mA/cm^2 to 1.1 mA/cm^2 when 5 wt% Ir(ppy)$_3$ is added into the MEH-PPV:PCBM (1:1) composite. It can be seen from the photocurrent action spectra in Figure 6.1b that the addition of Ir(ppy)$_3$ increases the I$_{SC}$ in the entire spectral range from 370 nm to 700 nm. The power
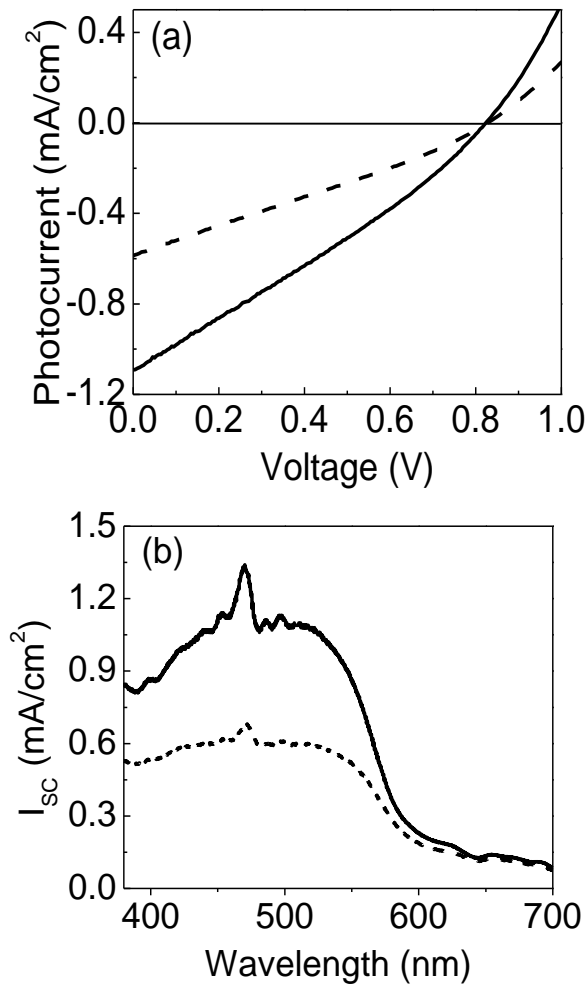
Figure 6.1 (a) Current-voltage (I-V) characteristics of MEH-PPV:PCBM (1:1) and 5wt%

Ir(ppy)$_3$ doped MEH-PPV:PCBM (1:1) devices under the mono-wavelength light

illumination of 8 mW/cm^2 at 500 nm. (b) Photocurrent spectra for devices of

ITO/MEH-PPV:PCBM(1:1)/Al and ITO/(5wt%)Ir(ppy)$_3$:MEH-PPV:PCBM(1:1)/Al. Dash

and solid lines are for MEH-PPV:PCBM (1:1) and (5wt%)Ir(ppy)$_3$:MEH-PPV:PCBM

(1:1) composites, respectively.

conversion efficiency (PCE) was consequently improved by 80% due to the dispersion of Ir(ppy)$_3$ in the MEH-PPV:PCBM (1:1) composite.

6.3.2 Ir(ppy)$_3$ Effect on MFP

To understand the Ir(ppy)$_3$-induced PV enhancement, the magnetic field effects on photocurrent (MFP) were investigated for the MEH-PPV upon Ir(ppy)$_3$ doping. It can be seen in Figure 6.2 that the MFP consists of two components: a rapid increase from 0 to10 mT and then a very slow decrease from 10 to 150 mT for both pure MEH-PPV and Ir(ppy)$_3$ doped MEH-PPV devices. The rapid increase and slow decrease components can be attributed to magnetic field-dependent exciton dissociation[26, 35] and triplet-charge reaction,[38, 39] respectively. In general, the photoexcited states undergo exciton dissociation and exciton-charge reaction in the generation of photocurrent in conjugated polymers, as shown in Figure 6.3. The electroluminescence (EL) and photoluminescence (PL) studies indicate that a low magnetic field can significantly affect the intersystem crossing K_{ISP} in polaron-pair states while the intersystem crossing K_{ISC} in excitonic states does not show appreciable magnetic dependence at low field.[105] Because singlet polaron pairs have a larger dissociation rate as compared to triplet polaron pairs, a low magnetic field can increase the photocurrent by reducing the singlet-triplet intersystem crossing K_{ISP} in polaron-pair states through Zeeman effects. On the other hand, an external magnetic field can reduce triplet-charge reaction yield by changing the reaction rate,

Figure 6.2 MFP from the MEH-PPV with different Ir(ppy)$_3$ doping concentrations under the mono-wavelength light illumination of 4 mW/cm^2 at 500 nm.

leading to a negative component in MFP. It is particularly noted in Figure 6. 2 that the amplitude of MFP decreases with increasing the dispersed Ir(ppy)$_3$ concentration. The 5wt% Ir(ppy)$_3$ dispersion reduces the amplitude of MFP by about 50%. We note that enhancing spin-orbit coupling can weaken the influence of an external magnetic field on the singlet-triplet intersystem crossing and consequently quenches the MFP. Therefore, the reduction of MFP amplitude (Figue 6. 2) suggests that the dispersed Ir(ppy)$_3$ increases the spin-orbit coupling in the MEH-PPV. This enhancement of spin-orbit coupling can be explained as follows. The delocalized π electrons of the MEH-PPV can penetrate into the large orbital magnetic field of the Ir(ppy)$_3$, forming an intermolecular spin-orbit magnetic
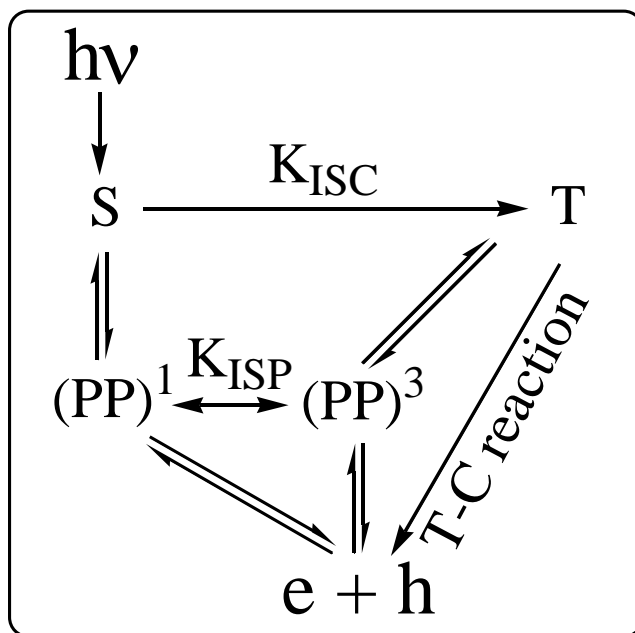
Figure 6.3 Photoexcitation and photovoltaic processes in organic semiconductors. S and T are singlet and triplet excitons. $(pp)^1$ and $(pp)^3$ represent singlet and triplet polaron pairs. K_{ISC} and K_{ISP} are intersystem crossing in excitonic and polaron-pair states. e and h are free electron and hole. Two PV processes are shown for exciton dissociation (through polaron-pair states) and charge reaction (through triplet excitons).

interaction when the MEH-PPV chains and the $Ir(ppy)_3$ molecules are placed within close proximity at their interface. This intermolecular magnetic interaction can increase the effective spin-orbit coupling of the MEH-PPV.

To confirm the modification of spin-orbit coupling due to intermolecular magnetic interaction, we compared the effects of heavy-metal complex $Ir(ppy)_3$ and light-metal complex Alq_3 on the MFP. It is noted that the heavy-metal complex $Ir(ppy)_3$ and light-metal complex Alq_3 have similar lowest unoccupied orbital (LUMO) and highest occupied orbital (HOMO) with the values of 3.0 eV and 5.4 eV for $Ir(ppy)_3$ [60] and 3.2 eV and 5.7 eV for Alq_3 [61], respectively. Figure 6.4 shows that the light-metal complex Alq_3 does not appreciably reduce the MFP in the MEH-PPV:Alq_3 composite device. This comparison indicates that the light-metal complex Alq_3 has little influence on the spin-orbit coupling of MEH-PPV. Therefore, the observed significant reduction of MFP amplitude in Figure 6.2 confirms that the heavy-metal complex $Ir(ppy)_3$ can form intermolecular magnetic interaction and leads to the modification of spin-orbit coupling of the polymer matrix in organic solar cells.

6.3.3 $Ir(ppy)_3$ Effect on PV processes

We now consider the effects of heavy-metal complex $Ir(ppy)_3$ on excited states processes in the $Ir(ppy)_3$: MEH-PPV:PCBM composite. It is known that the MEH-PPV and PCBM can form donor-acceptor interaction that dissociates photogenerated excitons in organic
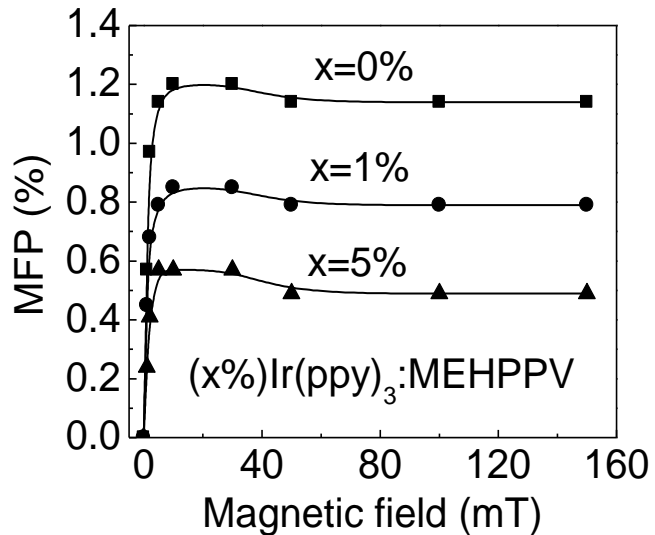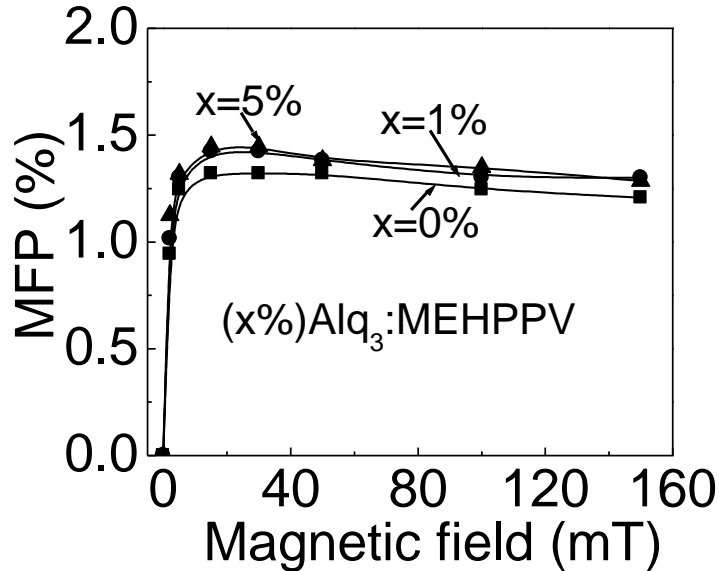
Figure 6.4 MFP from the MEH-PPV with different Alq_3 doping concentrations under the mono-wavelength light illumination of 4 mW/cm^2 at 500 nm.

bulk-heterojunction solar cells. The photoinduced absorption studies have found that free charge carriers are generated immediately (~40 fs) through dissociation process at the polymer/fullerene interfaces after photoexcited states are formed in polymer fullerene composites.[13] The dissociation of photoexcited states is inevitably accompanied by significant PL quenching, as shown in Figure 6.5a. The remaining PL from the heavily doped MEH-PPV:PCBM composites with 1:1 and 1:4 ratios comes from either incomplete dissociation of excited states or recombination of dissociated charge carriers. It is noted that the dispersed $Ir(ppy)_3$ further decreases the PL from the composite (Figure 6.5b). This further quenched PL suggests that the dispersed $Ir(ppy)_3$ consumes singlet

116
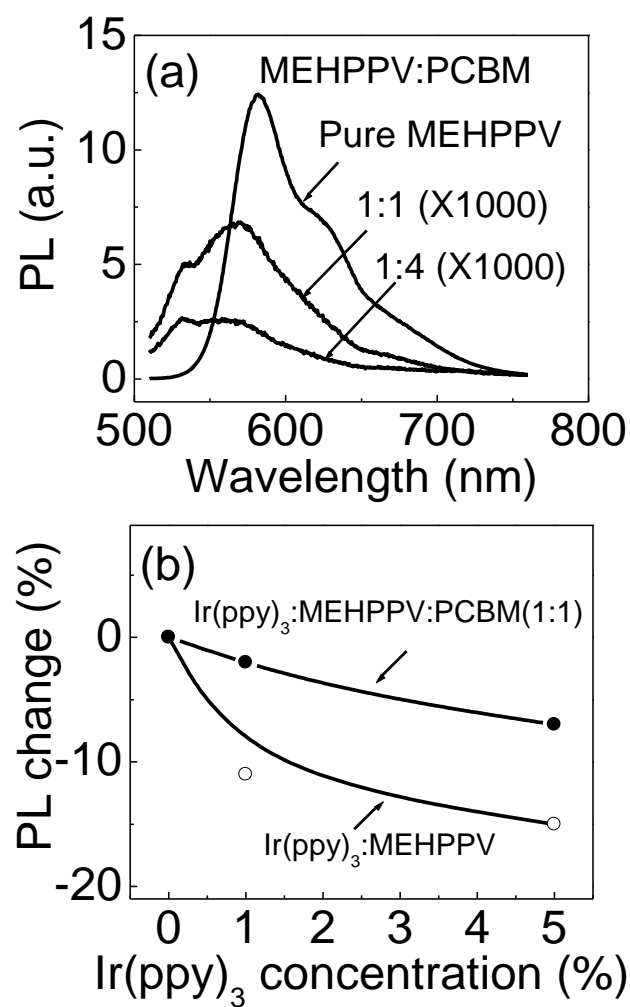
Figure 6.5 (a) PL spectra for pure MEH-PPV and MEH-PPV:PCBM composites with 1:1 and 1:4 ratios. (b) PL intensity as a function of Ir(ppy)$_3$ concentration for Ir(ppy)$_3$ doped MEH-PPV and PCBM:MEH-PPV composite. The excitation wavelength was 490 nm. The PL intensity was integrated for the entire spectrum.

excitons through intersystem crossing. Now we discuss whether the Ir(ppy)$_3$-associated

intersystem crossing can occur before the PCBM-induced dissociation of excited states. It

can be seen in Figure 6.6a that 1wt% PCBM doping reduces the positive MFP amplitude

but induces the negative MFP component in the MEH-PPV:PCBM solar cell. The

reduction of positive MFP implies that the low PCBM doping unequally dissociates the

singlet and triplet polaron pairs respectively, and thus decreases field-dependent K_{ISP}.

However, the negative MFP indicates that the low PCBM doping also increases the

reaction between triplet excitons and trapped charge carriers in conjugated polymer

matrix. Interestingly, the dispersed 5wt% Ir(ppy)$_3$ further increases the negative MFP:

triplet-charge reaction in the MEH-PPV:(1wt%)PCBM composite solar cell. Based on the

fact that low field-dependent triplet-charge reaction arises from the change of triplet

exciton density,[106] this further increased negative MFP confirms that that the 5wt%

Ir(ppy)$_3$ increases the triplet exciton ratio and the resultant triplet-charge reaction. It

should be noted that the MFP becomes flat when the PCBM doping increases to 5wt%.

Because the observed magnetic dependence at low field (< 150 mT) is due to the

field-dependent intersystem crossing K_{ISP} in polaron-pair states, this flat MFP is an

evidence that the 5wt% PCBM doping completely dissociates both singlet and triplet

polaron pairs in the MEH-PPV:PCBM composites. It should be noted that, at a given

PCBM concentration, the change in intersystem crossing due to spin-orbit coupling can

affect the completion of dissociation of both singlet and triplet polaron pairs because the
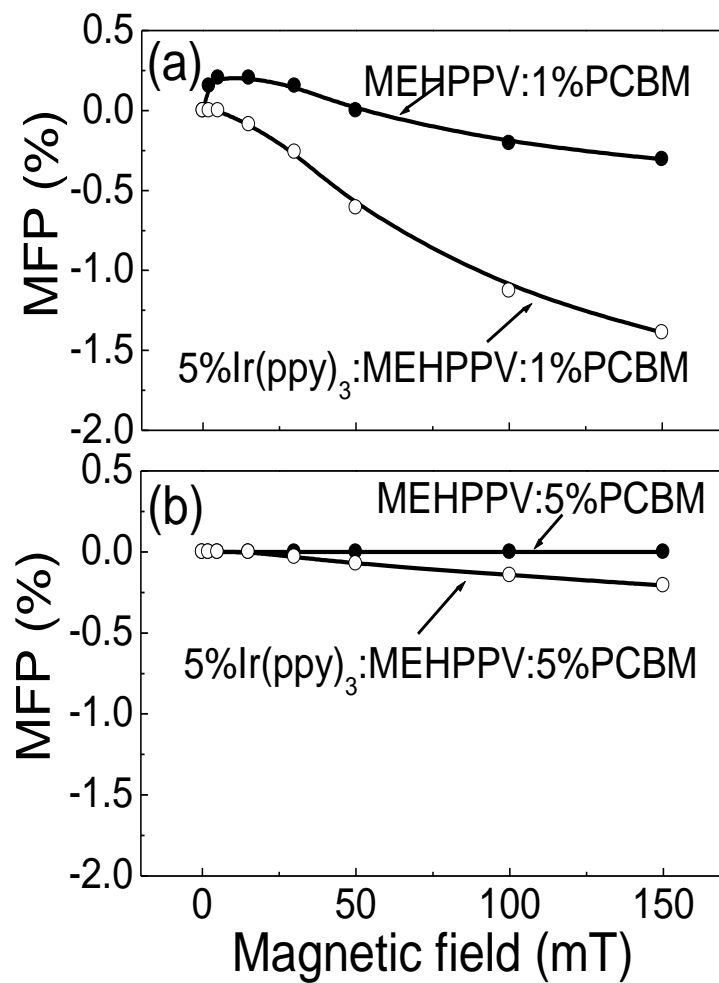
Figure 6.6 Ir(ppy)$_3$ doping effects on MFP for 1wt% (a) and 5wt% (b) PCBM doped

MEH-PPV, respectively

singlet and triplet polaron pairs also have different dissociation rates. Figure 6.6b shows that the dispersion of Ir(ppy)$_3$ in 5wt% PCBM doped MEH-PPV results in a slight negative MFP, so called triplet-charge reaction. This Ir(ppy)$_3$-induced negative MFP suggests that the Ir(ppy)$_3$ increases the intersystem crossing K$_{ISP}$ and thus the triplet exciton density through the conversion of triplet polaron pairs to triplet excitons in the lightly (5wt%) PCBM doped MEH-PPV.

In heavily PCBM doped MEH-PPV, the formation of polaron-pair states can be completely removed by direct exciton dissociation, leading to a flat MFP in a low magnetic field (< 150 mT). It is interesting to note in Figure 6.7 that at high magnetic field (> 200 mT) the heavily PCBM doped MEH-PPV shows a positive MFP. While this positive MFP is almost completely quenched in the 5% Ir(ppy)$_3$ dispersed MEH-PPV:PCBM composite. This high-field MFP indicates that charge transfer complexes are formed at MEH-PPV/PCBM interfaces. The strong spin exchange interaction in CT states causes a large energy difference between singlet and triplet CT complexes, and the large energy difference requires a relatively high field to change the intersystem crossing. It can be therefore suggested that the dispersed Ir(ppy)$_3$ molecules can change the singlet and triplet exciton ratios in exciton and CT complex states through intersystem crossing by modifying the spin-orbit coupling in the heavily PCBM doped MEH-PPV system.

We now discuss how the Ir(ppy)$_3$ dopant affects the polymer excited states processes
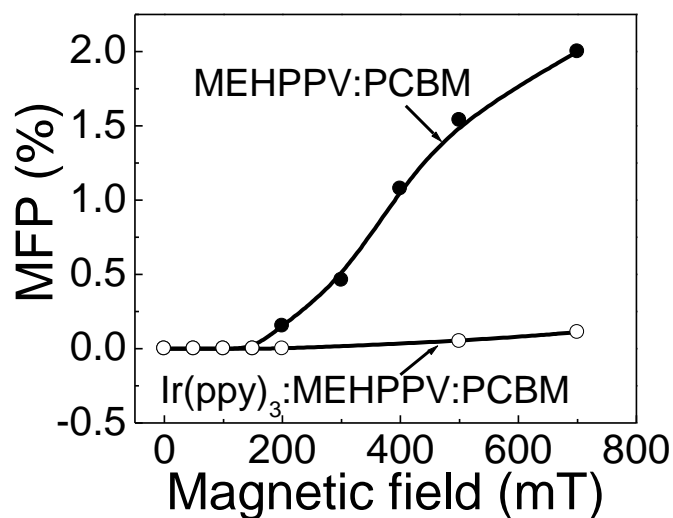
Figure 6.7 High-field MFPs for heavily PCBM doped MEH-PPV (1:1 ratio) without and with 5wt% Ir(ppy)$_3$.

when the PCBM is existed in organic bulk-heterojunction solar cell. It can be seen in Figure 6.8a that the PL temperature dependence of pure MEH-PPV shows a typical quenching due to multi-phonon nonradiative emission as temperature increases from 50 K to 300 K. When the 5 wt% Ir(ppy)$_3$ are uniformly dispersed into the MEH-PPV, the PL shows a slight increase and then decrease with increasing the temperature. This increase component is the typical behavior of the excitons formed by transferred charge carriers.[107-109] Therefore, it can be suggested that the dispersed Ir(ppy)$_3$ molecules form close contacts with MEH-PPV chains for introducing intermolecular magnetic interaction through the penetration of polymer π electrons into the orbital magnetic field of Ir(ppy)$_3$.
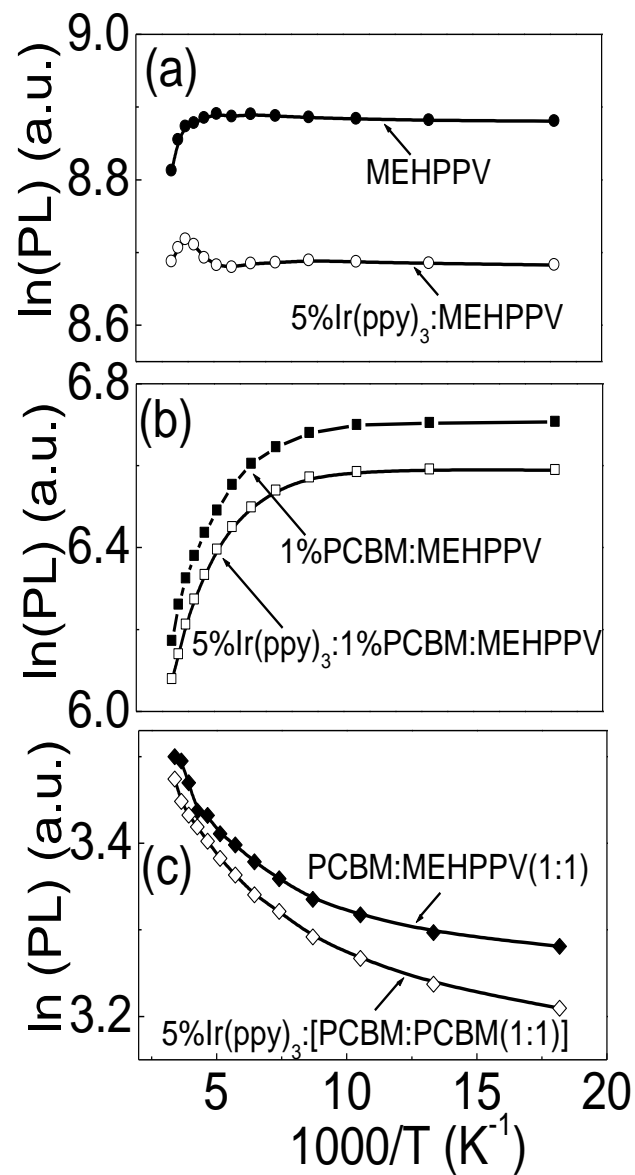
Figure 6.8 Ir(ppy)$_3$ doping effects on PL temperature dependence for (a) pure MEH-PPV,

(b) lightly PCBM doped MEH-PPV, and (c) heavily PCBM doped MEH-PPV.

We note that the low-concentration 1wt% PCBM dopant significantly increases the temperature-dependent PL quenching through multi-phonon process in the PCBM:MEH-PPV composite (Figure 6.8b). However, at high PCBM concentration, the PL temperature dependence only shows the increase component as the temperature changes from 50 K to 300 K (Figure 6.8c). This increase component in the PL temperature dependence implies that the dissociated charge carriers can recombine[110-112] and give rise to the PL at heavily PCBM doped MEH-PPV. There are three channels for dissociated electrons and holes to recombine in the PCBM:MEH-PPV composite. Firstly, the dissociated electrons come back to the MEH-PPV chains from the PCBM molecules to form MEH-PPV-type excitons for radiative emission. Secondly, the dissociated electrons and holes form exciplex between the PCBM molecules and MEH-PPV chains for light emission. Thirdly, the dissociated electrons and holes recombine with nonradiative emission. Here, the different PL temperature dependence between pure MEH-PPV and heavily PCBM doped MEH-PPV suggests that the recombination of dissociated electrons and holes may lead to radiative emission, in addition to the dominant nonradiative decay channel. The effects of PCBM dopant on excited states can be divided into two parts: increasing the multi-phonon nonradiative emission and dissociating excited states in the MEH-PPV:PCBM composite. We further note that the recombination rate of electrons and holes is proportional to exp $(-\Delta E/KT)$, where the ΔE is the potential barrier for electrons and holes to overcome for recombination. It can be

seen in Figure 6.8c that the dispersed Ir(ppy)$_3$ increases the PL temperature dependence in the (5%)Ir(ppy)$_3$:MEH-PPV:PCBM composite. We can therefore argue that the dispersed Ir(ppy)$_3$ molecules increase the potential barrier ΔE for electrons and holes to recombine. The Ir(ppy)$_3$-reduced recombination of dissociated charge carriers can be explained by the possible fact that the dissociated charge carriers from triplet excitons can experience a difficulty in recombination due to the repulsive magnetic interaction in parallel-oriented spin polarizations. As a result, the experimental results from MFP and PL temperature dependence suggest that the dispersed Ir(ppy)$_3$ molecules have two effects on the excited states: increasing the triplet exciton ratio and reducing the recombination of dissociated charge carriers in the Ir(ppy)$_3$: MEH-PPV:PCBM composite, which lead to the quenching of the magnitude of high-field MFP.

6.3.4 Ir(ppy)$_3$ Effect on Exciton Diffusion Length

We now consider the overall exciton diffusion length when the singlet and triplet ratios are changed by the Ir(ppy)$_3$ doping. Since both singlet and triplet excitons contribute to photocurrent, the measurement of thickness-dependent photocurrent [113] can lead to an estimate of the overall exciton diffusion length for pure MEH-PPV and Ir(ppy)$_3$-doped MEH-PPV devices. Especially, the effect of Ir(ppy)$_3$ dopant on the overall exciton diffusion length can be explored when the thickness of active layer is changed in the double-layer PV cell of ITO/MEH-PPV:(5wt%)Ir(ppy)$_3$/C$_{60}$(30nm)/Al. The exciton

diffusion length L_D can then be calculated based on the optimal thickness (d_{opt}) for maximal photocurrent efficiency, according to the equation[113]:

$$d_{opt} = \frac{L_D \ln(\alpha L_D)}{\alpha L_D - 1}$$ (Equation 6.1)

where α is absorption coefficient. We find that the overall exciton diffusion length L_D increases from 3.5 nm to 6.0 nm after 5 wt% Ir(ppy)$_3$ is dispersed into the MEH-PPV, as shown in Figure 6.9a. This result reflects that the enhancement of spin-orbit coupling leads to an increase of triplet ratio through intersystem crossing upon the Ir(ppy)$_3$ doping in the MEH-PPV:Ir(ppy)$_3$ composite.

Furthermore, PL quenching can also give an estimate of diffusion length of singlet excitons based on the double-layer organic/C$_{60}$ device. Particularly, when the thickness d of active layer is sufficiently thin ($<<$ optical absorption length L_A), the L_D of singlet excitons can be calculated based on the d-dependent PL quenching according to the following equation[114]:

$$\frac{PL_1}{PL_2} = 1 - \frac{L_D}{d} \frac{\left[1 - \exp(-2d/L_D)\right]}{\left[1 + \exp(-2d/L_D)\right]}$$ (Equation 6.2)

where the PL$_1$ and PL$_2$ are the PL intensities from the MEH-PPV devices without and with the quenching layer of C$_{60}$, respectively. The singlet exciton diffusion length L_D is found to be 9.2 nm in the MEH-PPV and 9.0 nm in the MEH-PPV:(5wt%)Ir(ppy)$_3$
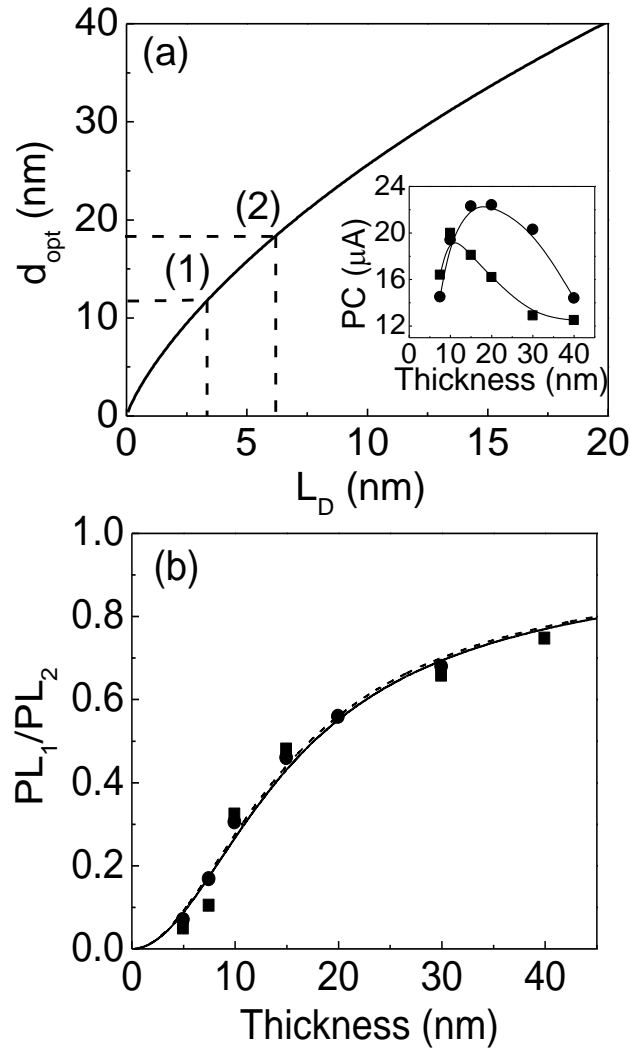
Figure 6.9 (a) Optimal active-layer thickness d_{opt} versus exciton diffusion length L_D. (1) and (2) are for MEH-PPV and MEH-PPV:(5wt%)Ir(ppy)$_3$, respectively. Absorption coefficient α was determined to be 0.01 nm^{-1} for MEH-PPV at 500 nm. Inset: thickness dependent photocurrent for MEH-PPV (square) and MEH-PPV:(5wt%)Ir(ppy)$_3$ (dot) devices. (b) Experimental data of PL_1/PL_2 versus thickness d for MEH-PPV (squares) and MEH-PPV:(5wt%)Ir(ppy)$_3$ (dots). The solid and dashed lines are the curves fitted by the equation (1) for pure MEH-PPV and 5wt% Ir(ppy)$_3$ doped MEH-PPV, respectively.

(Figure 6.9b), when the C_{60} thin film of 4 nm is used as a quenching layer in the devices. This result indicates that the dispersed Ir(ppy)$_3$ does not change the singlet exciton diffusion length of MEH-PPV. We should note that the L_D of singlet excitons derived from the PL quenching is larger than the value determined by the photocurrent. This difference can be attributed to the poor-defined MEH-PPV/C_{60} interface in the double-layer device due to the C_{60} penetration upon its vacuum deposition. This C_{60} penetration can lead to an over estimation of singlet exciton diffusion in the PL quenching experiment.[115] Nevertheless, the Ir(ppy)$_3$-induced increase of overall exciton diffusion length calculated from photocurrent (Figure 6.9a) must be due to the increase of triplet density in the Ir(ppy)$_3$: MEH-PPV:PCBM composite.

6.3.5 PCBM Concentration Effect on PV Efficiency

Because the singlet and triplet excitons have different contributions to exciton dissociation, exciton-charge reaction, and recombination of dissociated charge carriers, adjusting the singlet and triplet densities by dispersing the heavy-metal complex Ir(ppy)$_3$ can form a mechanism to improve the PV response in organic bulk-heterojunction solar cells. When the exciton dissociation is considered, the singlets should have a larger contribution to the PV response as compared to the triplets due to the lower binding energy. However, the triplet excitons can effectively diffuse to the donor-acceptor interaction sites for dissociation due to the longer diffusion length. Therefore, both

127

singlets and triplets can contribute to the exciton dissociation for photocurrent generation. When the exciton-charge reaction is considered, the triplets can be largely involved in the PV response relative to the singlets because of the longer lifetime. In addition, the dispersed $Ir(ppy)_3$ can also reduce the recombination of dissociated charge carriers due to the increase of triplet ratio and the related spin interaction. Therefore, increasing triplet ratio by introducing the heavy-metal complex $Ir(ppy)_3$ may lead to a further improvement of PV response in organic bulk-heterojunction PV cells. It is noted that the $Ir(ppy)_3$ molecules can be uniformly dispersed in the spin-cast films of conjugated polymers at the concentration up to 5wt% with the selected solvent of chloroform.[116] When the singlet and triplet exciton ratios are fixed by dispersing the $Ir(ppy)_3$ at the doping concentration of 5wt%, the PCBM concentration determines the density of donor-acceptor bulk-heterojunctions, the exciton diffusion distance for dissociation, and the density of dissociated charge carriers for triplet-charge reaction. Therefore, changing the PCBM concentration can lead to an optimization of PV response through adjusting the exciton dissociation and exciton-charge reaction. The Transmission Electron Microscopic (TEM) results indicate that the PCBM:MEH-PPV with the 1:1 ratio shows a uniform morphology while the higher PCBM concentration results in an aggregation in the MEH-PPV matrix, as shown in Figure 6.10. The analysis of electron dispersion spectrum (EDS) confirms that the 5wt% $Ir(ppy)_3$ was homogenously dispersed in the spin-cast film of $Ir(ppy)_3$:MEH-PPV:PCBM composite. It can be seen in Figure 6.11 that the PCBM
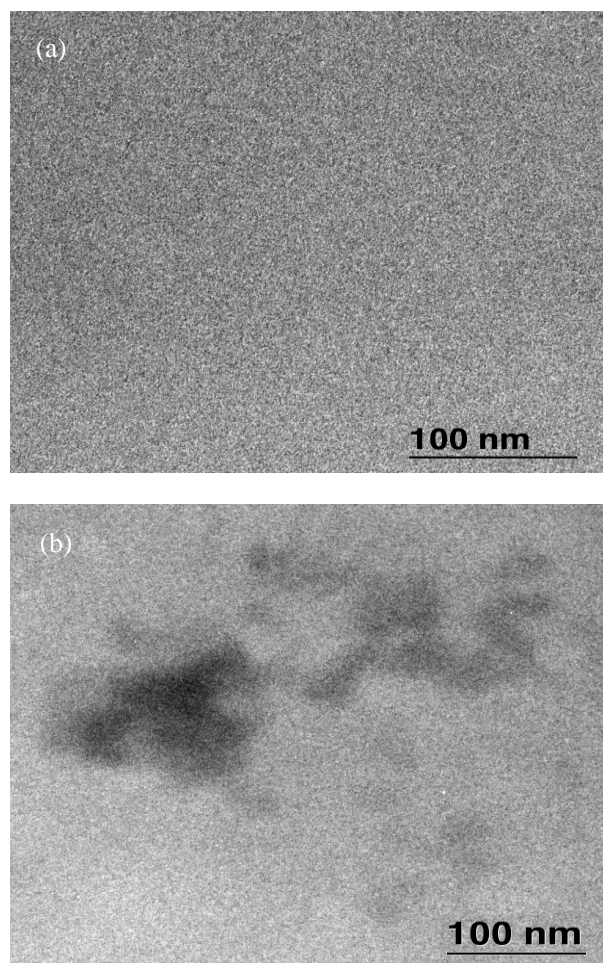
Figure 6.10 TEM images observed from the spin-cast films of PCBM doped (5wt%)Ir(ppy)$_3$:MEH-PPV composites. (a) MEH-PPV:PCBM = 1:1. (b) MEH-PPV:PCBM = 1:4.
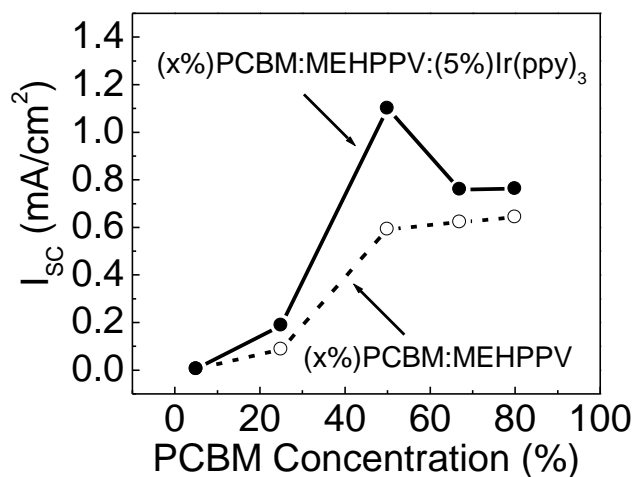
Figure 6.11 Short-circuit photocurrent (I_{SC}) as a function of PCBM concentration for ITO/MEH-PPV:(x%)PCBM/Al and ITO/(5wt%)Ir(ppy)$_3$:MEH-PPV:(x%)PCBM/Al solar cells.

concentration essentially controls the Ir(ppy)$_3$-induced PV enhancement in the Ir(ppy)$_3$:MEH-PPV:PCBM bulk-heterojunction solar cell. The PCBM with 1:1 ratio to the MEH-PPV gives rise to a maximal PV enhancement in the (5wt%)Ir(ppy)$_3$:MEH-PPV:PCBM composite solar cell.

6.4 Conclusions

In summary, the PV response of MEH-PPV:PCBM solar cell was improved by uniformly dispersing phosphorescent heavy-metal complex Ir(ppy)$_3$ molecules. The MFP results suggest that the dispersed Ir(ppy)$_3$ increases the spin-orbit coupling in conjugated

polymer MEH-PPV. The enhancement of spin-orbit coupling implies that the delocalized π electrons of MEH-PPV can penetrate into the large orbital magnetic field of Ir(ppy)$_3$, forming an intermolecular magnetic interaction at the Ir(ppy)$_3$/MEH-PPV interface. The photocurrent data indicates that the triplet exciton ratio was increased upon the dispersion of Ir(ppy)$_3$ through singlet-triplet intersystem crossing based on the enhancement of spin-orbit coupling. Furthermore, the PL temperature dependence shows that the PCBM dopant has two effects: increasing the multi-phonon nonradiative emission and dissociating excited states in conjugated polymers at low and high doping concentrations, respectively. Moreover, the dispersed Ir(ppy)$_3$ can reduce the recombination of dissociated charge carriers through changing the singlet and triplet ratios. The PCBM concentration-dependent Ir(ppy)$_3$-induced PV enhancement suggests that adjusting exciton dissociation, exciton-charge reaction, and recombination of dissociated charge carriers forms a new pathway to improve the PV response in organic bulk-heterojunction solar cells by tuning singlet and triplet exciton ratios through dispersing heavy-metal complex Ir(ppy)$_3$ based on the modification of spin-orbit coupling.

CHAPTER 7

CONCLUSIONS

The magnetic field effect on the intersystem crossing of excitons, polaron pairs and CT complexes has been studied. MFPL measurement indicates that external magnetic field does not affect the ISC in exciton state due to large $\Delta_{S\text{-}T}$. Electric field and excitation wavelength dependent MFP results confirmed that the low field MFP originates from the MF dependent ISC in polaron pair state. Introducing PCBM into MEH-PPV dissociates all the excitons and polaron pairs in the polymer matrix, providing the opportunity to study the magnetic field effect on CT complexes. The high-field MFP from MEH-PPV:PCBM was attributed to the magnetic field dependent intersystem crossing in CT complexes. The turn-on field of MFP from CT complexes is determined by the charge separation distance. And the magnitude of high-field MFP is determined by charge separation distance, the population of CT complexes and the nonmagnetic photocurrent.

The mechanism of the negative MFP was studied by tuning the density of triplet excitons and trapped charges, respectively. The magnitude of the negative MFP in PFO has been enhanced by increasing triplet ratio in PFO using phosphorescent Iridium dyes as dopants. And the negative MFP in MEH-PPV has been enhanced by increasing the density of trapped charges using low doping of PCBM. Based on these results, the mechanism of the negative MFP was attributed to the MFE on triplet-charge reaction. It

has been further investigated that spin-orbit coupling strength is important parameter in determining the magnetic field effect on the rate constant of triplet-charge reaction.

The photocurrent and MFP studies indicate that the triplet excitons mainly dissociate directly into free charge carriers at the metal-electrode interface due to their long diffusion length in the phosphorescent $Ir(ppy)_3$ PV cell while the singlet excitons experience significant bulk dissociation into polaron pairs due to their short diffusion length in the fluorescent Alq_3 PV cell. The interfacial dissociation of triplet excitons at the metal electrode leadS to enhanced PV response from phosphorescent materials as compared to the bulk dissociation of singlet excitons in fluorescent materials.

MFP measurements were used to study the charge carrier photogeneration processes in P3HT and P3HT:PCBM solar cells. It was found that dissociation of polaron pairs, triplet-charge reaction, and dissociation of hot excitons are the main carrier generation process in cells of P3HT or P3HT doped with low concentration of PCBM. When P3HT was doped with high concentrations of PCBM, the predominant photovoltaic channel is photoinduced charge transfer at donor/acceptor interface. In terms of photocurrent generation, photoinduced charge transfer in the most efficient PV channel, followed by direct dissociation of hot excitons. Dissociation of polaron pairs has the lowest efficiency for free charge carrier generation. Furthermore, high-field magnetic field dependence of photocurrent reflects the recombination of dissociated electrons and holes towards the formation of singlet and triplet charge-transfer complexes in bulk-heterojunction organic

solar cells. It is also indicative that the recombination of dissociated electrons and holes is a function of intermolecular donor-acceptor density and morphology. It was found that thermal annealing significantly reduces the density of CT complexes formed at the donor-acceptor interfaces by adjusting the film morphology and charge mobilities. This result suggests that completely removing the formation of CT complexes will further enhance the PV efficiency of organic bulk-heterojunction solar cells.

The PV efficiency of MEH-PPV:PCBM solar cells was improved by uniformly dispersing phosphorescent heavy-metal complex Ir(ppy)$_3$ molecules. The MFP results suggest that the dispersed Ir(ppy)$_3$ increases the spin-orbit coupling in conjugated polymer MEH-PPV. The enhancement of spin-orbit coupling implies that the delocalized π electrons of MEH-PPV can penetrate into the large orbital magnetic field of Ir(ppy)$_3$, forming an intermolecular magnetic interaction at the Ir(ppy)$_3$/MEH-PPV interface. The photocurrent data indicates that the triplet exicton ratio was increased upon the dispersion of Ir(ppy)$_3$ through singlet-triplet intersystem crossing based on the enhancement of spin-orbit coupling. Furthermore, the PL temperature dependence shows that the PCBM dopant has two effects: increasing the multi-phonon nonradiative emission and dissociating excited states in conjugated polymers at low and high doping concentrations, respectively. Moreover, the dispersed Ir(ppy)$_3$ can reduce the recombination of dissociated charge carriers through changing the singlet and triplet ratios. The PCBM concentration-dependent Ir(ppy)$_3$-induced PV enhancement suggests that adjusting

exciton dissociation and recombination of dissociated charge carriers forms a new pathway to improve the PV response in organic bulk-heterojunction solar cells by tuning singlet and triplet exciton ratios through dispersing heavy-metal complexes.

REFERENCES

1 A.E. Becquerel, Compt. Rend. Acad. Sci. **9**,145 (1839).

2 W. Smith, Nature **7,** 303 (1873).

3 A. Pochettino, Acad. Lincei Rend. **15,** 355 (1906).

4 M. Volmer, Ann. Physik **40,** 775(1913).

5 D. M. Chapin, C.S. Fuller, G.L. Pearson, J. Appl. Phys. **25**, 676(1954).

6 M. A. Green, K. Emery, Y. Hishikawa, W. Warta, Prog. Photovol. **16,** 61 (2008).

7 A. Goetzberger, C. Hebling, and H. W. Schock, Mater. Sci. Eng. R **40**, 1 (2003).

8 H. Spanggaard, and F. C. Krebs, Sol. Energy Mater. Sol. Cells, **83**, 125 (2004).

9 H. Hoppe and N. S. Sariciftci, J. Mater. Res. **19**,1924 (2004).

10 C.W. Tang and A.C. Albrecht, J. Chem. Phys. **62,** 2139 (1975).

11 C.W. Tang, Appl. Phys. Lett. **48,** 183 (1986).

12 J. Xue, S. Uchida, B. P. Rand, and S. R. Forrest, Appl. Phys. Lett. **85**, 5757 (2004).

13 N. S. Sariciftci, L. Smilowitz, A. J. Heeger, and F. Wudl, Science **258**, 1474 (1992).

14 G. Li, V. Shrotriya, J Huang, Y. Yao, T. Moriarty, K Emery, and Y. Yang, Nature Mater. **4**, 864 (2005).

15 W. L. Ma, C. Y. Yang, X. Gong, K. Lee, and A. J. Heeger, Adv. Funct. Mater. **15**,1617 (2005).

16 B. A. Gregg, J. Phys. Chem. B **108** (2004) 17285.

17 M. Chandross, S. Mazumdar, S. Jeglinski, X. Wei, Z. V. Vardeny, E. W. Kwock, and T.M. Miller, Phys. Rev. B **50**, 14702 (1994).

18 D. P. Craig, S. H. Walmskey, *Excitons in molecular crystals*. Benjamin, New York,

1968.

[19] U. E. Steiner and T. Ulrich, Chem. Rev. **89**, 51 (1989).

[20] A. Köhler and D. Beljonne, Adv. Funct. Mater. **14**, 11 (2004).

[21] I. V. Khudyakov, Y. A. Serebrennikov, and N. J. Turro, Chem. Rev. **93**, 537 (1993).

[22] S. P. McGlynn, J. Daigre, and F. J. Smith, J. Chem. Phys. **39**, 675(1963).

[23] D. Beljonne, Z. Shuai, G. Pourtois, and J. L. Bredas, J. Phys. Chem. **105**, 3899 (2001).

[24] H. D. Burrows, J. Seixas de Melo, C. Serpa, L. G. Arnaut, M. da G. Miguel, A. P. Monkman, I. Hamblett, and S. Navaratnam, Chem. Phys. **285**, 3 (2002).

[25] G. Ruani, C. Fontanini, M. Murgia, and C. Taliani, J. Chem. Phys. **116**, 1713 (2002).

[26] E. L. Frankevich, A. A. Lymarev, I. Sokolik, F. E. Karasz, S. Blumstengel, R. H. Baughman, and H. H. Horhold, Phys. Rev. B **46**, 9320 (1992).

[27] A. Köhler, H. F. Wittmann, R. H. Friend, M. S. Khan, and J. Lewis, Synth. Met. **77**, 147 (1996).

[28] F. Guo, Y. G. Kim, J. R. Reynolds, and K. S. Schanze, Chem. Comm. **17**, 1887 (2006).

[29] Y. Shao and Y. Yang, Adv. Mater. **17**, 2841 (2005).

[30] J. Kalinowski, M. Cocchi, D. Virgili, P. D. Marco, and V. Fattori, Chem. Phys. Lett. **380**, 710 (2003).

[31] J. Wilkinson, A. H. Davis, K. Bussmann, and J. P. Long, Appl. Phys. Lett. **86**, 111109 (2005).

[32] Z. H. Xiong, D. Wu, Z. V. Vardeny, and J. Shi, Nature, **476**, 821 (2004).

[33] T. L. Francis, O. Mermer, G. Veeraraghavan, M. Wohlgenannt, New J. Phys. **6**, 185 (2004).

[34] J. Kalinowski, J. Szmytkowski, and W. Stampor, Chem. Phys. Lett. **378**, 380 (2003).

[35] F. Ito, T. Ikoma, K. Akiyama, A. Watanabe, and S. T. Kubota, J. Phys. Chem. B **109**, 8707 (2005).

[36] E. Frankevich, A. Zakhidov, K. Yoshino, Y. Maruyama, and K. Yakushi, Phys. Rev. B **53**, 4498 (1996).

[37] R. C. Johnson, R. E. Merrifield, R. Avakian, and R. B. Flippen, Phys. Rev. Lett. **19**, 285 (1967).

[38] I. V. Tolstove, A. V. Belov, M. G. Kaplunov, I. K. Yakuschenko, N. G. Spitsina, M. M. Triebel, E. L. Frankevich, J. Lumin. **112**, 368 (2005).

[39] V. Ern, R. E. Merrifield, Phys. Rev. Lett. **21**, 609 (1968).

[40] D. V. Konarev, A. Y. Kovalevsky, S. S. Khasanov, G. Saito, D. V. Lopatin, A. V. Umrikhin, A. Otsuka, and R. N. Lyubovskaya, Eur. J. Inorg. Chem. **9,** 1881 (2006).

[41] T. Ikoma, F. Ito, T. Ogiwara, K. Akiyama, and S. Tero-Kubota, Chem. Lett. **34**, 1424 (2005).

[42] I. D. Parker, J. Appl. Phys. **75**, 1656 (1994).

[43] F. C. Chen, Q. Xu, and Y. Yang, Appl. Phys. Lett. **84**, 3181(2004).

[44] R. A. J. Janssen, J. C. Hummelen, and N. S. Sariciftci, MRS Bull. **30**, 33 (2005).

[45] V. Cimrova, I. Kminek, S. Nespurek, and W. Schnabel, Synth. Met. **64**, 271 (1994).

[46] V. I. Arkhipov, E. V. Emelianova, and H. Bassler, Chem. Phys. Lett. **340**, 517 (2001).

[47] E. Hendry, J. M. Schins, L. P. Candeias, L. D. A. Siebbeles, and M. Bonn, Phys. Rev. Lett. **92**, 196601 (2004).

[48] S. Bath, and H. Bassler, Phys. Rev. Lett. **79**, 4445 (1997).

[49] H. D. Burrows, J. Seixas de Melo, C. Serpa, L. G. Arnaut, A. P. Monkman, I. Hamblett, and S. Navaratnam J. Chem. Phys. **115**, 9601 (2001).

[50] M. Wohlgenannt, Z. V. Vardeny, J. Phys.: Condens. Mater. **15**, R83(2003).

[51] M. A. Baldo, D. F. O'Brien, M. E. Thompson, and S. R. Forrest, Phys. Rev. B **60**, 14422 (1999).

[52] G. Yu, J. Gao, J. C. Hummelen, F. Wudl, and A. J. Heeger, Science **270**, 1789 (1995).

[53] B. Kraabel, J. C. Hummelen, D. Vacar, D. Moses, N. S. Sariciftci, A. J. Heeger. and F. Wudl, J. Chem. Phys. **104**, 4267 (1996).

[54] X. Wei, Z. V. Vardeny, N. S. Sariciftci, and A. J. Heeger, Phys. Rev. B **53**, 2187 (1996).

[55] Z. Xu, and B. Hu, Adv. Funct. Mater. **18**, 1 (2008).

[56] J. M. Frost, F. Cheynis, S. M. Tuladhar, and J. Nelson, Nano Lett. **6**, 1674 (2006).

[57] I. V. Tolstove, A. V. Belov, M. G. Kaplunov, I. K. Yakuschenko, N. G. Spitsina, M. M. Triebel, E. L. Frankevich, J. Lumin. **112**, 368 (2005).

[58] W. Holzer, A. Penzkofer, and T. Tsuboi, Chem. Phys. **308**, 93 (2005).

[59] U. E. Steiner and T. Ulrich, Chem. Phys. **89**, 51(1999).

[60] N. Matsusue, S. Ikame, Y. Suzuki, and H. Naito, Appl. Phys. Lett. **85**, 4046 (2004).

[61] M. Yamaguchi and T. Nagatomo, Thin Solid Films **363**, 21(2000).

[62] Y. Wu, B. Hu, and J. Howe, J. Appl. Phys. **98**, 103510 (2005).

[63] M. Sudhakar, P. I. Djurovich, T. E. Hogen-Esch, and M. E. Thompson, J. Am. Chem. Soc. **125**, 7796 (2003).

[64] N. Corcoran, A. C. Arias, J. S. Kim, J. D. Mackenzie, and R. H. Friend, Appl. Phys.

Lett. **82**, 299 (2003).

65 D. V. Konarev, A. Y.   Kovalevsky, S. S. Khasanov, G. Saito, D. V. Lopatin, A.V.

Umrikhin, A. Otsuka, and R. N. Lyubovskaya, Eur. J. Inorg. Chem. **9**, 1881 (2006).

66 C. Rothe and A. P. Monkman, Phys. Rev. B **68**, 075208 (2003).

67 A. J. Cadby, P. A. Lane, H. Mellor, S. J. Martin, M. Grell, C. Giebeler, D. D. C.

Bradley, M. Wohlgenannt, C. An, and Z. V. Vardeny, Phys. Rev. B **62**, 15604 (2000).

68 M. Granström, K. Petritsch, A. C. Arias, A. Lux, M. R. Anderson, and R. H. Friend,

Nature (London) **395**, 257 (1998).

69 S. E. Shaheen, C. J. Brabec, N. S. Sariciftci, F. Padinger, T. Fromherz, and J. C.

Hummelen, Appl. Phys. Lett. **78**, 841 (2001).

70 C. Daniel, D. Guillaumont, C. Ribbing, and B. Minaev, J. Phys. Chem. **103**, 5766

(1999).

71 F. Q. Guo, Y. G. Kim, J. R. Reynolds, and K. S. Schanze, Chem. Communi. **17**,

1887(2006).

72 S. Naka, H. Okada, H. Onnagawa, Y. Yamaguchi, and T. Tsutsui, Synth. Met. **111**,

331 (2000).

73 N. Matsusue, Y. Suzuki, and H. Naito, Jpn. J. Appl. Phys. **44**, 3691 (2005).

74 H. D. Burrows, M. Fernandes, J. S. Melo, A. P. Monkman, and S. Navaratnam, J. Am.

Chem. Soc. **125**, 15310 (2003).

75 A. K. Ghosh and T. Feng, J. Appl. Phys. **49**, 5982 (1978).

76 K. C. Tang, K. L. Liu, and I. C. Chen, Chem. Phys. Lett. **386**, 437 (2004).

[77] I. Sokolik, R. Rriestley, A. D. Walser, R. Dorsinville, and C. W. Tang, Appl. Phys. Lett. **69**, 4168 (1996).

[78] A. D. Walser, R. Priestley, and R. Dorsinville, Synth. Met. **102**, 1552 (1999).

[79] J. Szmytkowski, W. Stampor, J. Kalinowski, and Z. H. Kafafi, Appl. Phys. Lett. **80**, 1465 (2002).

[80] J. Wilkinson, A. H. Davis, K. Bussmann, and J. P. Long, Appl. Phys. Lett. **86**, 111109 (2005).

[81] V. I. Adamovich, S. R. Cordero, P. I. Djurovich, A. Tamayo, M. E. Thompson, B. W. D'Andrade, S. R. Forrest, Org. Electron. **4**, 77 (2003).

[82] J. M. Leng, S. Jeglinski, X. Wei, R. E. Benner, Z. V. Vardeny, F. Guo, and S. Mazumdar, Phys. Rev. Lett. **72**, 156 (1994).

[83] S. F. Alvarado, P. F. Seidler, D. G. Lidzey, and D. D. C. Bradley, Phys. Rev. Lett. **81**, 1802 (1998).

[84] S. Barth, H. Bässler, U. Scherf, and K. Müllen, Chem. Phys. Lett. **288**, 147 (1998).

[85] V. I. Arkhipov, E. V. Emelianova, and H. Bässler, Phys. Rev. Lett. **82**,1321 (1999).

[86] V. I. Arkhipov, E. V. Emelianova, S. Barth, and H. Bässler, Phys. Rev. B **61** 8207 (2000).

[87] J. G. MüLLER, U. Lemmer, J. Feldmann, and U. Scherf, Phys. Rev. Lett. **88**, 147401 (2002).

[88] Y. Zaushitsyn, V. Gulbinas, D. Zigmantas, F. L. Zhang, O. Inganäs, V. Sundström, and A. Yartsev, Phys. Rev. B **70**, 075202 (2004).

[89] G. Dicker, M. P. de Haas, L. D. A. Siebbeles, and J. M. Warman, Phys. Rev. B **70**,

045203 (2004).

[90] E. Hendry, J. M. Schins, L. P. Candeias, L. D. A. Siebbeles, and M. Bonn, Phys. Rev. Lett. **92**, 196601 (2004)

[91] B. Kraabel, D. Moses, and A. J. Heeger, J. Chem. Phys. **103**, 5102 (1995).

[92] G. Ruani, C. Fontanini, M. Murgia, and C. Taliani, J. Chem. Phys. **116**, 1713 (2002).

[93] D. Y. Paraschuk, S. G. Elizarov, A. N. Khodarev, A. N. Shchegoikhin, S. A. Arnautov, and E. M. Nechvolodova, JETP Lett. **81**, 467 (2005).

[94] C. J. Brabec, G. Zerza, G. Cerullo, S. De Silvestri, S. Luzzati, J. C. Hummelen, and N. S. Sariciftci, Chem. Phys. Lett. **340**, 232 (2001).

[95] M. C. Scharber, N. A. Schultz, N. S. Sariciftci, and C. J. Brabec, Phys. Rev. B **67**, 085202 (2003).

[96] Y. Araki, Y. Yasumura, and O. Ito, J. Phys. Chem. B **109**, 9843 (2005).

[97] Y. Kim, S. A. Choulis, J. Nelson, D. D. C. Bradley, S. Cook, and J. R. Durrant, Appl. Phys. Lett. **86**, 063502 (2005).

[98] D. Chirvase, J. Parisi, J. C. Hummelen, and V. Dyakonov, Nanotechnology **15**, 1317 (1323).

[99] X. N. Yang, J. Loos, S. C. Veenstra, W. J. H. Verhees, M. M Wienk, J. M. Kroon, M. A. J. Michels, and R. A. J. Janssen, Nano Lett. **5**, 579 (2005).

[100] T. Erb, U. Zhokhavets, G. Gobsch, S. Raleva, B. Stűhn, P. Schilinsk, C. Waldauf, and C. J. Brabec, Adv. Funct. Mater. **15**, 1193 (2005).

[101] G. Li, Y. Yao, H. Yang, V. Shrotriya, G. W. Yang, and Y. Yang, Adv. Funct. Mater. **17**, 1636 (2007).

[102] J. Lewis, M. S. Khan, A. K. Kakkar, B. F. G. Johnson, T. B. Marder, H.B. Fyfe, F. Wittmann, R. H. Friend, and A. E. Dray, J. Organomet. Chem. **425**, 165 (1992).

[103] G. Kavarnos, T. Cole, P. Scribe, J. C. Dalton, and N. J. Turro, J. Am. Chem. Soc. **93**, 1032 (1971).

[104] Z. S. Romanova, K. Deshayes, and P. Piotrowiak, J. Am. Chem. Soc. **123**, 2444 (2001).

[105] Y. Wu, B, Hu, J. Howe, A. P. Li, and J. Shen, Phys. Rev. B **75**, 075413 (2007).

[106] Z. H. Xu, Y. Wu, and B. Hu, Appl. Phys. Lett. **89**, 131116 (2006).

[107] D. Chirvase, Z. Chiguvare, M. Knipper, J. Parisi, V. Dyakonov, and J. C. Hummelen, J. Appl. Phys. **93**, 3376 (2003).

[108] S. Guha, J. D. Rice, Y. T. Yau, C. M. Martin, M. Chandrasekhar, H. R. Chandrasekhar, R. Guentner, P. Scanduicci de Freitas, and U. Scherf, Phys. Rev. B **67**, 125204 (2003).

[109] G. Y. Zhong, X. M. Ding, J. Zhou, N. Jiang, W. Huang, and X. Y. Hou, Chem. Phys. Lett. **420**, 347 (2006).

[110] D. Veldman, T. Offermans, J. Sweelssen, M. M. Koetse, S. C. J. Meskers, R. A. J. Janssen, Thin Solid Films, **511**, 333 (2006).

[111] L. J. A. Koster, V. D. Mihailetchi, and P. W. M. Blom, Appl. Phys. Lett. **88**, 052104 (2006).

[112] H. Ohkita, S. Cook, Y. Astuti, W. Duffy, M. Heeney, S. Tierney, I. McCulloch, D. D. C. Bradley, and R. Durrant, Chem. Commun. **37**, 3939 (2006).

[113] T. Stubinger, and W. Brutting, J. Appl. Phys. **90**, 3632 (2001).

[114] P. Peumans, A. Yakimov, and S. R. Forrest, J. Appl. Phys. **93**, 3693 (2003).

[115] D. E. Markov, E. Amsterdam, P. W. M. Blom, A. B. Sieval, and J. C. Hummelen, J. Phys. Chem. A **109**, 5266 (2005).

[116] Y. Wu, B. Hu, and J. Howe, J. Appl. Phys. **98**, 103510 (2005).

VITA

Zhihua Xu was born in Dongyang, Zhejiang, China in July 1975. He attended Tianjin University in 1992, and received a Bachelor of Engineering from the Department of Chemical Engineering in 1996. After graduation he joined Sinopec, Inc and worked as an engineer for 4 years. In 2001 he entered Shanghai Institue of Ceramics, Chinese Academy of Sciences, and earned a Master of Science in Materials Science and Engineering in 2004. His research area was inorganic electroluminescent (EL) materials and devices. In August 2004, he attended the University of Tennessee, Knoxville for his doctoral degree. He has been working on organic solar cells since then.